*Stephan Calvet*
*Caminos de Agua*
*Federico Montes de Oca 2C, Independencia*
*San Miguel de Allende, Guanajuato, México*

# Chemical Treatment of Bone Char for Groundwater Fluoride Adsorption

A Thesis Presented to

The School of Engineering at

The University of Edinburgh

---

In Partial Fulfilment of the Requirements for the Degree of

Master of Engineering

---

*Industrial Supervisor:*

*Aaron Krupp*

*Academic Supervisor:*

*Dr Cher Hon Lau*

by

Stephan Calvet

April, 2019

# Abstract

The optimisation of cow bone based adsorbents for fluoride removal from groundwater was investigated. A series of batch tests followed by rapid small-scale column testing (RSSCT) was undertaken.

An initial batch test, assessing raw cow bone meal treated with 30 wt. % $H_2SO_4$, 30 wt. % $H_3PO_4$, 40 wt. % KOH and 32 wt. % NaOH as well as bone char (BC) doped with $CaO/Al_2(SO_4)_3$ yielded poor and unpredictable results.

A second batch test was undertaken, this time assessing BC treated with 0.1 M $H_2SO_4$ (0.97 wt. %), 0.1 M $H_3PO_4$ (0.97 wt. %), 38 wt. % HCl, 10 wt. % KOH, and 20 wt. % NaOH. BC produced with a shorter pyrolysis time (SPT), commercial Brazilian BC (BBC), and BC with the hard outer shell (BCO) separated from the softer inner core (BCI) was also tested.

The untreated BC had an adsorption capacity at an equilibrium fluoride concentration of 1.5 mg/L ($q_{1.5}$) of 2.99 mg/g (error: + 0.37 mg/g / - 0.46 mg/g). The best performing adsorbent was the $H_3PO_4$ treated BC, with a $q_{1.5}$ of 4.24 mg/g (error: + 0.47 mg/g / - 0.58 mg/g).

The $H_2SO_4$ and $H_3PO_4$ increased the adsorption capacity of the BC by 25.6 % (error: + 51.9 % / - 23.8 %) and 29.5 % (error: + 56.7 % / - 20.6 %) respectively. The KOH and NaOH decreased the adsorption capacity by 31.1 % (error: + 15.0 % / - 20.0 %) and 34.4 % (error: + 15.3 % / - 20.6 %) respectively. The HCl treated BC was almost completely destroyed (95 % production yield loss) and showed no fluoride adsorption. The SPT, BBC, BCO and BCI BC fluoride adsorption capacities were statistically indistinguishable from that of the untreated BC.

The $H_3PO_4$ treated BC was subjected to RSSCT along with the untreated BC. The untreated BC experienced breakthrough at 417 bed volumes (BV) and the $H_3PO_4$ treated BC at 520 BV, corresponding to a 24.7 % increase in performance, resulting in a 7.8 % total adsorbent cost reduction.

# Acknowledgements

I would like to thank the team at Caminos de Agua for so warmly welcoming me amongst them. During my time in Mexico, I have truly felt like I was working alongside not just colleagues, but good friends. Opening my eyes to such an important cause has lit a fire in me, and I wish to apply my experience to continue working on sustainable engineering projects to benefit those who need it the most, all around the world. Muchisima gracias a todxs!

In particular I wish to extend my complete gratitude to Aaron Krupp, who not only acted as a wise and helpful mentor, advising me throughout my project, but also a close friend, with whom I have shared many good times I will look back on with fondness.

I also wish to thank Dr 'Sam' Cher Hon Lau for his continuous support, guidance, and advice throughout my project; taking the time to write up helpful feedback on a monthly basis, as well as being available to discuss any issues I may have had. His last minute advice before my poster presentation was also invaluable to me!

I would like to give a special thank you to Dr Joshua Kearns, who during his brief visit to Caminos de Agua was able to provide me with huge amounts of invaluable advice, as well as his generous donation of RSSCT equipment to the organisation, without which a large part of this project would have been impossible to undertake.

Lastly, I wish to extend my thanks to all the others who touched my life in one way or another during my time in Guanajuato and other parts of Mexico. Whether or not this was related to my project, they have provided me with some life changing experiences I will never forget.

IV

# Contents

# Table of Figures

# Table of Tables

# Nomenclature

## Latin Letters

| Variable | Description | SI Units |
|:---:|:---|:---:|
| $a$ | Prausnitz-Radke isotherm model constant | $m^3/kg$ |
| $A$ | Packed bed area | $m^2$ |
| $A_1, A_2, A_3$ | Attractive dispersion force constants | - |
| $b$ | Prausnitz-Radke model constant | $(m^3/kg)^\beta$ |
| $B$ | Repulsive dispersion force constant | - |
| $Bi$ | Biot number | - |
| $c$ | Concentration | $kg/m^3$ |
| $\bar{c}_p$ | Intra-particle concentration averaged over pore volume | $kg/m^3$ |
| $d$ | Adsorption column diameter | $m$ |
| $d_p$ | Adsorbent particle diameter | $m$ |
| $D_L$ | Fickian axial dispersion coefficient | $m^2/s$ |
| $D_g$ | Pore solute distribution parameter | - |
| $\mathcal{D}$ | Diffusivity | $m^2/s$ |
| $\bar{\mathcal{D}}_i$ | Ionic self-diffusivity of species $i$ | $m^2/s$ |
| $EBCT$ | Empty bed contact time | $s$ |
| $Ed$ | Pore diffusion modulus | - |
| $G$ | Gibbs free energy | $J/kg$ |
| $Gr_p$ | Modified Reynolds number | - |
| $H$ | Enthalpy | $J/kg$ |
| $H_0$ | Limiting heat of adsorption | $J/kg$ |
| $J$ | Adsorbate diffusion flux | $kg/m^2s$ |
| $k$ | Rate constant | - |
| $k_a$ | Adsorption rate constant | - |
| $k_f$ | Mass transfer coefficient | $m/s$ |
| $K$ | Adsorption equilibrium constant | - |
| $L$ | Packed bed depth | $m$ |
| $m$ | Adsorbent mass | $kg$ |

## Latin Letters

| Variable | Description | SI Units |
|----------|-------------|----------|
| $n$ | Freundlich adsorption intensity constant | - |
| $n_i$ | Number of moles of adsorbate species $i$ | - |
| $\bar{n}$ | Number of adsorbate moles over the adsorbent particle volume | - |
| $N$ | Adsorbate flux at adsorbent particle surface | kg/m$^2$s |
| $P$ | Column pressure | Pa |
| $P$ | Peclet number | - |
| $q$ | Adsorbate mass | kg |
| $Q$ | Flowrate | m$^3$/s |
| $r$ | Radial position/distance | m |
| $R$ | Ideal gas constant | J/kgK |
| $Re$ | Reynolds number | - |
| $S$ | Entropy | J/kgK |
| $S_A$ | Outer surface area of the adsorbent particle | m$^2$ |
| $Sc$ | Schmidt number | - |
| $SF$ | Scaling factor | - |
| $Sh$ | Sherwood number | - |
| $St$ | Stanton number | - |
| $t$ | Time | s |
| $T$ | Temperature | K |
| $v$ | Interstitial fluid velocity | m/s |
| $v_f$ | Hydraulic loading rate | m/s |
| $v_s$ | Superficial fluid velocity | m/s |
| $V$ | Volume | m$^3$ |
| $x$ | Axial position/distance | m |
| $X$ | Diffusivity factor | - |
| $y$ | fluid phase adsorbate mole fraction | - |
| $z$ | Longitudinal position/distance | m |
| $z_i$ | Charge of ionic species $i$ | - |

## Greek Letters

| Variable | Description | SI Units |
|---|---|---|
| $\beta$ | Prausnitz-Radke isotherm model exponent | - |
| $\Delta$ | Difference | - |
| $\epsilon$ | Lennard-Jones force constant | J/kg |
| $\varepsilon$ | Void fraction | - |
| $\varepsilon_b$ | Packed bed void fraction | - |
| $\theta$ | Adsorbent fractional coverage | - |
| $\mu$ | Fluid viscosity | Pa·s |
| $\upsilon$ | Viscous diffusion rate | m$^2$/s |
| $\rho$ | Density | kg/m$^3$ |
| $\rho_b$ | Bulk solution density | kg/m$^3$ |
| $\sigma$ | Lennard-Jones force constant | m |
| $\tau$ | Tortuosity | - |
| $\phi$ | Adsorption potential | J |

## Subscripts

| Variable | Description |
|---|---|
| 0 | Initial |
| 1 | 1$^{st}$ order |
| 1.5 | 1.5 mg/L equilibrium fluoride concentration |
| 2 | 2$^{nd}$ order |
| 1000 | 1000 mg/L equilibrium fluoride concentration |
| $adsorbed$ | Adsorbed species |
| $a$ | Species $a$ |
| $b$ | Species $b$ |
| $bed$ | Column bed |
| $D$ | Dipole |
| $e$ | Equilibrium |
| $F$ | Freundlich |

## Subscripts

| Variable | Description |
|---|---|
| $i$ | Species $i$ |
| $in$ | Internal |
| $l$ | Liquid |
| $lam$ | Laminar |
| $L$ | Langmuir |
| $LC$ | Large column |
| $LJ$ | Lennard-Jones |
| $n$ | $n^{th}$ order |
| $p$ | Pore |
| $Q$ | Field quadrupole gradient |
| $r$ | Radial position/distance |
| $R$ | Repulsion |
| $s$ | Saturation |
| $solution$ | Bulk solution |
| $sur$ | Surface |
| $S$ | Adsorbate-adsorbate |
| $SC$ | Small column |
| $turb$ | Turbulent |
| $\mu$ | Field dipole gradient |

# 1.0  Introduction

The purpose of this report is to introduce the reader to the work that was undertaken over the period of six months, from June to December 2018 with the NGO Caminos de Agua (CdA), in the Guanajuato state located in Central Mexico.

The aim of the work completed during this period was to optimise a bone char (BC) fluoride adsorbent produced by CdA to increase the fluoride adsorption capacity of this, by investigating variations on the production process of this, including, but not limited to, chemical treatment.

This introduction serves to contextualise the reader with the current state of drinking water quality in Mexico, specifically in communities served by the Independencia Basin located in Guanajuato, as well as the work that CdA undertakes to provide these communities with safe, healthy and sustainable drinking water.

## 1.1  Water Stress in Mexico

According to the National Commission of Water in Mexico; 77 % of the country's water use is for agricultural purposes [1]. Of the total water volume allocated for off-stream uses, 37 % of this originates from groundwater sources. As of 2008, 101 of the country's 653 aquifers are considered over-exploited, where the ratio of water withdrawal to recharge (water stress) is greater than 1 [1]. This over-exploitation of aquifers has led to water stress levels as high as 1.73 [2], creating the serious risk of water supply collapses across the country. Alongside the risk of water shortages, the depleting water levels within aquifers are exposing populations (whose domestic water supply relies heavily on groundwater) to fossil waters with increased levels of heavy metals and other contaminants such as fluoride, causing skeletal fluorosis and various forms of cancer, with the younger population facing the most significant risks [3-5].

## 1.2   Independencia Basin

80 % of the population of Mexico live in the Central and Northern regions, where less than 20 % of the available water in the country is located [2]. In the state of Guanajuato, the population was 5.86 million as of 2015 [6]. One of the groundwater basins providing water to populations and industries in Guanajuato is the Independencia Basin, and is considered an over-exploited aquifer [1]. 99 % of domestic water supply to populations living in Guanajuato and 100 % of industrial water use is groundwater based. 60 % of agricultural production is also groundwater based, and contributes to over 84 % of the total groundwater use of the Independencia Basin [7].

Since the 1950s, the federal government of Mexico has assisted the region to undergo explosive development in the industrial and agricultural sectors. This rapid development has resulted in a large population growth in the region. This economic and population growth has led to an increase in water demand, and has led to a rapid increase in deep-well construction, shown in figure 1.2.1, despite legislation being put into place to prevent this – a Veda was placed in 1983 making it illegal to construct more wells on the aquifer [8].
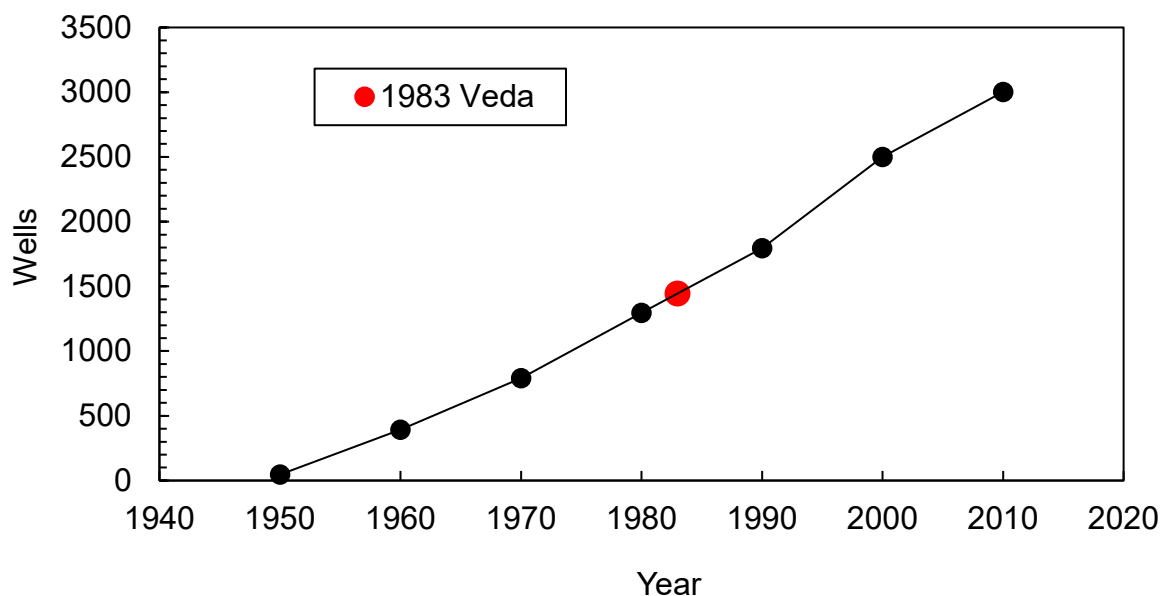


Figure 5.2.1 - Number of wells extracting groundwater from the Independencia Basin. Red data point represents the point at which the 1983 Veda was declared – making the drilling of wells illegal [8]

Poor enforcement of this Veda, resulting from a combination of historic corruption and lack of monitoring (10 CONAGUA inspectors for the entire Guanajuato state, with over 20,000 total wells [8]) has resulted in the digging of additional and deeper wells. Groundwater extraction from the Independencia Basin has therefore been steadily rising, and total water extraction is currently over 800 million m$^3$ per year [7]. This level of extraction is greater than the natural regenerative rate of the aquifer, and therefore water levels have been dropping by 3 - 4 m per year [8]. As groundwater levels drop, the water must be extracted from increasingly deeper parts of the basin, and has resulted in a steadily increasing level of groundwater contaminants naturally occurring in deep parts of the aquifer; predominantly arsenic and fluoride [9]. Figures 1.2.2 and 1.2.3 show the arsenic and fluoride concentrations respectively of groundwater samples taken from wells and other sources providing groundwater from the Independencia Basin [10]. It can be seen from these figures that 54 % and 32 % of sources had arsenic and fluoride contaminations larger than the World Health Organisation (WHO) limits respectively. These limits are outlined in section 1.2.1.
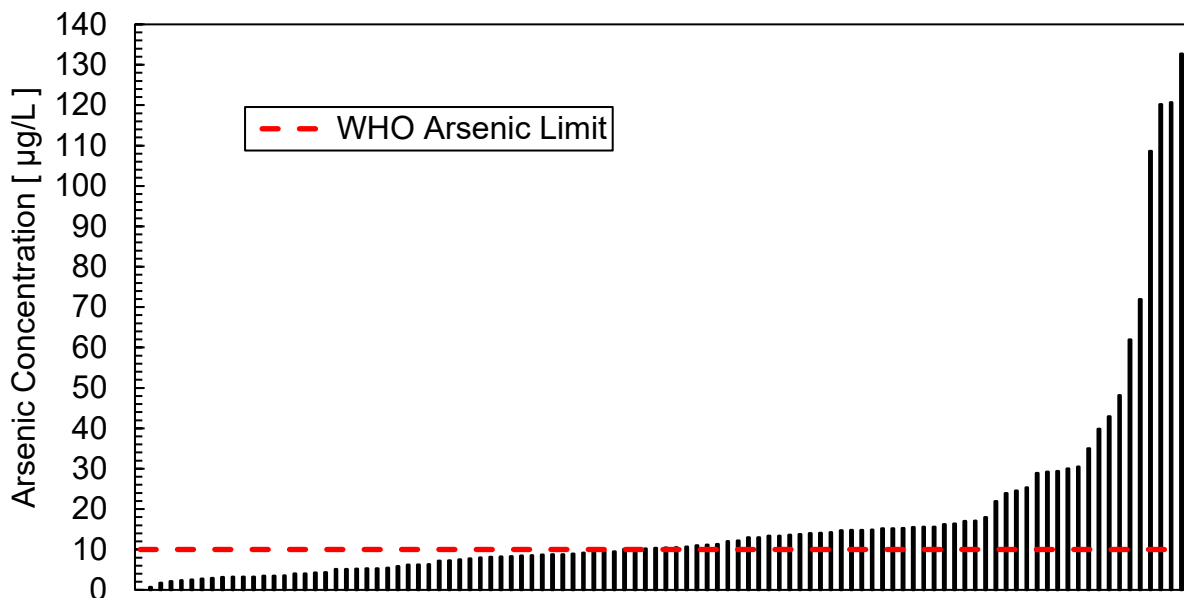


Figure 1.6.2 - Arsenic contamination of groundwater from 101 sample points taken in the Independencia Basin region [10]
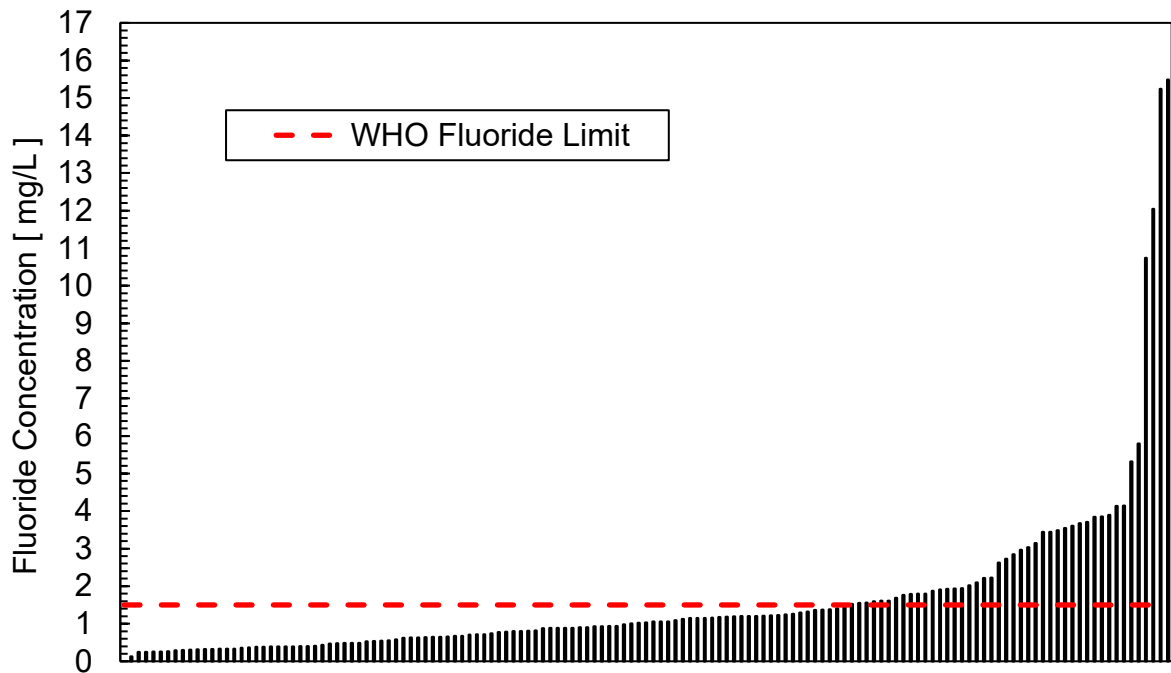
Figure 1.2.7 - Fluoride contamination of groundwater from 142 sample points taken in the Independencia Basin region [10]

## 1.2.1 WHO Guideline Arsenic and Fluoride Values

The WHO has set out recommendations for the maximum concentrations of various contaminants in drinking water before these pose a health risk to populations. The limits for arsenic and fluoride, the two primary sources of inorganic contamination found in the groundwater from the Independencia Basin, are given in table 1.2.1.1.

Table 5.2.1.1 - WHO guideline arsenic and fluoride concentrations in drinking water

| Species | Concentration Limit | Source |
|---------|--------------------|--------|
| Fluoride | 1.5 mg/L | [11] |
| Arsenic * | 10 µg/L | [12] |

*While the WHO acknowledges that there is strong evidence of correlation between elevated levels of arsenic in drinking water and instances of cancer (particularly of the skin, bladder, and lung [13]), there remains considerable uncertainty over the actual risks at low concentrations. Therefore, the 10 µg/L limit is a provisional recommendation based on best data available [12].*

## 1.3 Fluoride Health Effects

Current research indicates that an excess of consumed fluoride ions alters the rate at which enamel proteins break down, as well as the rate at which by-products from this process are removed by the maturing enamel. This interference with normal enamel growth activity indirectly results in a decrease in free calcium ion concentration, resulting in severely hypo-mineralised and weakened enamel [14].

Another effect of excess fluoride consumption is the conversion of hydroxyapatite (HAP) to fluorohydroxyapatite (FHAP) through the proposed ion-exchange reaction given below in equation 1.3.1 [15].

$$Ca_{10}(PO_4)_6(OH)_2 + F^- \rightarrow Ca_{10}(PO_4)_6(OH)F + H_2O \qquad (1.3.1)$$
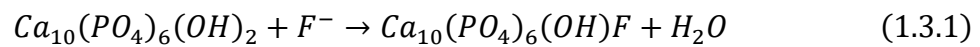
HAP constitutes approximately 70 wt. % of human bones and teeth. Due to FHAP being less dense than HAP, as well as darker in colour; this reaction causes weakening of dental structure, as well as a discoloration of teeth [15].

The Thylstrup-Fejerskov index (TFI), named after the authors who developed it, is often used to determine the severity of dental fluorosis in individuals [16, 17]. The index has a scale of 1 - 9, with descriptions of the dental surface provided to enable determination of the level of dental fluorosis in the individual. Examples of teeth at various levels on the TFI are shown in table 1.3.1.

Table 1.3.1 - TFI levels with analogue visual representation of teeth at these levels [18]

| Example | TFI Index Level |
| --- | --- |
|  | 2 |
|  | 3 |
|  | 4 |
|  | 5 |
|  | 6 |
|  | 7 |
|  | 8 |

Children and adolescents are at the highest risk of dental fluorosis due to their developing teeth. A 2016 study of 307 participants between the ages of 11 - 20 from rural areas in Guanajuato showed that 92 % of these suffered from dental fluorosis [19]. 62 % of these had a TFI greater than 4. With a continued increase in fluoride concentrations in groundwater, an imminent health crisis could result in the first cases of skeletal fluorosis appearing in populations; resulting in serious, irreversible damage and deformations of the skeletal bone structure. Again, children and teenagers are most at risk.

## 1.4 Caminos de Agua

Caminos de Agua (CdA) is a registered 501(c)(3) non-profit organisation in the U.S. as well as a Mexican Asociación Civil. CdA's mission is to provide open-source water solutions for at-risk communities on the Independencia Basin in Central Mexico, and leverage those solutions for others confronting similar water challenges throughout the world [20]. CdA takes four approaches to implementing water solutions:

1  **Technology development:** working in the lab, in the field or alongside various universities, organisations and other institutions to develop low-cost technologies allowing access to drinking water.
2  **Community-led implementation:** working with local grassroots organisations and community coalitions by following the initiatives and desires of community members.
3  **Education:** undertaking various events and educational programs to prevent the spread of misinformation, teach people about water issues and solutions, and provide training to allow communities to become independent in the management of their water systems.
4  **Monitoring and evaluation:** rigorously following up on implemented projects to allow for continuous improvement of these, as well as maintenance and constant surveying to track the developing situation and contamination levels of groundwater in the region.

The primary projects undertaken in the research and technology department of CdA include:

**Rainwater harvesting:** the community-led construction and implementation of rainwater cisterns.

**Ceramic filter manufacture:** the production of low-cost, silver-coated ceramic water filters to remove suspended solids and pathogens from water. These are implemented in conjunction with rainwater harvesting cisterns.

**Bone char production:** in-house pyrolysis of cow bone to produce BC for the removal of fluoride contaminants from groundwater.

**Groundwater treatment system (GTS):** a fixed-bed lead-lag adsorption column system comprised of several components, including BC filters for fluoride removal and bayoxide columns for arsenic removal.

### 1.4.1 Context of the Project within Work Undertaken by Caminos de Agua

Early economic estimates undertaken in-house by CdA have indicated that the total cost of currently used BC fluoride adsorbents used in the lead-lag fixed bed adsorption column GTS are greater than that of the bayoxide imported from Germany to attain the treatment objectives set by the WHO. These objectives are given in table 1.2.1.1.

The optimisation of fluoride removing adsorbents is therefore an economic priority in the development of the GTS, to reduce costs for end users.

## 2.0  Theory

The following section will take the reader through the underlying theoretical principles of the work conducted at CdA, primarily discussing the topics of adsorption from solution and adsorption systems.

## 2.1  Fluoride Removal Process Selection

Mohapatra *et al.* [21] conducted a comprehensive review of current technologies for removal of fluoride from drinking water. Chibi and Haarhoff [22] also detail the relative advantages and disadvantages of the prevailing techniques. These features, coupled with the constraints that CdA faces when seeking to develop and deploy fluoride removal systems in rural communities across Guanajuato and beyond, serve as the basis for process selection for such a system.

Table 2.1.1 highlights the primary process types, along with their relative advantages and disadvantages.

Table 6.1.1 – Fluoride removal process features and characteristics

| Process Type | Description | Advantages | Disadvantages |
|---|---|---|---|
| **Ion-exchange** | The release of ions from a medium in exchange for ions present in solution [23]. | • Resins developed to have large exchange capacities and high selectivity to fluoride ions<br><br>• Do not produce sludge | • Resins must be regenerated once saturated, producing a concentrated waste stream which requires appropriate disposal<br><br>• High capital costs for specialised ion-exchange resins |
| **Adsorption** | The removal of fluoride from solution through adsorption processes. May involve chemical or physical adsorption processes. Some adsorbents may also have ion exchange processes occurring. | • Many adsorbents have a relatively low capital cost<br><br>• Do not produce sludge | • Adsorbents tend to have a lower removal capacity and selectivity than specialised ion exchange resins or membranes<br>• Media must be regenerated once saturated, producing a concentrated waste stream which requires appropriate disposal |
| **Membrane processes** | Physical separation of ionic constituents such as fluoride through the pressurisation of water through a semi-permeable membrane [24]. | • Extremely high fluoride selectivity and removal capacity | • High capital, operational and maintenance costs<br>• Concentrate stream produced requiring appropriate disposal |
| **Chemical precipitation** | The addition of chemicals such as lime [25-27], magnesium [28] or aluminium sulphate [29] to precipitate fluoride from water solution. | • Certain techniques, such as magnesium or aluminium sulphate addition, have high fluoride removal rates | • Excess and costly doses required<br>• Sludge disposal necessary, raising operation and maintenance costs |

9

## 2.1.1 Fluoride Adsorbent Selection

Given the strict constraints on process economy, it can be seen from table 2.1.1 that adsorption is the most viable fluoride removal process type. There are several types of possible adsorbent that can be used. The primary types of these are described in table 2.1.1.1.

Table 2.1.1.1 – Fluoride adsorbent type comparison

| Adsorbent Type | Advantages | Disadvantages |
|---|---|---|
| **Activated alumina** | <ul><li>Costs are about 10 % those of commonly used ion-exchange resins [22]</li><li>Relatively high adsorption capacity [30]</li><li>Greater affinity to fluoride than many other anionic species commonly found in groundwater [22]</li></ul> | <ul><li>Hydroxide and phosphate species, commonly found in groundwater from the Independencia Basin, have a higher affinity to activated aluminas than fluoride [22]</li><li>Low point of zero charge of pH 5 - 6 so will experience low adsorption capacities when exposed to more basic groundwater [30, 31], such as is the case for groundwater from the Independencia Basin</li><li>High capital costs compared to other adsorbents</li></ul> |
| **Activated carbon** | <ul><li>Large surface area and adsorption capacity, although not as high as activated aluminas [22]</li></ul> | <ul><li>Low fluoride selectivity</li><li>Relatively high capital costs</li></ul> |
| **Bone char** | <ul><li>Greater affinity to fluoride than many other anionic species commonly found in groundwater [22]</li><li>Low capital costs</li></ul> | <ul><li>Lower adsorption capacity than aluminas</li></ul> |

BC's affinity to fluoride as well as its low cost, ease of manufacture and high adsorption capacity compared to other low-cost adsorbents make it an ideal choice for fluoride adsorption in rural settings.

## 2.2   Adsorption Types

Adsorption is the adhesion of molecules of gas, liquid or dissolved solids onto a surface [32]. The removal of fluoride from groundwater in the context of CdA's work, as well as the project undertaken with the organisation, involves the adsorption of dissolved fluoride ions in solution. Therefore, mechanisms and equations from this point forward will refer to adsorption from solution, where appropriate.

The two primary types of adsorption are physical adsorption, involving only relatively weak intermolecular forces; and chemisorption, involving the formation of a chemical bond between the adsorbent surface and the adsorbate species.

Ruthven [33] concisely describes the primary differences between the two adsorption types, shown in table 2.2.1.

Table 2.2.1 - Primary differences between physical adsorption and chemisorption

| Physical Adsorption | Chemisorption |
|---|---|
| Low heat of adsorption (< 2 or 3 times latent heat of evaporation) | High heat of adsorption (> 2 or 3 times latent heat of evaporation) |
| Non-specific | Highly specific |
| Monolayer or multilayer | Monolayer only |
| No dissociation of adsorbed species | May involve dissociation |
| Significant only at relatively low temperatures | Possible over a wide range of temperatures |
| Rapid, non-activated and reversible | Activated, may be slow and reversible |
| No electron transfer, although polarisation of adsorbent may occur | Electron transfer leading to bond formation between adsorbate and adsorbent surface |

The divide between chemisorption and physical adsorption is not always clear, and can depend on the adsorption energy [34] (also known as the heat of adsorption).

Previous work by Medellin-Castillo *et al.* [35, 36] has shown that the adsorption of fluoride onto the surface of hydroxyapatite (HAP) is due to the electrostatic interactions between fluoride ions in water and the surface charge of the HAP surface, with a low heat of adsorption and therefore a physical adsorption process occurring.

For this reason, the theory and mechanisms of physical adsorption will be described in the following section, and, from this point forward, the term adsorption will refer to physical adsorption.

## 2.3   Fundamental Entropic Basis of Adsorption

Adsorption is fundamentally an exothermic process. This can be shown through an entropic argument, wherein the adsorbed species has at most two degrees of translational freedom, always fewer degrees of rotational freedom than the species in solution, and therefore a lower entropy (i.e. $S_{solution} > S_{adsorbed}$). Therefore, the entropy change upon adsorption will be negative. This is shown in equation 2.3.1.

$$\Delta S = S_{adsorbed} - S_{solution} \qquad (2.3.1)$$

Where:      $\Delta S$ is the total entropy change of adsorption

$S_{adsorbed}$ is the entropy of the adsorbed species

$S_{solution}$ is the entropy of the species in solution

If adsorption is to occur spontaneously, the change in Gibbs free energy ($\Delta G$) must be negative, and therefore from equation 2.3.2, this requires the enthalpy change of adsorption ($\Delta H$) to be positive – i.e. exothermic adsorption [33].

$$\Delta G = \Delta H - T\Delta S \qquad (2.3.2)$$

Where:      $\Delta G$ is the change in Gibbs free energy

$\Delta H$ is the enthalpy change of adsorption

$T$ is the temperature of the system

$\Delta S$ is the total entropy change of adsorption

## 2.4 Forces and Energies of Adsorption

Physical adsorption involves both van der Walls (dispersion – repulsion) forces and electrostatic interactions (specifically, in the case of ionic fluoride adsorption, Coulombic forces).

### 2.4.1 Dispersion - Repulsion Energy

The attractive potential arising from dispersion forces between two isolated molecules is shown in equation 2.4.1.1.

$$\phi_D = -\frac{A_1}{r_{a,b}^6} - \frac{A_2}{r_{a,b}^8} - \frac{A_3}{r_{a,b}^{10}}$$ (2.4.1.1)

Where:    $\phi_D$ is the attractive potential

$r_{a,b}$ is the distance between the centres of interacting molecules $a$ and $b$

$A_1$, $A_2$, and $A_3$ are constants

The sixth power term ($\frac{A_1}{r_{a,b}^6}$), which is largely dominant, arises from instantaneous dipole – induced dipole interactions, meaning that attractive forces decay at a rate of ($\frac{1}{r^6}$).

The repulsive forces, given by equation 2.4.1.2, describe the Pauli Exclusion principle [36][37], which forbids pairs of electrons to occupy the same quantum state:

$$\phi_D = \frac{B}{r_{a,b}^{12}}$$ (2.4.1.2)

Where:    $\phi_R$ is the repulsive potential

$r_{a,b}$ is the distance between the centres of interacting molecules $a$ and $b$

$B$ is a constant

This repulsive force decays at a rate of ($\frac{1}{r^{12}}$).

These attractive and repulsive forces, when both considered, give rise to the Lennard-Jones potential, described in equation 2.4.1.3.

$$\phi_{LJ} = 4\epsilon \left[ \left( \frac{\sigma}{r_{a,b}} \right)^{12} - \left( \frac{\sigma}{r_{a,b}} \right)^{6} \right] \tag{2.4.1.3}$$

Where:    $\phi_{LJ}$ is the Lennard-Jones potential

$r_{a,b}$ is the distance between the centres of interacting molecules $a$ and $b$

$\epsilon$ and $\sigma$ are force constants characteristic of the species considered

Figure 2.4.1.1 depicts the graphical representation of the Lennard-Jones potential:
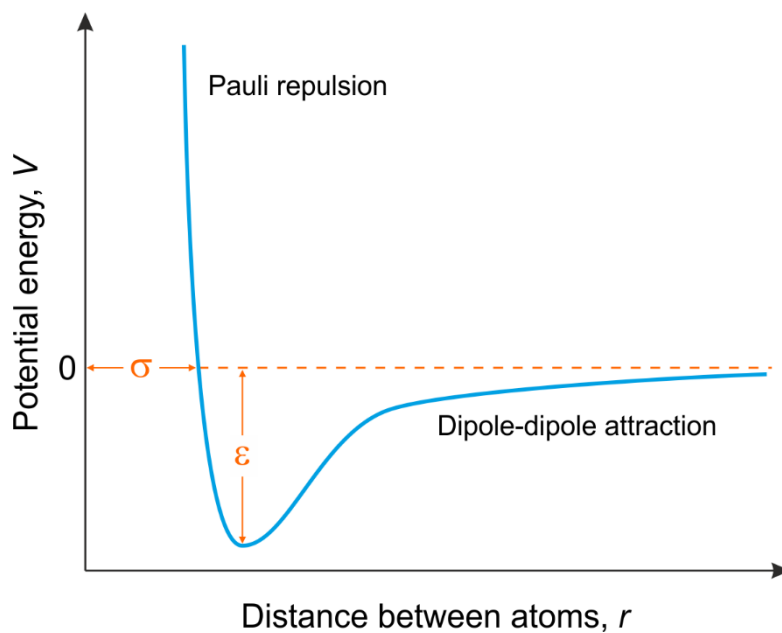


Figure 2.4.1.1 - Lennard-Jones potential well [38]

The point at which the graph crosses zero on the potential energy axis shows where repulsive forces become attractive.

### 2.4.2 Electrostatic Energy

Electrostatic contributions to the adsorption energy arise when the surface of an adsorbent or adsorbate has significant electric fields. Additional contributions to the energy of adsorption arise from polarisation ($\phi_P$), field dipole ($\phi_\mu$), field gradient quadrupole ($\phi_Q$), and adsorbate-adsorbate ($\phi_s$) interactions [33].

Together with dipole and repulsive interactions, the overall potential is given by equation 2.4.2.1.

$$\phi = \phi_D + \phi_R + \phi_P + \phi_\mu + \phi_Q + \phi_S \qquad (2.4.2.1)$$

Where:       $\phi$ is the total adsorption potential

                       $\phi_D$ is the attractive (dipole) potential

                       $\phi_R$ is the repulsive potential

                       $\phi_\mu$ is the field dipole potential

                       $\phi_Q$ is the field gradient quadrupole potential

                       $\phi_S$ is the adsorbate-adsorbate potential

## 2.5   Point of Zero Charge

The point of zero charge (PZC) describes the condition at which the surface charge density of an adsorbent is zero.

The PZC relates strongly to the pH of the solution in which the adsorbent is immersed: at pH values below the PZC, the acidic water protonates the surface of the adsorbent, yielding a positive surface electrical field, which in turn attracts anions such as fluoride. At pH values below the PZC, negative hydroxyl ions are present on the surface of the adsorbent and attract cations (i.e. repel anions) [39, 40].

For this reason, the PZC of adsorbents has a significant effect on the adsorption capacity of these at different solution pH values. The average pH of groundwater in the Independencia Basin is between pH 7.3 to pH 7.7 [10, 41, 42]. Therefore, adsorbents with a PZC below this point will likely have a significantly better adsorption capacity than those with a greater PZC, due to the electrostatic attraction of negatively charged fluoride ions to their surface.

## 2.6　Adsorption Isotherms

Adsorption isotherms, in the case of adsorption from solution, depict the adsorption capacity of an adsorbent species as a function of the adsorbate concentration at fixed temperatures. The shapes of these isotherms are based both on theoretical and empirical models of adsorption behaviours. Brunauer *et al.* [43] first proposed a classification of the primary adsorption isotherm behaviours observed throughout literature into five different types. The International Union of Pure and Applied Chemistry (IUPAC) has since expanded this to six types, shown in figure 2.6.1.
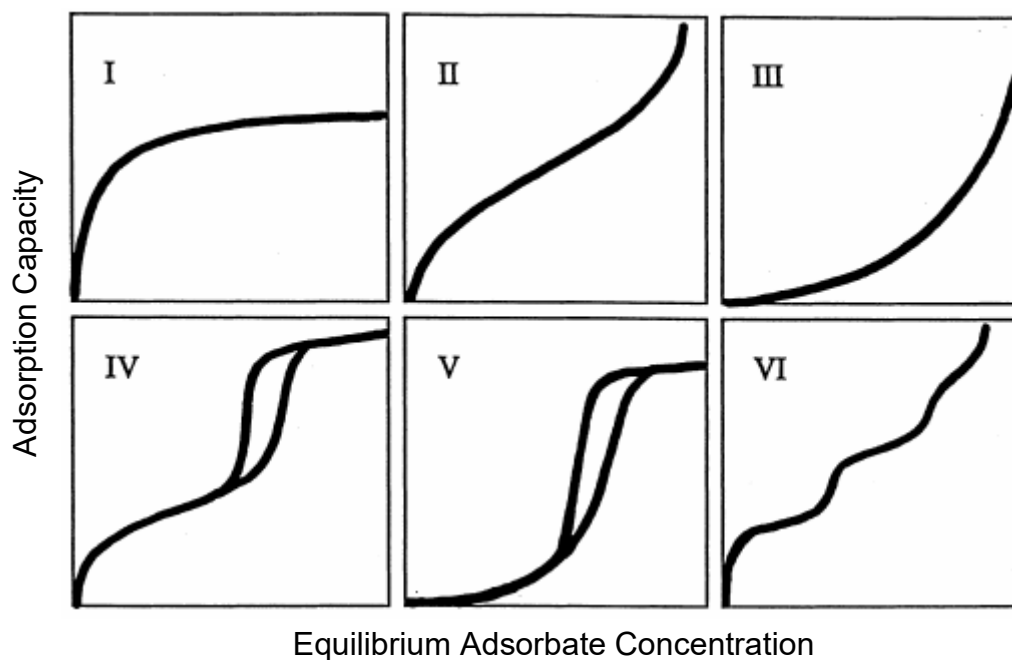


Figure 2.6.1 - IUPAC adsorption isotherm classification, types I – VI [44]

The reversible type I isotherm is typically attributed to microporous adsorbents with relatively small external surfaces. This is due to the definite saturation limit corresponding to the filling of the adsorbent micropores by the adsorbate (such as in activated carbons and zeolites) [45].

Previous experiments involving fluoride adsorption from water with BCs indicate that these show type I isotherm behaviours [35, 46]. Results of adsorption batch experiments in this project also indicate that the treated BCs show type I isotherm behaviour (see section 5.1.2). For this reason, the theoretical and empirical adsorption models explained below will be those describing type I isotherm behaviours that were used to model the adsorption of fluoride to BC.

## 2.6.1 Freundlich Isotherm

Freundlich first described the empirical relationship between the concentration of adsorbate on the surface of an adsorbent and its concentration in solution in 1909 [47].

Initially, the relation proposed was derived from work observing the mass of gas particles adsorbed onto the surface of an adsorbent as a function of pressure. However, this relationship is analogous to that observed in solid-liquid adsorption, and is shown in equation 2.6.1.1.

$$\frac{q}{m} = K_F c^{\left(\frac{1}{n}\right)}$$

(2.6.1.1)

Where:  $q$ is the adsorbate mass

$m$ is the adsorbent mass

$c$ is the concentration of adsorbate in solution

$K_F$ is the Freundlich distribution coefficient [48]

$n$ is the Freundlich adsorption intensity constant [48]

Although this isotherm is originally empirical in nature, the isotherm is now interpreted as adsorption to heterogeneous surfaces, and gives an expression that defines the surface heterogeneity and exponential distribution of active sites and their energies [49, 50].

The model assumes that stronger binding sites are occupied by the adsorbate first, and that the strength of adsorption decreases as the fraction of occupied sites increases [51].

One of the limitations of the Freundlich isotherm is its inability to predict an adsorption maximum. The distribution coefficient, $K$, implies that the energy of adsorption is independent of surface coverage of the adsorbent, for homogeneous surfaces [52].

### 2.6.2 Langmuir Isotherm

The Langmuir isotherm is the simplest theoretical model for monolayer adsorption [33].

The model works under four basic assumptions:

1. Molecules are adsorbed at a fixed number of well-defined, localised sites

2. Each site holds one adsorbate molecule

3. All sites are energetically equivalent

4. There is no interaction between molecules adsorbed on neighbouring sites

A simplified derivation of the isotherm, based on kinetic principles, is outlined in equations 2.6.2.1 to 2.6.2.9.

The rate of adsorption is simply:

$$k_a c (1 - \theta) \tag{2.6.2.1}$$

With:

$$\theta = \frac{q}{q_s} \tag{2.6.2.1.1}$$

Where:     $k_a$ is the adsorption rate constant

        $c$ is the concentration of adsorbate in solution

        $\theta$ is the fractional coverage

        $q$ is the adsorbate mass

        $q_s$ is the saturation adsorbate mass

The rate of desorption is:

$$k_d \theta \tag{2.6.2.2}$$

Where:     $k_d$ is the desorption rate constant

At equilibrium, adsorption and desorption rates are equal:

$$\frac{\theta}{1 - \theta} = \frac{k_a}{k_d} c = K_L c \tag{2.6.2.3}$$

Where:     $K_L$ is the Langmuir adsorption equilibrium constant

Equation 2.6.2.3 can be rearranged to the form:

$$\theta = \frac{q}{q_s} = \frac{K_L c}{1 + K_L c}$$

(2.6.2.4)

This form of the expression clearly shows the asymptotic behaviour of the Langmuir monolayer adsorption, where, as $c \to \infty$, $q \to q_s$ and $\theta \to 1$.

At lower adsorbate concentrations, the linear adsorption behaviour, given by a variation of Henry's law [53] for adsorption from solution is observed:

$$\lim_{c \to 0} \left(\frac{q}{c}\right) = K_L q_s = K'$$

(2.6.2.5)

Where:     $K'$ is the Henry adsorption coefficient

The saturation adsorbent mass, $q_s$, represents a fixed number of adsorption sites (from assumption 1 given above), and is therefore a temperature independent constant.

The equilibrium constant however, has a temperature dependence which follows the van 't Hoff equation [54], shown below:

$$K_L = K_{L,0} exp\left(\frac{-\Delta H_0}{RT}\right)$$

(2.6.2.6)

Where:     $K_{L,0}$ is the limiting adsorption equilibrium constant

$\Delta H_0$ is the limiting heat of adsorption

$R$ is the ideal gas constant

$T$ is the temperature

Due to the exothermic nature of adsorption (i.e. $\Delta H$ is negative), $b$ should decrease with increasing temperature.

From the assumption of no interaction between adsorbed species at different sites, it is implied that the heat of adsorption is independent of adsorbent surface coverage.

By taking the derivative of equation 2.6.2.3, and using the Clausius-Clapeyron equation [55, 56], it can therefore be seen that the isosteric heat of adsorption ($-\Delta H_s$) is the same as the limiting heat of sorption ($-\Delta H_0$), shown in equation 2.6.2.7.

$$\left(\frac{\partial \ln c}{\partial T}\right)_q = \frac{\Delta H_s}{RT^2} = \frac{d \ln K_L}{dT} = \frac{d \ln K'}{dT} = \frac{\Delta H_0}{RT^2} \qquad (2.6.2.7)$$

Common ways to fit experimental data to Langmuir models involve plotting either $\frac{c}{q}$ against $c$ or $\frac{1}{q}$ against $\frac{1}{c}$ and rearranging equation 2.6.2.4 to equations 2.6.2.8 or 2.6.2.9.

$$\frac{c}{q} = \frac{1}{K_L q_s} + \frac{c}{q_s} \qquad (2.6.2.8)$$

*or*

$$\frac{1}{q} = \frac{1}{q_s} + \frac{1}{K_L q_s}\left(\frac{1}{c}\right) \qquad (2.6.2.9)$$

## 2.6.3  Prausnitz-Radke Isotherm

The Prausnitz-Radke isotherm is a type I isotherm model developed in 1972 [57].

The model takes the form shown in equation 2.6.3.1.

$$q = \frac{ac}{1 + bc^\beta} \qquad (2.6.3.1)$$

Where:    $q$ is the adsorbate mass

$c$ is the concentration of adsorbate in solution

$a$ and $b$ are Prausnitz-Radke model constants

$\beta$ is the Prausnitz-Radke model exponent

The model parameters $a$, $b$ and $\beta$ are obtained by a non-linear statistical fit to experimental data [58].

The Prausnitz-Radke model has several important properties making it suitable for many adsorption systems:

- At low adsorbate concentrations, this isotherm reduces to a linear form

- At high adsorbate concentrations, it becomes the Freundlich isotherm

- In the special case where the model parameter $b$ is one, the isotherm becomes the Langmuir isotherm

The model is in particular preferred for adsorptive systems with low adsorbate concentrations [49], and gives a good fit for many type I isotherms over a wide concentration range. Therefore, it is often preferred to other type I isotherm models such as Langmuir or Freundlich [59].

## 2.7 Adsorption Mass Transport

The mass transport mechanisms that determine the kinetics in adsorption processes such as the fixed bed adsorption columns used by CdA can be divided into two primary types:

1. Intra-particle transport mechanisms

2. Extra-particle transport and dispersion mechanisms

### 2.7.1 Intra-Particle Transport

Since there is a negligible amount of bulk flow occurring through adsorbent pores, intra-particle transport is considered a diffusive process defined by Fick's first law [60], given in equation 2.7.1.1.

$$J = -\mathcal{D}(c)\frac{\partial c}{\partial x} \tag{2.7.1.1}$$

Where:       $J$ is the adsorbate diffusion flux

$\mathcal{D}$ is the diffusivity of the adsorbate

$c$ is the concentration of adsorbate in solution

$x$ is the position of the adsorbate

In general, intra-particle diffusion may occur by several different mechanisms depending on the adsorbent pore size, adsorbate concentration and other conditions specific to the adsorption system [61].

### 2.7.1.1     *Macro-pore Diffusion*

Macro-pore diffusion involves the diffusion transport of adsorbate species into pores large enough such that the adsorbate is unaffected by any effects from electrostatic or dispersion-repulsion force fields on the surface of the adsorbent [61]. Therefore, the driving force of diffusion is the concentration gradient of diffusing adsorbate species.

The diffusion flux in macro-pore diffusion can be expressed in terms of the pore diffusion coefficient (diffusivity), $\mathcal{D}_{pi}$:

$$J_i = -\varepsilon_p \mathcal{D}_{pi} \frac{\partial c_{pi}}{\partial r} \qquad (2.7.1.1.1)$$

Where:       $J_i$ is the adsorbate diffusion flux for species $i$

$\varepsilon_p$ is the adsorbent pore void fraction

$\mathcal{D}_{pi}$ is the pore diffusivity

$c_{pi}$ is the pore concentration of adsorbate species $i$

$r$ is the adsorbent pore radius

Due to the non-ideal shape of pores in BC, the real diffusion coefficient is smaller than the diffusivity in a straight, ideal, cylindrical pore ($\mathcal{D}_i$). This is accounted for by including a correction factor, tortuosity ($\tau_p$).

$\tau_p$ can be estimated when enough information about the pore structure, size and shape distribution is known. This data can obtained through adsorbent characterisation methods [62].

Other equations have been proposed in literature for estimating the tortuosity factor [63-65]:

$$\tau_p = \frac{\left(2 - \varepsilon_p\right)^2}{\varepsilon_p} \qquad (2.7.1.1.2)$$

$$\tau_p = \frac{1}{\varepsilon_p} \qquad (2.7.1.1.3)$$

$$\tau_p = \varepsilon_p + 1.5\left(1 - \varepsilon_p\right) \qquad (2.7.1.1.4)$$

Where:       $\tau_p$ is the tortuosity of the adsorbent pore

Special cases of macro-pore diffusion may occur, such as Knusden diffusion in low-pressure gas-phase diffusion, where the molecular mean free path length may be greater than the pore diameter [66]. Another special case is the liquid phase diffusion of large adsorbate molecules, where the ratio of molecular to pore diameter is significantly greater than zero; in which case diffusivity is hindered by steric interferences with the pore wall as well as hydrodynamic resistance [67]. These processes however do not occur in the case of fluoride adsorption by BC and will therefore not be discussed in this report.

### 2.7.1.2 *Surface Diffusion*

Surface diffusion occurs in micro- and meso-porous regions, in which the adsorbate is unable to escape the force field experienced at the adsorbent surface. Adsorbate species therefore 'jump' between adsorbent fixed sites. The driving force in this case is approximated by the concentration gradient of the adsorbate in its adsorbed state [61].

The diffusion flux in the case of surface diffusion is given in equation 2.7.1.2.1.

$$J_i = -\rho_p \mathcal{D}_{sur,i} \frac{\partial n_i}{\partial r} \qquad (2.7.1.2.1)$$

Where:     $\rho_p$ is the pore density

$\mathcal{D}_{sur,i}$ is the surface diffusivity

$n_i$ is the number of moles of adsorbate species $i$

The surface diffusion flux is generally much smaller than the pore diffusion flux, however, the concentration of adsorbed species is often far greater [61].

In diffusion involving the electrostatic interactions between charged ionic adsorbent surfaces and ionic adsorbate species, such as the surface diffusion of fluoride ions along a positively charged BC surface, this diffusion is further complicated by electrical coupling effects. These electrostatic effects on ionic diffusion are accounted for through the Nernst-Planck equations [68], where in a system containing $M$ counterions, the surface flux is expressed as:

$$J_i = -\rho_p \frac{1}{z_i} \sum_{J=1}^{M-1} \overline{\mathcal{D}}_{i,j} \frac{\partial z_j n_j}{\partial r} \qquad (2.7.1.2.2)$$

With:

$$\overline{\mathcal{D}}_{i,j} = -\frac{\overline{\mathcal{D}}_i (\overline{\mathcal{D}}_j - \overline{\mathcal{D}}_M) z_i^2 n_i}{\sum_{k=1}^{M} \overline{\mathcal{D}}_k z_k^2 n_k} \qquad (2.7.1.2.3a)$$

And

$$\overline{\mathcal{D}}_{i,i} = -\frac{\overline{\mathcal{D}}_i (\overline{\mathcal{D}}_i - \overline{\mathcal{D}}_M) z_i^2 n_i}{\sum_{k=1}^{M} \overline{\mathcal{D}}_k z_k^2 n_k} \qquad (2.7.1.2.3b)$$

Where:      $z_i$ is the charge of ionic species $i$

                 $\overline{\mathcal{D}}_i$ is the ionic self-diffusivity of species $i$

## 2.7.2 Extra-Particle Mass Transport

The external mass transfer occurring outside of the adsorbent pores is described by a mass transfer coefficient, $k_f$.

The adsorbate flux at the adsorbent particle surface therefore becomes:

$$N = k_f (c - c_{sur}) \qquad (2.7.2.1)$$

Where:      $N$ is the adsorbate flux at the adsorbent particle surface

                 $k_f$ is the mass transfer coefficient

                 $c_{sur}$ is the concentration of the adsorbate at the outer surface of the adsorbent

The mass transfer coefficient is estimated from correlations involving the Sherwood and Schmidt numbers:

$$Sh = \frac{k_f d_p}{\mathcal{D}} \tag{2.7.2.2}$$

Where:     $Sh$ is the Sherwood number

$d_p$ is the adsorbent particle diameter

$\mathcal{D}$ is the adsorbate diffusivity

$$Sc = \frac{\upsilon}{\mathcal{D}} \tag{2.7.2.3}$$

Where:     $Sc$ is the Schmidt number

$\upsilon$ is the viscous diffusion rate

Several empirical correlations have been proposed for packed columns, based on the Reynolds number of the liquid flowing through these [65, 69, 70]:

$$Sh = 1.85 \left(\frac{1-\varepsilon}{\varepsilon}\right)^{0.33} Re^{0.33} Sc^{0.33} \; for \; Re < 40 \tag{2.7.2.4}$$

$$Sh = \frac{1.09}{\varepsilon} Re^{0.33} Sc^{0.33} \; for \; 0.0015 < Re < 55 \tag{2.7.2.5}$$

$$Sh = \frac{0.25}{\varepsilon} Re^{0.69} Sc^{0.33} \; for \; 55 < Re < 1050 \tag{2.7.2.6}$$

Where:     $Re$ is the Reynolds number

## 2.8   Adsorption Kinetics

There are two approaches to kinetic modelling of adsorption from solution: diffusional modelling, where diffusion is considered the rate-limiting step, and kinetic modelling, which works under the assumption that surface adsorption and desorption is rate-limiting [50, 71].

Adsorption and desorption rates in porous adsorbents are often controlled by the rates of diffusion of adsorbate species within the porous network rather than the adsorption kinetics at the surface of the adsorbent, with exception of certain chemisorption processes, where the kinetics of bond formation may be rate limiting.

In the case of microporous adsorbents such as BC, there is negligible bulk flow through macro-pores [33]. There is also no evidence of chemisorption of fluoride to the surface of the char [35].

## 2.8.1 Diffusional Adsorption Model

The overall adsorption rate of fluoride on an adsorbent using the diffusional adsorption model is assumed to take place by a mechanism consisting of three consecutive steps [72]:

1. External mass transport

2. Intra-particle diffusion

3. Adsorption rate on a site inside the pores

The diffusional model assumes that intra-particle diffusion is exclusively due to diffusion in the adsorbent pore volume (i.e. Fick diffusion), and that the rate of adsorption on an active site is instantaneous.

A mass balance of the adsorbate in solution for batch adsorption yields:

$$V\frac{dc}{dt} = -mS_A k_f(c - c_{sur}) \qquad (2.8.1.1)$$

Where:     $S_A$ is the outer surface area of the adsorbent particle

$c_{sur}$ is the concentration of the adsorbate at the outer surface of the adsorbent

By taking a mass balance of the adsorbate on a differential volume of a spherical adsorbent particle, the partial differential shown in equation 2.8.1.2 is obtained.

$$\varepsilon_p \frac{\partial c_r}{\partial t} + \rho_p \frac{\partial q}{\partial t} = \frac{1}{r^2}\frac{\partial}{\partial r}\left[r^2\left(\mathcal{D}_p \frac{\partial c_r}{\partial r}\right)\right] \qquad (2.8.1.2)$$

Where:     $c_r$ is the concentration of adsorbate in the pore volume at a distance $r$

$\mathcal{D}_p$ is the effective pore volume diffusivity

$r$ is the distance in the radial direction of the adsorbate from the adsorbent surface

The two terms on the left of equation 2.8.2.1 represent the accumulation of adsorbate in the adsorbent pore volume and pore surface. The term on the right represents the adsorbent pore volume diffusion.

Introducing the following initial and boundary conditions enables a mathematical relationship between $c_r$ and $q$ to be obtained in the form $q = f(c_r)$:

$$c_r = 0 \; at \; t = 0, 0 \leq r \leq R \tag{2.8.1.2a}$$

$$\left. \frac{\partial c_r}{\partial r} \right|_{r=0} = 0 \tag{2.8.1.2b}$$

$$\mathcal{D}_p \left. \frac{\partial c_r}{\partial r} \right|_{r=R} = k_f(c - c_s) \tag{2.8.1.2c}$$

Local equilibrium exists between the adsorbate in the pore volume and that adsorbed on the pore surface, since it is assumed that the adsorption rate occurs instantaneously [72].

## 2.8.2  Kinetic Adsorption Model

An overall mass balance on the adsorbate yields equation 2.8.2.1.

$$m \frac{dq}{dt} + V \frac{dc}{dt} = 0 \tag{2.8.2.1}$$

Where:  $m$ is the adsorbent mass

$q$ is the adsorbate mass

$V$ is the solution volume

$c$ is the concentration of adsorbate in solution

$t$ is the time

The equation obtained has no concentration gradients of adsorbate species. Therefore, intra-particle diffusion and external mass transport is neglected, since they are assumed much faster than the adsorption rate at the surface of the adsorbent.

### 2.8.2.1 First-order kinetics

By setting boundary conditions $q = 0$ at $t = 0$, equation 2.8.2.1.1 can be integrated to yield:

$$q = \frac{V(c_0 - c)}{m}$$

(2.8.2.1.1)

Where:    $c_0$ is the initial concentration of adsorbate in solution

Taking the first-order adsorption rate expressed in equation 2.8.2.1.2:

$$\frac{dq}{dt} = k_1(q_e - q)$$

(2.8.2.1.2)

Where:    $k_1$ is the first-order rate constant

$q_e$ is the adsorbate mass at equilibrium

This can be integrated, using the same initial conditions shown above, to yield:

$$q = q_e(1 - e^{-k_1 t})$$

(2.8.2.1.3)

Using equation 2.8.2.1.1, equation 2.8.2.1.3 can be expressed in terms of $c$ and $c_e$ [33]:

$$c = c_e + (c_0 - c_e)e^{-k_1 t}$$

(2.8.2.1.4)

### 2.8.2.2 Second-order kinetics

The adsorption rate of a second-order reaction is represented by the following reaction [73]:

$$\frac{dq}{dt} = k_2(q_e - q)^2$$

(2.8.2.2.1)

Where:    $k_2$ is the second-order rate constant

Integrating this results in equation 2.8.2.2.2.

$$\frac{1}{(q_e - q)} - \frac{1}{q_e} = k_2 t$$

(2.8.2.2.2)

This relationship can again be expressed in terms of $c$ and $c_e$, similarly to the first-order rate equation [33]:

$$c = c_0 - \left(\frac{m}{V}\right) \frac{k_2[(V/m)(c_0 - c_e)]^2 t}{(1 + k_2[(V/m)(c_0 - c_e)]t)} \tag{2.8.2.2.3}$$

### 2.8.2.3    $n^{th}$-order kinetics

The $n^{th}$-order adsorption rate is similar to second-order kinetic rate equation, given in equation 2.8.2.2.1, and takes the form:

$$\frac{dq}{dt} = k_n(q_e - q)^n \tag{2.8.2.3.1}$$

Where:      $k_n$ is the $n^{th}$-order rate constant

When written in terms of $c$ and $c_e$, this yields:

$$\frac{dc}{dt} = -k'_n(c - c_e)^n \tag{2.8.2.3.2a}$$

Where the relationship between $k_n$ and $k'_n$ is:

$$k'_n = \left(\frac{V}{m}\right)^{n-1} k_n \tag{2.8.2.3.2b}$$

Adsorption reaction rate constants can therefore be determined from experimental data [33].

## 2.9    Adsorption Systems

Due to the finite adsorption capacity of adsorbents, any interactions during an adsorption process will eventually lead to a thermodynamic equilibrium between the adsorbent and adsorbate phases [74]. At equilibrium, the net loading of adsorbent cannot increase due to adsorption and desorption rates becoming equal. For further adsorption to occur, the adsorbent species must be regenerated or replaced.

There exist multiple systems for adsorption to be studied or applied. The systems discussed in this section will involve those that were used during the project or are in use by CdA.

### 2.9.1 Batch Adsorption

The basic conservation equation for batch adsorption is expressed below [75]:

$$c_0 V - cV + qm \qquad (2.9.1.1)$$

Where: $c_0$ is the initial adsorbate concentration in solution

$V$ is the volume of solution in the batch system

$c$ is the adsorbate concentration in solution

$q$ is the adsorbate mass

$m$ is the adsorbent mass

Batch adsorption is often used to characterise the performance, adsorption mechanisms and kinetics of various adsorbents [76]. Various parameters such as pH, temperature and solution composition can be easily adjusted in experiments to determine their effects on adsorption capacity. For adsorption for water treatment, batch systems are very useful for studying various adsorption systems and determining their properties and behaviours, making these important in an analytical context. However, these systems are impractical for field water treatment applications and are seldom used at the field scale.

### 2.9.2 Fixed Bed Columns

In most applied adsorption processes, the adsorbent is in contact with the liquid phase in a packed column.

#### *2.9.2.1  Material Balance*

At the microscale, the adsorbate species exists at three locations [33]:

1.  In the adsorbed phase

2.  Inside the pore fluid

3.  In the fluid outside of particles

Therefore, material balances involve the number of adsorbate moles $(n)$, the intra-particle adsorbate concentration $(c_p)$ and the extra-particle (solution) concentration, $(c)$.

The material balance for a fixed-bed process therefore takes the following form, given in equation 2.9.2.1.1 [61].

$$\rho_b \frac{\partial \hat{n}}{\partial t} + \varepsilon \frac{\partial c}{\partial t} + \varepsilon \frac{\partial (vc)}{\partial z} = \varepsilon D_L \frac{\partial}{\partial z}\left(c \frac{\partial y}{\partial z}\right) \qquad (2.9.2.1.1)$$

With:

$$\hat{n} = \bar{n} + \left(\frac{\varepsilon_i}{\rho_i}\right)\bar{c}_p = \bar{n} + \left[(1 - \varepsilon_b)\frac{\varepsilon_i}{\rho_b}\right]\bar{c}_p \qquad (2.9.2.1.1a)$$

Where: $\rho_b$ is the bulk solution density

$t$ is the time

$\varepsilon$ is the packed bed void fraction

$c$ is the adsorbate concentration in solution

$v$ is the interstitial fluid velocity

$z$ is the longitudinal position in the column

$D_L$ is the Fickian axial dispersion coefficient

$y$ is the fluid phase adsorbate mole fraction

$\bar{n}$ is the number of adsorbate moles over the adsorbent particle volume

$\varepsilon_i$ is the adsorbent particle void fraction

$\rho_i$ is the adsorbent particle density

$\bar{c}_p$ is the intra-particle adsorbate concentration averaged over pore fluid volume

### 2.9.2.2    *Pressure*

Variables such as particle size, fluid velocity and bed dimensions will have an impact on process economy, due to their effect on the pressure of the system. This influences pumping costs, or in the case of gravity driven flows, the static head requirements which in turn affect the capital costs of a fixed bed column adsorption system [61].

The pressure drop in flow through a packed bed in an adsorption column can be expressed in terms of the dimensionless friction factor using the Ergun equation [77]:

$$f = \frac{\Delta P}{L} \frac{d_p}{\rho_b v_s^2} \left( \frac{\varepsilon_b^3}{1 - \varepsilon_b} \right) \qquad (2.9.2.2.1)$$

Where:       $\Delta P$ is the pressure drop across the column

$L$ is the packed bed length

$d_p$ is the spherical adsorbent particle diameter

$\rho_b$ is the bulk fluid density

$v_s$ is the superficial fluid velocity

$\varepsilon_b$ is the packed bed void fraction

Several correlations exist to determine the friction factor, notably [77, 78]:

$$f = \frac{805}{Re} \; for \; Re < 40 \qquad (2.9.2.2.1a)$$

$$f = \frac{38}{Re^{0.15}} \; for \; Re > 40 \qquad (2.9.2.2.1b)$$

Where:       $Re$ is the Reynolds number

And:

$$f = \frac{150}{Gr_p} + 1.75 \qquad (2.9.2.2.1c)$$

With:

$$Gr_p = \frac{\rho_b v_s d_p}{(1 - \varepsilon)\mu} \qquad (2.9.2.2.1d)$$

Where:       $Gr_p$ is the modified Reynolds number

$\mu$ is the fluid viscosity

### 2.9.2.3 Axial Dispersion

Fluids passing through packed beds have a tendency to axially disperse, i.e. mix along the length of the column [61]. Axial dispersion is an undesirable behaviour that reduces separation efficiency.

The axially dispersed plug flow model is represented in equation 2.9.2.3.1.

$$-D_L \frac{\partial^2 c}{\partial z^2} + \frac{\partial}{\partial z}(v_s c) + \frac{\partial c}{\partial t} + \left(\frac{1-\varepsilon}{\varepsilon}\right)\frac{\partial q}{\partial t} = 0 \qquad (2.9.2.3.1)$$

Where:        $q$ is the adsorbate mass

The effects of the various mechanisms contributing to this axial mixing effect are collected together and represented under the single axial dispersion coefficient, $D_L$. There are however many cases where axial dispersion may be neglected when modelling the flow behaviour through a packed bed, in which case ideal plug flow is assumed [33].

### 2.9.2.4 Fixed Bed Transitions

Fixed bed transitions involve modelling the concentration profile of the adsorbate solution passing through the bed [61]. These enable the prediction of system behaviours such as the number of bed volumes that can be passed through a fixed bed column before breakthrough (the point at which the treatment objective is no longer met). There exist various methods for the analysis of fixed-bed transitions.

Local equilibrium theory bases itself on the stoichiometry and nonlinearities of a system – transitions can therefore be simple wave (i.e. gradual), shock (abrupt) transitions, or a combination of these. Local equilibrium theory however omits mass-transfer resistance. The asymptotic behaviour of transitions that are under the influence of mass-transfer resistances are shown in figure 2.9.2.4.1.
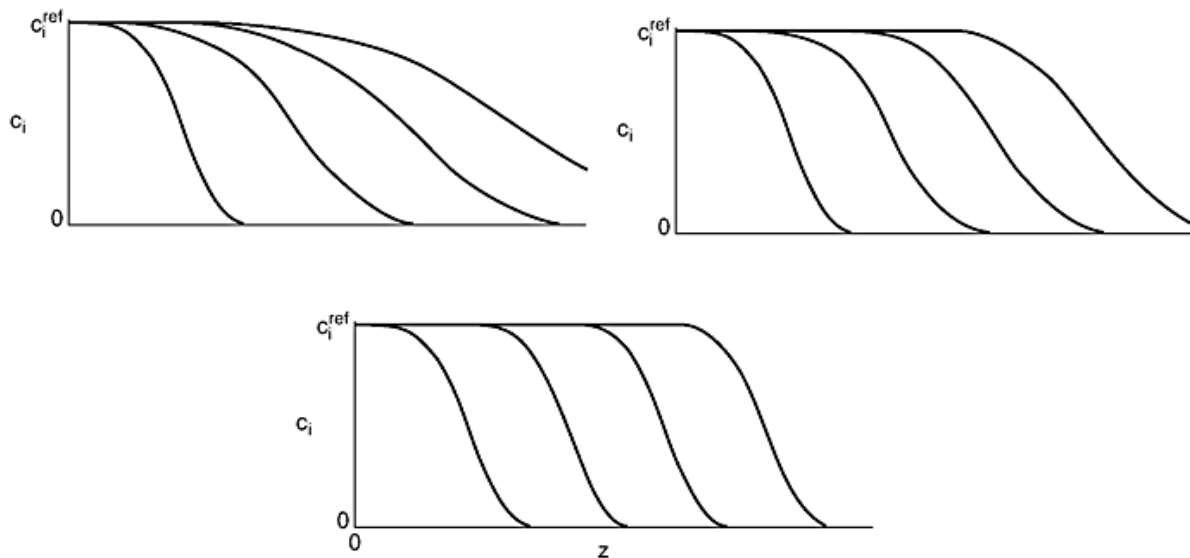
Figure 2.9.2.4.1 - Top left: unfavourable isotherm transition behaviour. Top right: square root spreading for linear isotherm. Bottom: favourable isotherm constant spreading behaviour. [79]

The transition waves represented in figure 2.9.4.1 show the change in concentration of adsorbate from feed concentration to outlet concentration as a function of the bed length. The unfavourable isotherm transition width becomes proportional to the bed depth passed through. The linear isotherm transition width becomes proportional to the square root of the bed depth. The favourable isotherm transition width approaches a constant, also known as the constant pattern [61].

The mass transfer zone (MTZ) resembles a constant pattern, the length of which, alongside stoichiometry, can be used to determine how long a bed can be used before breakthrough. Upstream of the MTZ, the adsorbent is in equilibrium with the feed. Downstream, the adsorbent is at initial state. Within the MTZ, the fluid phase adsorbate concentration drops from feed levels to column outlet concentrations. Equilibrium with the feed is not attained in the MTZ. Due to the fact that adsorption beds are typically removed shortly after breakthrough, the full bed capacity is not utilised. This is shown on the graphs in figure 2.9.2.4.2.
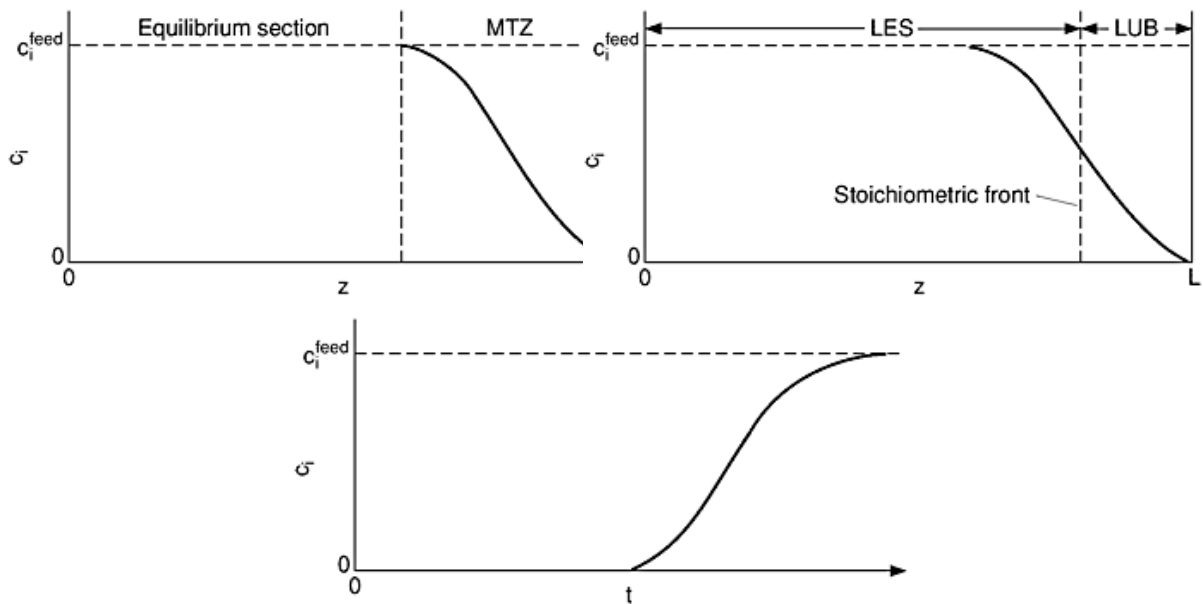
Figure 2.9.2.4.2 - Top left: bed profile showing the MTZ and equilibrium section at breakthrough. Top right: bed profile showing the length of the equilibrium section and the length of the equivalent unused bed. Bottom: breakthrough curve. [61]

It can be seen from figure 2.9.2.4.2 that the greater the width of the MTZ, the greater the length of the equivalent unused bed (LUB). The LUB and the length of the equivalent equilibrium section (LES) divide the MTZ in equal parts, with the stoichiometric (equilibrium) front dividing the two. The effluent concentration profile against time is known as the breakthrough curve.

The effluent adsorbate concentration will remain at essentially zero until the MTZ reaches the outlet, at which point the adsorbate concentration will rise until eventually reaching initial inlet concentrations. Before the effluent reaches inlet concentrations, it will have passed the treatment objective, the time of this known as the breakthrough time. After breakthrough, the adsorbent must either be replaced or regenerated [61].

## 2.9.3 Lead-Lag Column Systems

It has been suggested that single columns are a viable option for adsorption systems if the MTZ is short, and the single column length is 3 - 5 times longer than the MTZ [80, 81]. However, despite having a lower capital cost, a single column is likely to have the highest adsorbent replacement cost [82].

There exist various column configurations that can be used when the MTZ is too long, or the adsorbent costs are high enough to justify the capital costs of adding extra columns. These include lead-lag, parallel column, and configurations which could also include a bypass line system. Previous research undertaken by CdA has shown that lead-lag systems reduce bone-char use rates more greatly than staged-parallel configurations (46 % reduction as opposed to 29 %) [83].

Bypass lines are also inappropriate for fluoride removal applications for drinking water, due to the requirement that all water be treated. Therefore, only lead-lag systems will be discussed in this section.

Lead-lag systems comprise two adsorption columns: a lead and a lag. Water flows first through the lead and then through the lag, allowing the MTZ to pass through the configuration. When the effluent target is reached, column positions are changed, so the lag becomes the lead. Exhausted adsorbent from the previous lead column is changed out with fresh adsorbent and placed in the lag position, allowing the process to be continued.

A diagram showing this process is shown in figure 2.9.3.1.

Lead-lag systems are preferred when the breakthrough curve is gradual and a low effluent to inlet concentration ratio ($c/c_0$) is required. It has been suggested that lead-lag systems are appropriate when $c/c_0 \leq 0.05$ and when the MTZ can be contained in one column [80]. Lead-lag systems typically achieve higher fractional utilisation than parallel columns and therefore may be preferred if economics make it essential to use as much of the adsorbent as possible.

Fresh adsorbent

Mass transfer zone

Saturated adsorbent

moved into lead position    Char replaced

BT    TO reached

BT    TO reached

moved into lead position    Char replaced

Abbreviations:
BV = Bed volume treated
TO = Treatment objective
BT = Breakthrough

Figure 2.9.3.1 - Top: lead-lag column configuration showing MTZ front travelling through the system. Bottom: column replacement cycle. [84]

## 2.9.4  Rapid Small-Scale Column Testing (RSSCT)

Determining the breakthrough curve of an adsorbent at the pilot scale requires many weeks or even months. A rapid way to screen various adsorbents and determine their breakthrough curves in a matter of hours or days is through RSSCT - developed by Crittenden *et al.* in 1986 [85]. With an accurate RSSCT model, the pilot scale data can be represented with accuracy [86].

Advantages of RSSCT aside from shorter testing times include the lack of necessity of kinetic studies to predict the performance of a full-scale column from RSSCT, the fact that RSSCT can be performed at the laboratory bench scale, and the low sample water volume requirements.

There are several primary assumptions made in RSSCT, including [86]:

- Backwashing, which may obliterate the mass transport zone, is not be taken into consideration

- The scaling procedure is based on the dispersed-flow, pore-surface-diffusion model

- It is not possible to regenerate the adsorbent in the short duration of RSSCT time through biological activity

- The limiting factor is internal mass transfer, meaning the media should be micro-porous in nature

- Distribution of pore size is independent of the radius of the particle size

- There are no variations in the properties of the adsorbent such as the adsorption capacity, porosity and bulk density when it is crushed from complete size to minute size

- The interaction of the adsorbate species with the adsorption sites should depend on the size of the particle

Large column parameters considered for scaling purposes are listed in table 2.9.4.1 [85].

Table 2.9.4.1 - Large column parameters considered for RSSCT design

| Parameter | Symbol |
|---|---|
| Empty bed contact time | $EBCT$ |
| Hydraulic loading rate (velocity) | $v_f$ |
| Mean particle size | $d_p$ |
| Column internal diameter | $d_{in}$ |
| Bed depth (depth of adsorbent media) | $L$ |
| Flowrate | $Q$ |

There are two common RSSCT design approaches:

1. Constant diffusivity (CD)

2. Proportional diffusivity (PD)

CD assumes that intra-particle diffusivity does not depend on adsorbent particle size, whereas PD assumes that intra-particle diffusivity is directly proportional to particle size [86]. There is currently no clear superior approach to modelling pilot scale columns with either RSSCT model [87]. However, work by Badruzzaman *et al.* and Westerhoff *et al.* [88, 89] has shown that the PD model offers a better approach at modelling arsenic breakthrough in granular ferric hydroxide fixed bed contactors and was therefore selected as the approach for RSSCT modelling in this project. For this reason, only the PD model will be discussed in detail in the following section.

### 2.9.4.1 RSSCT Model

The generic RSSCT design equation is given in equation 2.9.4.1.1 [90, 91].

$$\frac{EBCT_{SC}}{EBCT_{LC}} = \left[\frac{d_{p,SC}}{d_{p,LC}}\right]^{2-X} = SF^{X-2} = \frac{t_{SC}}{t_{LC}} \qquad (2.9.4.1.1)$$

Where:

$EBCT_{SC}$ is the empty bed contact time of the small RSSCT column

$EBCT_{LC}$ is the empty bed contact time of the large pilot column

$d_{p,SC}$ is the adsorbent particle diameter in the small column

$d_{p,LC}$ is the adsorbent particle diameter in the large column

$X$ is the diffusivity factor

$SF$ is the scaling factor

$t_{SC}$ is the operation time of the small column

$t_{LC}$ is the operation time of the large column

In the CD model, the diffusivity factor, $(X)$ is 0. In the PD model, the diffusivity factor is 1. The scaling factor (SF) can then be determined from the relative particle diameters of the large and small columns [90, 91]:

$$SF = \frac{d_{p,LC}}{d_{p,SC}} = \frac{v_{f,SC}}{v_{f,LC}} \qquad (2.9.4.1.2)$$

Where:

$v_{f,SC}$ is the hydraulic loading rate of the small column

$v_{f,LC}$ is the hydraulic loading rate of the large column

From this, the scaled required hydraulic loading rate is found for the small column, which enables the calculation of the various dimensionless parameters used in mass transfer models for column design.

The column bed depth can be determined [90, 91]:

$$L_{SC} = v_{f,SC} \times EBCT_{SC} \qquad (2.9.4.1.3)$$

Where:

$L_{SC}$ is the bed depth of the small column

The bed depth is used to determine the RSSCT design flow rate by dividing the hydraulic loading rate by the by EBCT.

It should be noted that columns with low loading rates (i.e. large EBCTs and small Reynolds numbers) are prone to axial dispersion, where the adsorbate diffuses axially along the length of the column.

Westerhoff *et al.* [89] have shown that if $Re \times Sc > 200$, dispersion may be neglected from mass transfer models, and the flow through the column may be assumed as ideal plug flow, as explained in section 2.9.2.3.

## 3.0   Literature Review

This section will discuss work and research that has been undertaken into the adsorption of fluoride from solution with BC, as well as the production and characterisation of BC. The state of the art research into chemical treatment methods for BC fluoride adsorption capacity optimisation is also discussed.

### 3.1   Bone Char Production

Various methods for the production of BC have been proposed and implemented throughout literature [83, 84, 92-97]. Typically, cattle bone is used to produce BC, although BC produced from other species (such as fish [98]) has been investigated.

Cattle bone samples may crushed to bone powder prior to pyrolysis, however this technique is primarily used for laboratory experiments [93, 94]. A more practical method for BC production, suited to larger-scale production for use in full-size column systems, involves the pyrolysis of raw cattle bone followed by crushing, due to the weakened mechanical strength of the char, which may then be crushed manually, without the need for automated crushing equipment [83, 84].

Bone pyrolysis temperatures vary from 350 °C [92, 95] to 600 °C [83, 84, 94], as it has been found that continuous pyrolysis temperatures exceeding 600 °C decreases the surface area and pore volume of the BC, therefore decreasing the fluoride adsorption capacity of the char [93].

### 3.1.1 Caminos de Agua Bone Char Production

The production method for BC used by CdA is outlined step-by-step in this section:

1. BC is produced locally by CdA using cattle bones purchased from local butchers and abattoirs

2. The bones are purchased pre-cut into large chunks (approximately 10 cm in diameter) and are placed into a 30 L retort (CdA has previously experimented with using 19 L retorts, however it was found that a 30 L retort could produce a larger amount of BC per burn without affecting the quality of char produced)

3. The 30 L retort is then placed on top of a larger, 200 L retort, filled with biomass, which serves as the combustion fuel. CdA currently uses wooden pellets as combustion fuel – a side product of the local wood production industry. These wooden pellets are pyrolysed into biochar

4. Another 200 L retort with chimney is then placed on rails over the 30 L retort to serve as the combustion zone - both the lower and upper retorts serve as primary and secondary air intakes respectively

5. The primary air intake is created by drilling several holes in the bottom of retort

6. The second, smaller intake is formed by raising the combustion chamber on rails

7. The combustion fuel is then set on fire and allowed to burn from the top-down, creating a modified version of a top-lit-updraft (TLUD), known as a TLUD-K (based on designs by Kearns [99]), which does not limit the primary air intake as much as a typical TLUD

8. The pyrolysis gases rise to the upper combustion chamber and combust, creating a secondary pyrolysis reaction in the 30 L bone retort, using the excess energy produced from the pyrolysation of the wooden pellets into biochar

9. Temperatures in the combustion chamber are kept between 400-600 °C for a minimum of 1.5 hours, to achieve this, two 200 L biomass retorts are combusted consecutively [84, 100]

10. Pyrolysed BC chunks are then ground into smaller particles and sieved to standard US standard mesh size # 8 x # 30 (0.60 mm < x < 2.36 mm).

Figure 3.1.1.1 depicts the cross section of the TLUD-K gasifier.
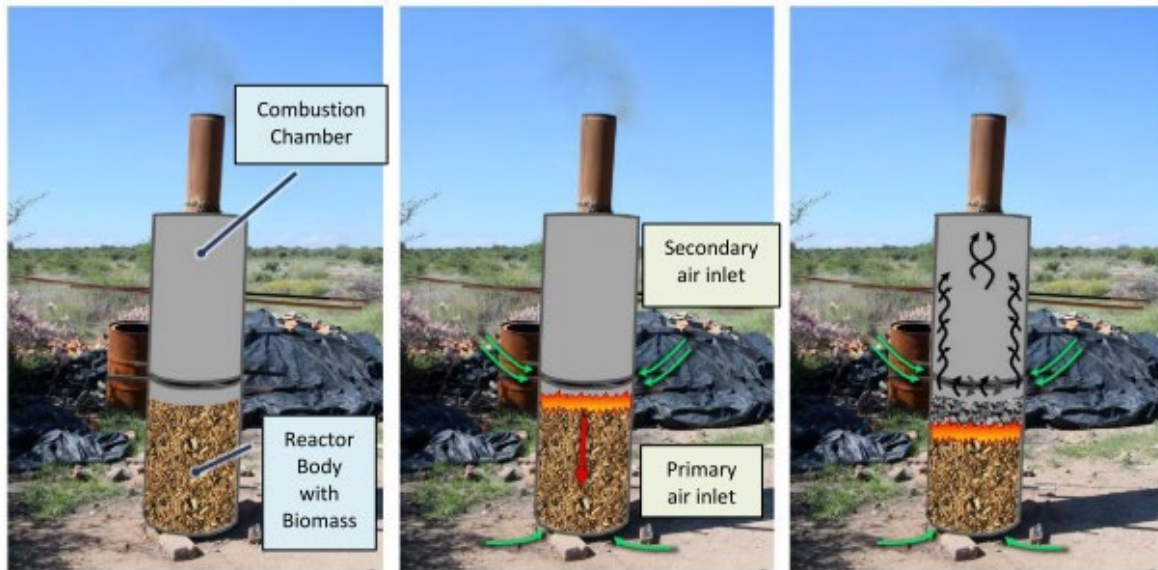


Figure 3.1.1.1 - Cross-section of the TLUD-K gasifier which produces BC [100]

## 3.2 Bone Char Characterisation

### 3.2.1 Morphology and Structure

The morphology and structure of BC has been extensively studied by most authors investigating the adsorption properties of this [36, 95, 101]. BC particles analysed using scanning electron microscopy (SEM) show that these particles are very irregular, with fractured, rough and porous surfaces. BC particles also do not have a uniform particle size distribution. Figure 3.2.1.1 shows the irregular structure of a typical BC particle using SEM.
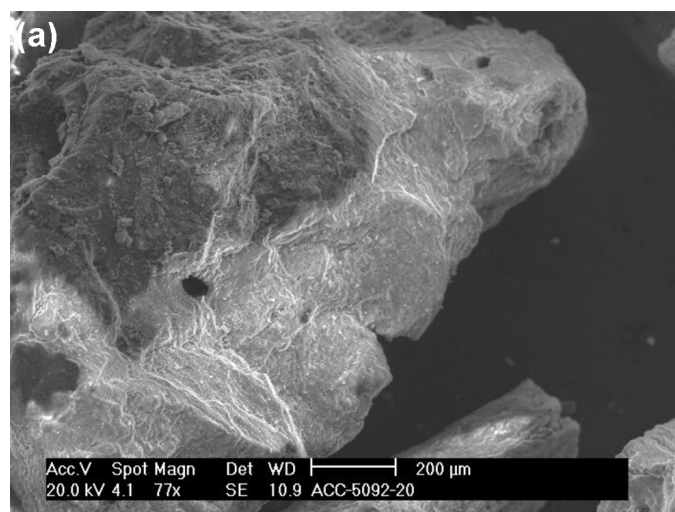


Figure 3.2.1.1 - SEM image of a BC particle [36]

43

### 3.2.2 Chemical Composition

X-ray diffraction (XRD) analysis of BC shows patterns largely consistent with the standard patterns of crystalline hydroxyapatite (HAP), indicating that BC is primarily composed of HAP, albeit with slightly less intense peaks in the case of BC.
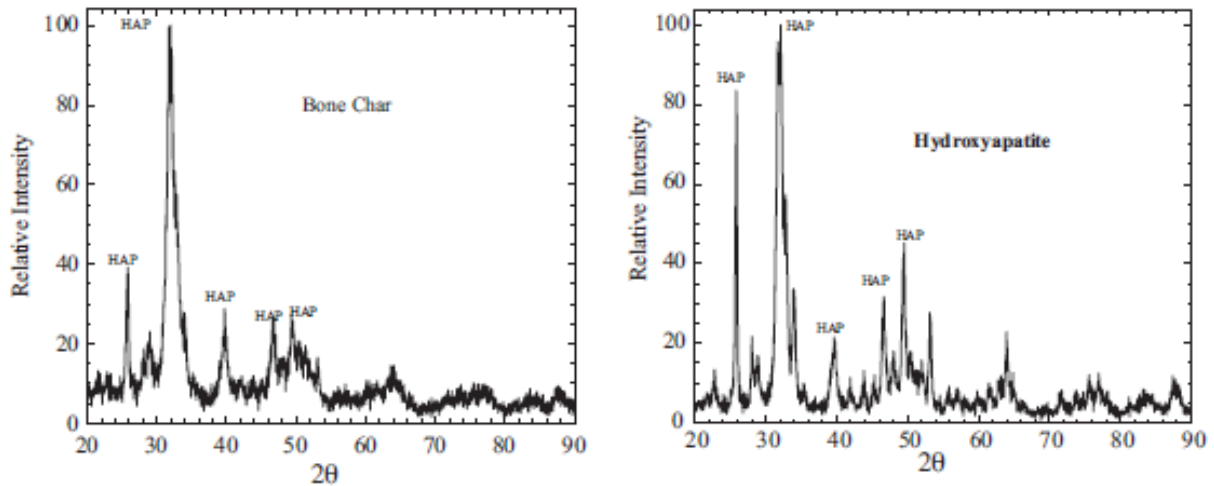


Figure 3.2.2 - Left: XRD spectrum of BC. Right: XRD spectrum of HAP (JCPDS card # 82-1943 (Joint Committee on Powder Diffraction Standard). [95]

The elemental analysis of BC shows that carbon content varies between 6 % [36, 102] and 11 % [35], with the remaining components being primarily calcite ($CaCO_3$) and HAP (76 % [36, 103] to 85 % [35]).

HAP is a mineral form of the calcium apatite crystal, with a unit cell consisting of $Ca_{10}(PO_4)_6(OH)_2$ [104].

### 3.2.3 Textural Properties

The nitrogen physisorption BET (Brunauer–Emmett–Teller) method is often used to determine the BET surface area of BC [36, 101, 105, 106].

Reported BET surface areas vary from 58 $m^2$/g [101] to as much as 104 $m^2$/g, reported by Medellin-Castillo *et al.* [36]. The authors suggest that the higher values of CB surface area compared to typical values for HAP reported in literature (45 $m^2$/g to 54.2 $m^2$/g) are due to the presence of carbon found in BC from organic materials still present in this.

$N_2$ adsorption isotherms on BC are of type IV and characteristic of meso-porous solids [107].

Reported pore sizes range between 7.5 nm [106] to 11.1 nm [36], and pore volumes from 0.1 $cm^3$/g [36] to 0.3 $cm^3$/g [101, 105, 106], corresponding to a meso-pore (2 nm - 50 nm) [108] content between 70 % and 80 %, with the rest of BC pores being microporous (< 2 nm) by nature [108].

### 3.2.4 Point of Zero Charge (PZC)

The PZC of BC can be determined by a titration method, first proposed by Babic *et al.* [109] where two KCl – KOH solutions, one containing BC and one without, are titrated by addition of HCl, and the changing solution volumes and pH are recorded. The intersection of the two solution pH curves represents the PZC of BC.

PZC values of BC are reported as varying from pH 7.6 [101, 106] to pH 8.4 [35, 36]. These values are slightly greater than the naturally occurring pH of waters in the Guanajuato region, which are reported to being in the range of pH 7.3 - pH 7.8 [10, 41, 42]. This means that typical BC samples will have a positive surface charge when exposed to this water, and will therefore be favourable for anionic fluoride adsorption, as explained in section 2.5.

## 3.3 Bone Char Isotherms

Researchers who have determined the adsorption isotherm behaviours of BC have found these to fit type I isotherm models [35, 36, 46, 71, 93, 95, 110].

Medellin-Castillo *et al.* [36] fitted BC adsorption data to the two-parameter Langmuir and Freundlich models as well as the three-parameter Prausnitz-Radke model. They determined the percentage deviation (% D) of the models using the average relative error method developed by Marquardt [49].

The saturation adsorbate mass parameter ($q_s$) obtained from the Langmuir model at pH 7 was found to be 5.44 mg/g. % D was 10.5, 16.9 and 17.1 for Prausnitz-Radke, Langmuir and Freundlich models respectively, they attributed Prausnitz-Radke's smallest error to the fact that it is a three-parameter model.

The authors also noted in previous work [35] that the Langmuir model is not ideal at higher fluoride concentrations due to experimental data not exhibiting the asymptotic behaviour at higher concentrations typical of the Langmuir isotherm.

Shahid *et al.* [95] used the Langmuir and Freundlich models, and determined model fits *via* the coefficient of determination ($R^2$) method.

They found $R^2$ values of 0.99 and 0.97 for Langmuir and Freundlich models, respectively. The authors noted the higher $R^2$ value of the Langmuir model indicated monolayer fluoride adsorption on the BC surface. The authors also mentioned that the Freundlich adsorption intensity constant ($n$) of 3.11 indicated heterogeneous layer formation on the adsorbent surface.

Abe *et al.* [46] determined the Freundlich adsorption intensity constant ($n$) of BC to be 2.56, similar to the value reported by Shahid *et al.* [95], and also noted that BC's Freundlich distribution coefficient ($K_F$ was largest of all carbonaceous materials tested, indicating that it had the greatest fluoride interaction and adsorption capacity.

Leyva-Ramos *et al.* [110] had very similar results to those reported by Medellin-Castillo *et al.* [36], finding that the Prausnitz-Radke isotherm had the best fit of the three isotherms discussed by the aforementioned authors. They found Freundlich distribution coefficients ($K_F$) of 2.84 and 2.72 and adsorption intensity constants ($n$) of 3.05 and 3.46 for BC particle diameters of 0.65 mm and 0.79 mm respectively, reflecting results similar to those reported by Abe *et al.* [46].

The authors also found that the Langmuir saturation adsorbate mass parameter ($q_s$) remained mostly constant at approx. 5.60 mg/g for particle diameters 0.65 mm and 0.79 mm respectively, indicating that the maximum adsorption capacity of BC is not correlated to particle diameter at this size range.

Hu *et al.* [71] fitted the BC adsorption behaviour at 283 K, 298 K, 308 K and 318 K to both Langmuir and Freundlich models. They determined the correlation of both models using $R^2$ and $X^2$ methods, and found the Langmuir model to be a better fit across all temperatures with both methods. The authors also found that the Langmuir saturation adsorbate mass parameter ($q_s$) increased with temperature.

## 3.4   BC Fluoride Adsorption

### 3.4.1 Mechanisms

There is a wide consensus in the scientific that the adsorption of fluoride on to the surface of hydroxyapatite (HAP) is primarily due to the electrostatic interactions between positively charged basic sites, which consist of phosphate and calcium hydroxyl functional groups found at the surface of HAP, monetite and similar structures which compose bones [93].

These functional groups get protonated at pH levels more acidic than the point of zero charge (PZC) (pH < $pH_{PZC}$) by the following reactions [35, 93, 110]:

$$\equiv P - OH + H^+ \rightarrow \equiv POH_2{}^+ \qquad\qquad (3.4.1.1a)$$

$$\equiv Ca - OH + H^+ \rightarrow \equiv Ca - OH_2{}^+ \qquad\qquad (3.4.1.1b)$$
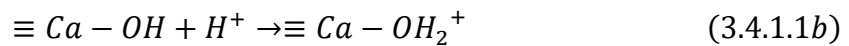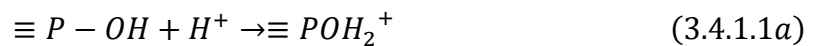
Acidic sites on the other hand are formed by the deprotonation of hydroxyl functional groups at pH levels more basic than the PZC (pH > $pH_{PZC}$):

$$\equiv P - OH \rightarrow \equiv PO^- + H^+ \qquad\qquad (3.4.1.2a)$$

$$\equiv Ca - OH \rightarrow \equiv Ca - O^- + H^+ \qquad\qquad (3.4.1.2b)$$
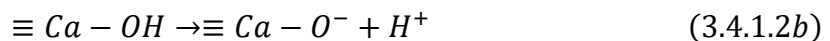
This phenomenon explains the drastic reduction in adsorption capacity of BC exposed to pH levels greater than the PZC, as fluoride anions are repelled from the surface of the adsorbents.

There is however, no clear consensus on which ion exchange mechanisms have a role to play in the adsorption of fluoride, and to which extent these occur.

Some authors such as Abe *et al.* [46] argue that fluoride ions exchange with $PO_4{}^{3-}$ ionic species on the HAP surface, and maintain that ion exchange between $OH^-$ ions does not play a role in the adsorption of fluoride. This is because the pH of solutions in the batch experiments undertaken by these authors remains largely unchanged before and after fluoride adsorption, implying there was an insignificant release of $OH^-$ ions. These observations agree with the measurements taken in batch experiments undertaken during this project, shown in figures 5.1.2.4 and 5.1.2.8.

However, the extent to which ion exchange of fluoride with phosphate ions contributes to the overall fluoride adsorption capacity of BC is also debated.

Abe *et al.* [46] have proposed that the ion exchange of fluoride ions with the $PO_4^{3-}$ ions represented between 18 % and 42 % of the fluoride adsorbed. However, Medellin-Castillo *et al.* [93] have found no significant changes in phosphate concentration before and after fluoride adsorption, and in fact found that in some experiments the mass of phosphate released when no fluoride was present was even higher than that of phosphate released when the fluoride was present in the solution. This implies that this ion exchange process may be minimal and that the presence of phosphate ions in solution are simply due to the dissolution of phosphate groups from the HAP surface.

Abe *et al.* [46] and Medellin-Castillo *et al.* [93] have also argued that due to the reversibility of fluoride adsorption to BC, chemisorption is to be disregarded [36, 46].

Other authors [95, 101, 111] have proposed that alongside ion exchange occurring between phosphates and fluoride, exchange with hydroxide ions is also occurring *via* the following reaction:

$$Ca_{10}(PO_4)_6(OH)_2 + 2\,F^- \rightarrow Ca_{10}(PO_4)_6F_2 + 2\,OH^- \qquad (3.4.1.3)$$
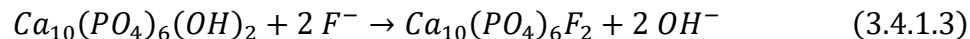
These conclusions were made through observing a decrease in the intensity of surface hydroxyl XPS peaks after fluoride adsorption, indicating that these were displaced by adsorbed fluoride ions.

He *et al.* [111] also note the appearance of a new band after adsorption, representing the OH-F bond indicative of FHAP, claiming some irreversible chemisorption through ion exchange is also occurring.

### 3.4.2 Kinetics

Kinetic studies of fluoride adsorption by BC have been undertaken by several authors [92, 95, 101, 110]. These are undertaken through batch tests, where a certain dose of BC is added to a water solution containing fluoride and shaken or stirred. Solution fluoride concentrations are then measured at various time intervals, to obtain concentration profiles.

Shahid *et al.* [95] and Leyva-Ramos *et al.* [110] investigated the effect of changing BC particle size on fluoride adsorption kinetics. Both authors found that second order kinetic plots had a better correlation for describing the behaviour of the BC.

Leyva-Ramos *et al.* [110]  also found that the smaller particles had a larger value for the second order rate constant ($k_2$) (with $k_2$ = 1.6 x $10^3$ g/mg min for $d_p$ = 0.65 mm and $k_2$ = 0.6 x $10^3$ g/mg min for $d_p$ = 1.29 mm).

Chatterjee *et al.* [101] investigated the effects of changing temperature on adsorption kinetics. The authors found that the effective pore volume diffusivity ($\mathcal{D}_p$) of fluoride slightly increased from $5.8 \times 10^{-12}$ m²/s at 30 °C to $6.2 \times 10^{-12}$ m²/s at 50 °C.

It was also found that residual fluoride concentrations increased with temperature, in line with findings by Shahid *et al.* [91][95] and Leyva-Ramos *et al.* [110]. This was attributed to the exothermic adsorption effect.

Finally, Jones [92] and Leyva-Ramos *et al.* [110] examined the effects of changing initial solution fluoride concentrations on the rate of adsorption, specifically 19 mg/L - 79 mg/L and 3.37 mg/L - 22.4 mg/L respectively. Very little variation in values of $k_2$ were observed by Leyva-Ramos *et al.* [110], which were between 0.9 x $10^3$ g/mg min and 1.3 x $10^3$ g/mg min for $c_0$ = 3.37 mg/L - 8.59 mg/L respectively, however at $c_0$ = 22.4 mg/L, $k_2$ was found to equal to 2.3 x $10^3$ g/mg min.

Jones [92] found similar trends, with $k_2$ increasing as $c_0$ increased. Both authors remarked that second and $n^{th}$ order kinetic models fit data best.

Leyva-Ramos *et al.* [110] also remarked that due to BC's adsorptive nature being highly dependent on solution pH, it is imperative to retain a constant solution pH when undertaking kinetic experiments.

All authors mentioned in this section reported keeping a constant pH of 7 during kinetic experiments.

### 3.4.3 Effect of pH

Authors who determined the effect of adsorbate solution pH on the adsorption capacity all remarked a significant decrease in adsorption capacity when increasing the pH of the solution [35, 36, 46, 93, 95]. In all cases, this effect was attributed to the PZC at the surface of the BC, with fluoride ions being repelled from the negative overall surface charge of BC at pH > PZC, as explained in section 2.5.

Medellin-Castillo et al. [36] also noted that when adsorption experiments were undertaken at an initial pH < PZC, the solution pH would increase after adsorption equilibrium had been reached (from pH 3, pH 5 and pH 7 to pH 6.9, pH 7.9 and pH 7.9 respectively), independently of initial fluoride concentration. However, adsorption experiments undertaken at initial pH > PZC, namely pH 9 and pH 12, saw little change in pH (to pH 8.1 and pH 11.8 respectively). The authors attributed the change in pH observed to the protonation and deprotonation reactions occurring at the amphoteric surface of BC, containing both acid and basic sites, as described in section 3.4.1.

## 3.5  BC Chemical Treatment

### 3.5.1 Treatment Methods

Several authors have investigated chemical modification of BC to increase the adsorption capacity of this [93, 96, 97, 101, 112].

Wang *et al.* [96] investigated modifying BC with lanthanum, by immersing a solution of 2:1 mass ratio of BC : $LaCl_3$ and stirring for 2 h.

Chatterjee *et al.* [101] proposed a method for chemically treating raw bone meal (RBM) and BC with calcium oxide and aluminium sulphate. The authors introduced 100 g of RBM to 1 L solutions of water containing between 5 g and 50 g of CaO and stirred this for 2 h. This was followed by addition of between 50 g and 1000 g of $Al_2(SO_4)_3$ for an additional 4 h. BC pyrolysed at 550 °C for 4 hours was also treated with CaO and $Al_2(SO_4)_3$.

Yami *et al.* [97] treated RBM with $H_2SO_4$, $H_3PO_4$ and ZnCl solutions, each at 20 wt. %, 30 wt. % and 50 wt. %. The RBM samples were immersed in a 1:1 mass ratio with the solutions, stirred and heated at 50 °C for 3 hours. One sample of each kind was also subjected to pyrolysis at 540 °C for 3 hours. Samples of BC were subjected to surface amendment with aluminium salts (1,000 ppm and 2,000 ppm $AlCl_3$ and 500 ppm, 1,000

ppm and 2,000 ppm $Al_2(SO_4)_3$). 12 g of BC was stirred at 200 rpm with 200 mL solution for 5 days.

Medellin-Castillo *et al.* [93] investigated the acid treatment of BCs pyrolysed at temperatures of 400 °C, 500 °C, 600 °C, 700 °C and 800 °C with 0.5 M, 1.0 M and 1.5 M $HNO_3$ solutions. 60 g of BC was submerged in 500 mL of solution, and continuously stirred at 80 °C for 24 h.

Tapia-Picazo *et al.* [112] proposed the surface modification of BC pyrolysed for 2 h at 700 °C with cerium salts. The soluble salts $Ce(NO_3)_3 \cdot 6H_2O$ and $(NH_4)_2Ce(NO_3)_6$ were used as precursors of $Ce^{3+}$ and $Ce^{4+}$ ions, respectively. 1 g of BC was treated with 50 mL of aqueous cerium solution at 30 °C, followed by another pyrolysation step. The authors used Taguchi experimental design arrays [113], choosing the following operating variables, given in table 3.5.1.1.

Table 7.5.1.1 - Taguchi experimental design variables for BC treatment with cerium solutions [112]

| Variable | $Ce(NO_3)_3 \cdot 6H_2O$ | $(NH_4)_2Ce(NO_3)_6$ |
|---|---|---|
| Cerium solution concentration [ M ] | 0.005, 0.01, 0.02 | 0.025, 0.05, 0.1 |
| BC reaction time with cerium solution [ h ] | 6, 12, 18, 24 | 2, 6, 12 |
| Final pyrolysis temperature [ °C ] | 200, 300, 400, 500 | 200, 300, 500 |
| Final pyrolysis duration [ h ] | 1, 2, 3, 4 | 1, 2, 4 |

## 3.5.2  Treated BC Characterisation

Wang *et al.* [96] used SEM to analyse the surface properties of the lanthanum-modified bone waste (LBW), and noted its more porous, irregular surface when compared to regular bone waste, as shown in figure 3.5.2.1. They remarked that the addition of the lanthanum could increase the specific surface area (SSA) of the adsorbent and therefore provide more available adsorption sites. The $N_2$-BET analysis of the LBW indicated an SSA of 85.4 $m^2/g$, a higher value than the SSA reported for BC, as shown in section 3.2.1.
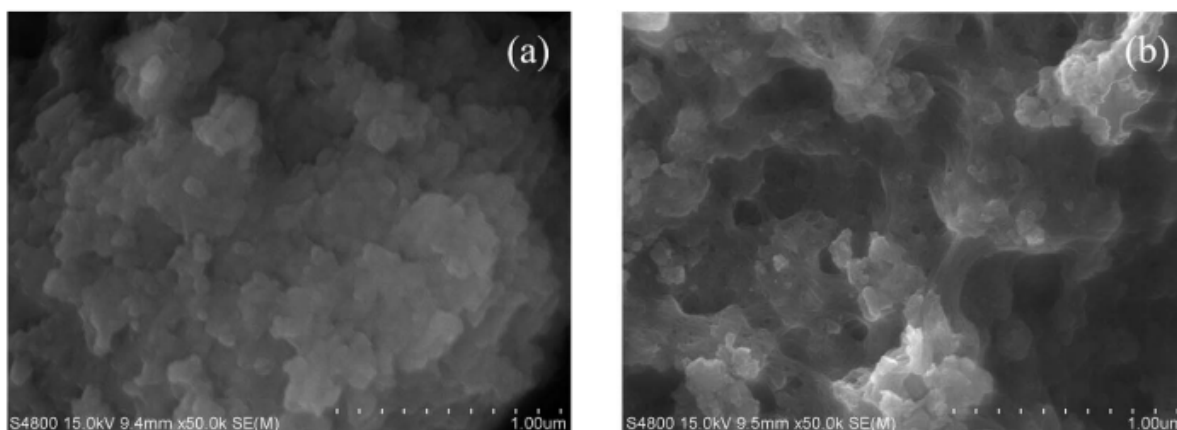
Figure 3.5.2.1 - Left: Untreated bone waste SEM image. Right: Lanthanum-modified bone waste SEM image. [96]

Chatterjee *et al.* [101] also found that the chemically treated bone meal (CTBM) surface was less smooth than regular BC. The authors also noted a deposition of aluminium hydroxide on the CTBM surface, but found no significant difference in the surface areas of the CTBM and BC. XRD analysis indicated the presence of calcium oxides, as well as an increased crystallinity of the CTBM, which has been shown to increase the fluoride uptake capacity [114].
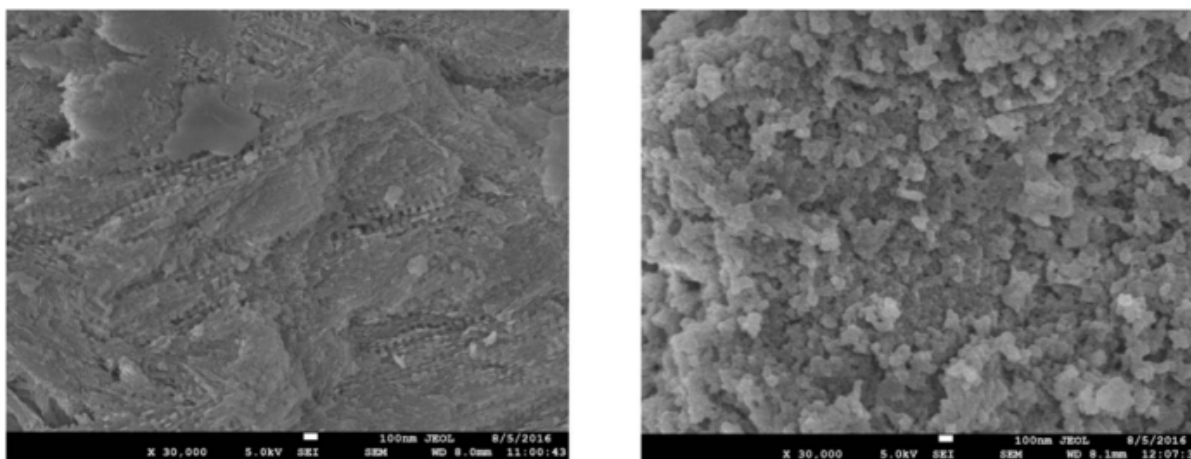


Figure 3.5.2.2 - Left: BC SEM image. Right CTBM SEM image. [101]

Yami *et al.* [97] reported SSAs of 134 m$^2$/g, 111 m$^2$/g and 106 m$^2$/g for 30 % $H_2SO_4$ treated bone (HSCB), 50 % KOH treated bone and 50 % Zn treated CB respectively. No correlation was found between SSA and fluoride uptake capacity for these samples. The authors also noted that the SSAs of the chemically activated bones were largely the same as SSAs of BCs quoted in literature, and therefore could not account

for their increased fluoride uptake capacity. The PZC of the best performing char, 30 % HSCB, was 6.6 – indicating that the net surface charge on the surface of the HSBC was negative during the experiments, carried out at pH 7, and therefore also could not explain the increased fluoride uptake.

XRD analysis of the 30 % HSCB revealed the presence of bassanite and monetite minerals ($CaSO_4 \cdot 0.5\ H_2O$ and $CaHPO_4$ respectively) not present in BC, indicating a crystal phase change as a result of the chemical activation.
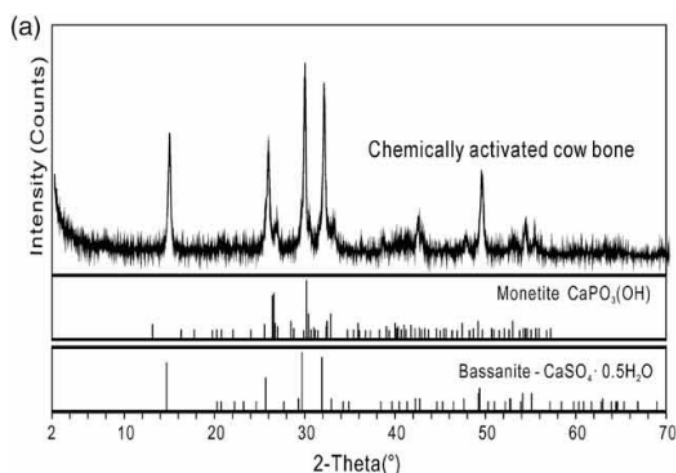


Figure 3.5.2.3 - Top: CAB XRD spectrum. Middle: monetite XRD spectrum. Bottom: bassanite XRD spectrum. [97]

Medellin-Castillo *et al.* [93] found through XRD analysis that treating BC with $HNO_3$ increased the hydroxyapatite crystallinity from 0.4 % to 30.2 % for untreated BC and BC treated at 0.5 M respectively. Increasing the concentration to 1 M increased the crystallinity of HAP further and also introduced the presence of monetite. At 1.5 M, the sample showed a complete conversion of HAP to monetite. This was attributed to reactions of HAP with protons in solution.

The authors found that the BET SSA of BC was drastically reduced after chemical treatment (e.g. untreated BC to BC treated at 1.5 M went from 134 $m^2$/g to 4.3 $m^2$/g). This was attributed to the destruction of the porous structure of the BC and the increased HAP and monetite crystallinity. However, Yami *et al.* [97] have argued that that this is likely due to the collapse of the mineral structure of the BC during the vacuum stage of the BET process, as the authors had noticed the same effect occurring while conducting similar research. This effect no longer occurred when the ethylene glycol monoethyl ether BET method was employed to determine SSA.

Medellin-Castillo et al. [93] noted that the PZC increased when pyrolysis temperature was increased, however increasing concentration of acid during chemical treatment decreased the PZC, which was at a minimum of 4.5 for BC treated at 1.5 M. The authors attributed this to the acidic nature of the monetite crystal surface.

Tapia-Picazo et al. [112] found through FTIR spectra analysis that cerium doping caused a partial dissolution of HAP structure of the BC and substitution of $Ca^{2+}$ by $Ce^{3+}$ or $Ce^{4+}$ on the BC surface. The authors noted that the incorporation of multivalent Ce cations in the HAP of BC caused changes in the molecular geometry including the creation of cationic vacancies and a transformation of the $OH^-$ groups to $O^{2-}$. The SEM images of the Ce doped BC was noted to appear more porous in nature than BC.

### 3.5.3 Batch Results

Table 3.5.3.1 shows the adsorption capacities of various BCs at an equilibrium fluoride concentration ($c_e$) of 1.5 mg/L ($q_{1.5}$).

It should be noted that batch conditions may differ between experiments and have an impact on final capacities, making perfect comparisons difficult. These differences, when stated by the authors, are mentioned in the notes column.

Where $q_{1.5}$ was not explicitly given by authors, this was calculated using best-fit isotherm parameters provided by these.

Table 3.5.3.1 - Untreated BC batch adsorption capacities

| Untreated Bone Char | | | |
|---|---|---|---|
| BC Type | $q_{1.5}$ [mg/g] | Notes | Reference |
| Fish BC | 0.9 | 1 h batch test at 200 rpm | [98] |
| BC | 1.2 | 3 h batch test at RTP | [46] |
| BC | 1.4 | 24 h batch test at 200 rpm, pH7 | [97] |
| BC | 2.1 | 24 h batch test at 200 rpm | [36] |
| CdA produced BC | 2.81 | 24 h batch test at 51 rpm, RTP, pH 8.3 | Author's work |

Table 3.5.3.1 shows $q_{1.5}$ values for various chemically treated bone and BCs reported across literature.

Table 3.5.3.2 - Chemically treated bone and BC adsorption capacities

| | Treated Bone and Bone Char | | |
|---|---|---|---|
| BC Type | $q_{1.5}$ [mg/g] | Notes | Reference |
| 50 % Zn treated bone | 0.5 | 24 h batch test at 200 rpm, pH 7 | [97] |
| 1000 ppm AlCl$_3$ doped BC | 1.2 | 24 h batch test at 200 rpm, pH 7 | [97] |
| 2000 ppm AlCl$_3$ doped BC | 1.2 | 24 h batch test at 200 rpm, pH 7 | [97] |
| 1000 ppm Al$_2$(SO$_4$)$_3$ doped BC | 1.2 | 24 h batch test at 200 rpm, pH 7 | [97] |
| 2000 ppm Al$_2$(SO$_4$)$_3$ doped BC | 1.2 | 24 h batch test at 200 rpm, pH 7 | [97] |
| Al$_2$(SO$_4$)$_3$/CaO doped BC | 1.27 | 24 h batch test at 150 rpm, pH 6.8 | [101] |
| Ce$_4^+$ doped BC | 1.34 | 24 h batch test at 120 rpm, RTP, pH 7 | [112] |
| 500 ppm Al$_2$(SO$_4$)$_3$ doped BC | 1.6 | 24 h batch test at 200 rpm, pH 7 | [97] |
| 50 % Zn treated bone pyrolysed at 500 °C | 2.2 | 24 h batch test at 200 rpm, pH 7 | [97] |
| 30 % KOH treated bone pyrolysed at 540 °C | 3.2 | 24 h batch test at 200 rpm, pH 7 | [97] |
| 30 % KOH treated bone | 3.3 | 24 h batch test at 200 rpm, pH 7 | [97] |
| 50 % KOH treated bone pyrolysed at 540 °C | 3.6 | 24 h batch test at 200 rpm, pH 7 | [97] |
| 50 % KOH treated bone | 3.8 | 24 h batch test at 200 rpm, pH 7 | [97] |
| 1.0 M HNO$_3$ treated BC | 4 | 7 day batch test at 0 rpm, pH 7 | [93] |

Table 3.5.3.2 - Chemically treated bone and BC adsorption capacities

**Treated Bone and Bone Char**

| BC Type | $q_{1.5}$ [mg/g] | Notes | Reference |
|---|---|---|---|
| 30 % $H_3PO_4$ treated bone | 5.4 | 24 h batch test at 200 rpm, pH 7 | [97] |
| Lanthanum-modified bone waste | 5.87 | 24 h batch test at 200 rpm, RTP, pH 7 | [96] |
| 30 % $H_2SO_4$ treated bone | 6.1 | 24 h batch test at 200 rpm, pH 7 | [97] |
| 30 % $H_2SO_4$ treated bone pyrolysed at 540 °C | 6.3 | 24 h batch test at 200 rpm, pH 7 | [97] |

## 3.5.4  Fluoride Adsorption Mechanisms

Wang *et al.* [96] remarked that the fast adsorption rate, as well as short adsorption equilibrium time from kinetic studies indicated a high active site density on the lanthanum-modified bone waste. SEM imaging as well as BET analysis showed micro- and meso-pores contributing to a large surface area, which in turn are favourable for fluoride adsorption.

PZC analysis indicated that the surface of the LBW is high (pH 11.4) and therefore the protonation of hydroxide groups facilitates electrostatic fluoride adsorption and ion exchange.

Shifts in peaks from XPS analysis indicated fluoride ions were likely removed by ion exchange with hydroxide and chloride ions on the LBW surface. The authors proposed that the La was attached to the surface in various forms, including R–La–OH, $La_2O_3$ or $La(OH)_3$ – the high affinity of the multivalent lanthanum ions towards fluoride ions creating an exchange between OH or Cl through the following reactions:

$$R - M - OH + F^- \rightarrow R - M - F + OH^- \qquad (3.5.3.1a)$$

$$M - OH + F^- \rightarrow M - F + OH^- \qquad (3.5.3.1b)$$

$$M - Cl + F^- \rightarrow M - F + Cl^- \qquad (3.5.3.1c)$$
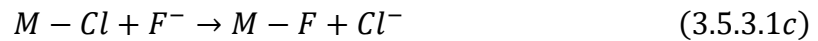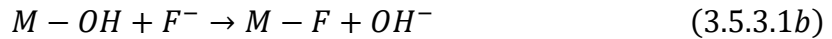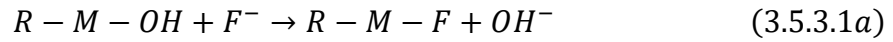
Where:    $R$ is the HAP base structure

   $M$ is the lanthanum surface group

Additionally, electrostatic adsorption was proposed to have the following mechanism:

$$R - M - OH_2{}^+ + F^- \rightarrow R - M - OH_2 \cdots F \qquad (3.5.3.2a)$$

$$MOH_2{}^+ + F^- \rightarrow MOH_2 \cdots F \qquad (3.5.3.2b)$$
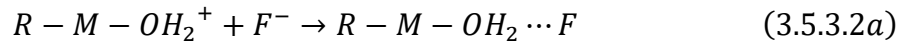
Chatterjee *et al.* [101] suggested the fluoride uptake mechanism of $Al_2(SO_4)_3$/CaO treated raw bone meal to occur *via* the following ion exchange mechanisms:

$$Ca_{10}(PO_4)_6(OH)_2 + 2\,F^- \rightarrow Ca_{10}(PO_4)_6F_2 + 2\,OH^- \qquad (3.5.3.3a)$$

$$2\,Al(OH)_3 + 2\,F^- \rightarrow 2\,Al - F + 6\,OH^- \qquad (3.5.3.3b)$$

$$Ca(OH)_2 + 2\,F^- \rightarrow CaF_2 + 2\,OH^- \qquad (3.5.3.3c)$$
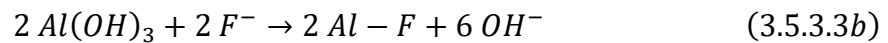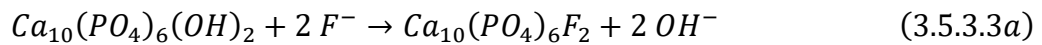
Yami *et al.* [97] remarked that research has suggested that the presence of $SO_4^{2-}$, $Ca^{2+}$ and $PO_4^{3-}$ increases the fluoride uptake capacity of samples [46, 115, 116]. The authors therefore postulated that the presence of sulphate and phosphate groups from bassanite and monetite phases respectively, formed during the crystal phase change of HAP after activation, may explain the improved adsorption capacity of the CAB. Specifically, through ion exchange mechanisms between fluoride ions and $SO_4^{2-}$, OH⁻ and $PO_4^{3-}$.

Medellin-Castillo *et al.* [93] stated that the Fourier-transform infrared spectroscopy (FTIR) bands of 1.0 M $HNO_3$ treated BC loaded with fluoride corresponding to $OH^-$ and $HPO_4^{2-}$ were displaced to lower wavenumbers than the untreated BC spectrum, indicating chemical interactions between the fluoride and hydroxyl or phosphates from the HAP and monetite. The authors suggested that ion exchange between fluoride ions and $OH^-$ ions on the BC was not relevant in the adsorption of fluoride from an aqueous phase. XPS analysis showed that binding energies corresponded to fluoride bonding to calcium and forming fluorite ($CaF_2$) and FHAP ($Ca_{10}(PO_4)_6F_2$). They stated that the fluoride ions present in the solution therefore reacted with the calcium in monetite and HAP as well as other calcium phosphate amorphous materials contained in the BC.

The authors suggested the adsorption of fluoride on HAP was described by the following reactions:

$$Ca_{10}(PO_4)_6(OH)_2 + 20\ F^- \rightarrow 10\ \equiv CaF_2 + 3\ PO_4{}^{3-} + 2\ OH^- \qquad (3.5.3.4a)$$

$$Ca_{10}(PO_4)_6(OH)_2 + 2\ F^- \rightarrow\ \equiv Ca_{10}(PO_4)_6F_2 + 2\ OH^- \qquad (3.5.3.4b)$$
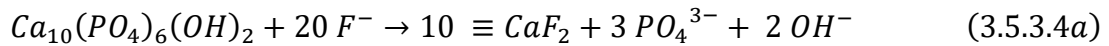
And the adsorption of fluoride to monetite *via* this mechanism:

$$\equiv CaHPO_4 + 2\ F^- \rightarrow\ \equiv CaF_2 + HPO_4{}^{2-} \qquad (3.5.3.5)$$
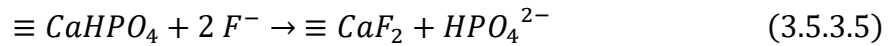
Tapia-Picazo *et al.* [112] noted that the FTIR spectra of cerium doped BC after fluoride adsorption showed displacements and decrements in adsorption bands of phosphate and hydroxide groups, suggesting these played a role in fluoride removal. The changes were noted to be more prominent with $Ce^{4+}$ modified BC.

The crystalline phase of $Ca_{10}(PO_4)_6F_2$ was identified in BC and Ce-doped BC samples after fluoride adsorption. The authors suggested these characterisation results indicate fluoride adsorption on cerium-containing BC may involve a mechanism where electrostatic interactions and an ion exchange process play a relevant role. In particular, the ion exchange mechanism can be defined by:

$$MOH + F^- \leftrightarrow RMF + OH^- \qquad (3.5.3.6)$$

Where:        *M* is the cerium surface group

# 4.0  Methodology

Three primary experiments were undertaken during the placement at CdA. These are described in some detail below. Full, detailed experimental methodologies are given in appendix B.

## 4.1  Apparatus

### 4.1.1 Adsorbent Synthesis

Treated bone and BC syntheses were undertaken in glass beakers on a magnetic stirring plate.

Drying for batch experiment 1 was done in a toaster oven with a thermocouple placed inside to display temperature – the oven was then manually turned on and off to ensure temperature remained as constant as possible – drying temperatures therefore varied by ± 20 °C. Figure 4.1.1.1 depicts the drying setup utilised.



Figure 8.1.1.1 - Toaster oven with thermocouple setup used to dry samples

Drying for batch experiment 2 was undertaken using the same toaster oven, which was modified after batch test 1 by implementing a PID temperature controller built into this, reducing temperature variation to ± 1 °C. Figure 4.1.1.2 depicts this.

Figure 4.1.1.2 - Top: PID oven system. Bottom: PID controller unit

A schematic of the reverse osmosis (RO) flushing system used to leach away any phosphate groups from the surface of synthesised adsorbents, to prevent any interference from colourimetry readings is shown in figure 4.1.1.3.
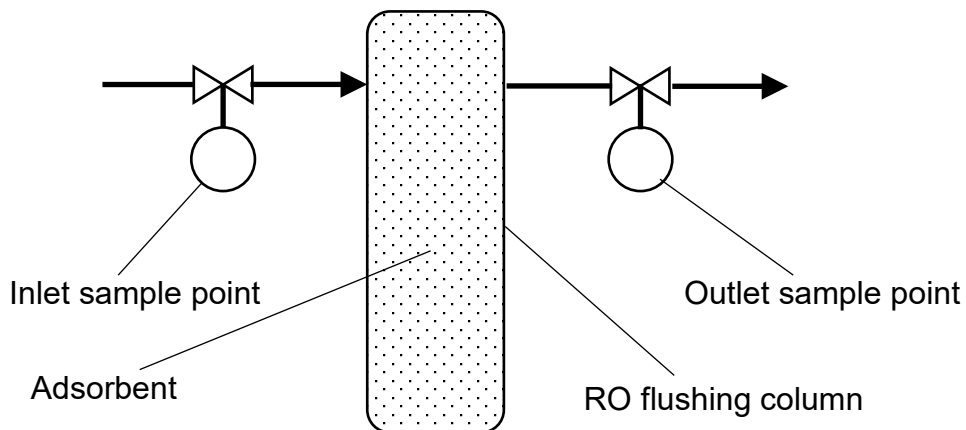


Figure 4.1.1.3 - RO adsorbent flushing system

## 4.1.2 Batch Testing

Adsorbent media doses (given in sections 4.2.3.1 and 4.3.3.1) were placed in sealed beakers along with sample water into a batch adsorbent sample tumbler. A schematic of this is shown in figure 4.1.2.1.
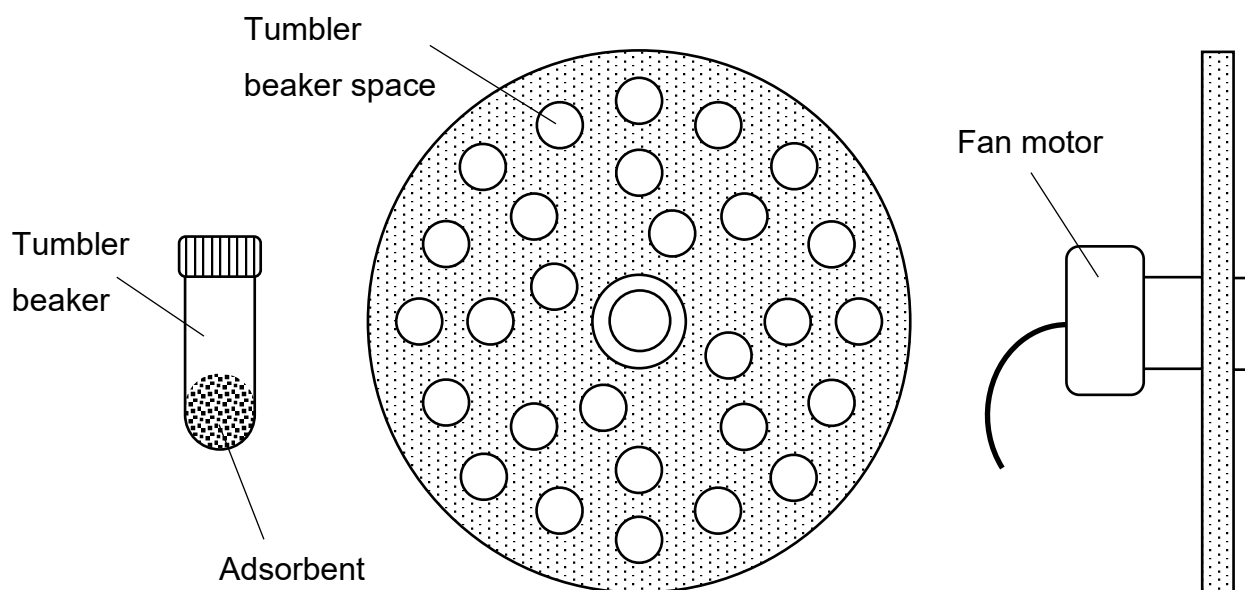
Figure 4.1.2.1 - Left: batch tumbler beaker containing sample and water to be treated. Middle: front view of batch adsorbent sample tumbler with holes for insertion of sample beakers. Right: side view of batch adsorbent sample tumbler with driving fan motor. [100]

The tumbler can accommodate up to 42 sample beakers. However, for batch experiments, the total number of samples including duplicates were split into equal numbers and tested in batch lots.

Samples further from the centre of the tumbler wheel experienced greater angular velocities, however these differences were deemed too small to have any significant impact on results due to equilibrium fluoride concentration similarities between duplicates.

After batch testing, treated water samples were filtered using Whatman™ glass microfiber filters, the full filtering procedure is detailed in appendix B 4.

### 4.1.3  RSSCT

Figure 4.1.3 shows a schematic of the RSSCT equipment setup used.
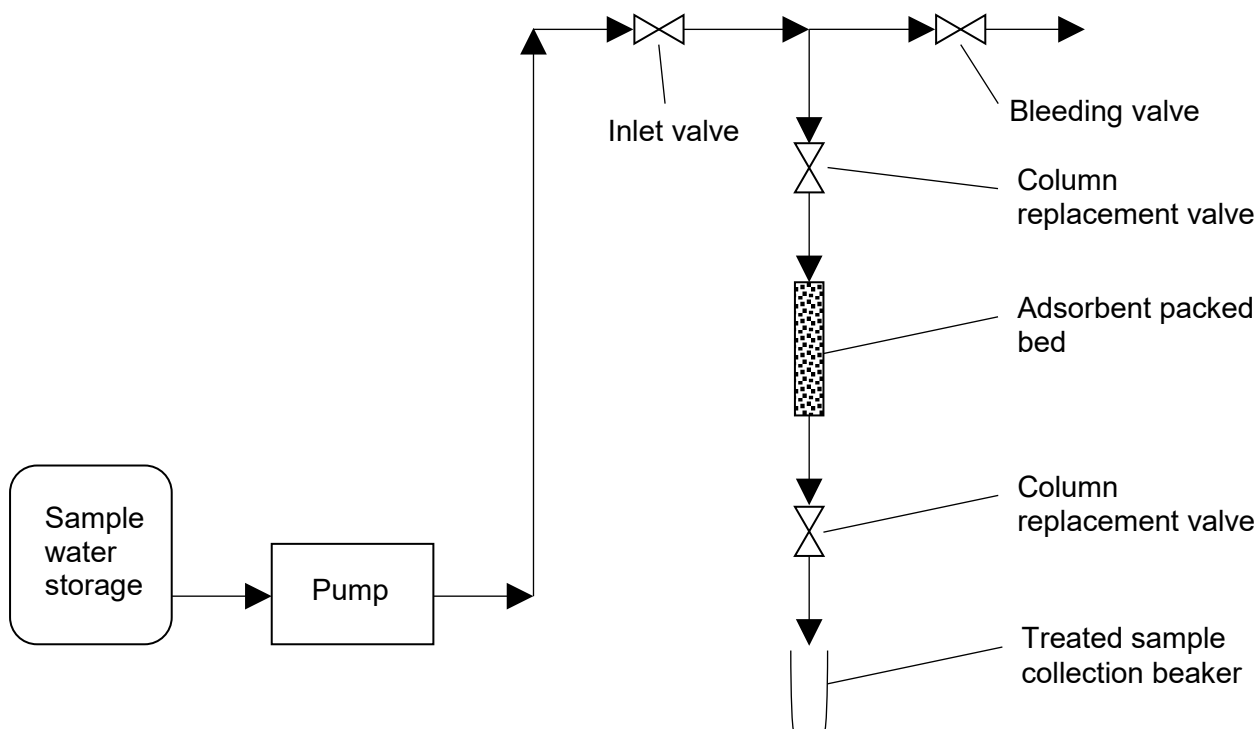
Figure 4.1.3 - RSSCT experimental setup schematic

## 4.1.4 Species Quantification

Sample water fluoride concentrations were determined by colourimetry using the Hach DR/890 portable colourimeter with the SPADNS 2 reagent [117] and using Extech Instruments fluoride ion selective electrode probe [118]. These are shown below in figure 4.1.4.1.



Figure 4.1.4.1 - Left: Hach DR/890 portable colourimeter with sample beakers [100]. Right: Extech Instruments FL700 fluoride ion selective electrode probe [118].

62

Total dissolved solids (TDS) and solution pH were determined using Juanjuan TDS and pH probes respectively [119], shown in figure 4.1.4.2:



Figure 4.1.4.2 - Left: Juanjuan pH probe. Right: Juanjuan TDS probe. [119]

Arsenic concentrations were determined using the ITS Quick Arsenic Econo II Test Kit [120], shown below in figure 4.1.4.3:



Figure 4.1.4.3 - ITS Quick Arsenic Econo II Test Kit [120]

## 4.2 Adsorbent Synthesis and Batch Test 1

An initial batch test aiming to replicate results produced by Yami *et al.* [97] as well as those by Chatterjee *et al.* [101], and compare these to the batch adsorption capacity of BC produced by CdA in the method described in section 3.1.1.

A secondary objective of batch test 1 was to determine the production yields of the synthesised adsorbents for subsequent cost estimation.

### 4.2.1 Synthesis Methodology

Table 4.2.1.1 shows a brief methodology of the adsorbent preparation for batch test 1.

Table 4.2.1.1 - Batch test 1 adsorbent synthesis methodologies

| Adsorbent | Synthesis Method | Based On |
|---|---|---|
| CdA BC (RBC) | 1. CdA BC produced according to procedure outlined in section 3.1.1<br>2. BC packed into a column and flushed with RO water until inlet and outlet fluoride concentrations are within ± 0.1 mg/L – ensuring that any $PO_4$ groups are flushed from the BC surface<br>3. Flushed sample removed from column and dried in oven for 1.5 h at 100 °C<br>4. Dried BC is then crushed, passed through a # 30 US standard mesh sieve, and weighed | |
| Chemically activated bone char (CABC) | 1. 20 g of # 8 x # 30 US standard mesh sieved CdA BC added to 200 g DI water<br>2. 3 g of CaO added to solution and stirred for 2 h at room temperature<br>3. 100 g of $Al_2(SO_4)_3$ added to solution and stirred for 2 h at room temp.<br>4. Sample filtered, packed into a column and flushed with RO water until inlet and outlet fluoride concentrations are within ± 0.1 mg/L – ensuring that any $PO_4$ groups are flushed from the CABC surface<br>5. Flushed sample removed from column and dried in oven for 1.5 h at 100 °C<br>6. Dried CABC is then crushed, passed through a # 30 US standard mesh sieve, and weighed | [101] |

Table 8.2.1.1 - Batch test 1 adsorbent synthesis methodologies

| Adsorbent | Synthesis Method | Based On |
|---|---|---|
| $H_2SO_4$ activated bone ($H_2SO_4$ CAB)<br><br>$H_3PO_4$ activated bone ($H_3PO_4$ CAB)<br><br><br>KOH activated bone (KOH CAB)<br><br><br><br>NaOH activated bone (NaOH CAB) | 1. 325 g of commercial bone meal soaked in 0.8 L of 13 wt. %. NaOCl for 48 h to remove organic impurities<br>2. Slurry filtered with coffee filter and rinsed with DI water<br>3. Slurry dried in oven for 3 h at 60 °C<br>4. Dried bone meal separated into 4 samples<br>5. Samples added to 30 wt. % $H_2SO_4$, 30 wt. % $H_3PO_4$, 40 wt. % KOH, and 32 wt. % NaOH solution respectively, in a 1:1 bone meal to solution mass ratio<br>6. Solutions stirred for 4 h<br>7. Samples filtered, packed into a column and flushed with RO water until inlet and outlet fluoride concentrations are within ± 0.1 mg/L – ensuring that any $PO_4$ groups are flushed from the CAB surface<br>8. Flushed samples removed from column and dried in oven for 1.5 h at 100 °C<br>9. Dried CAB samples are then crushed, passed through a # 30 US standard mesh sieve, and weighed | [97] |

## 4.2.2 Batch Sample Water Preparation

To determine the effectiveness of fluoride uptake of adsorbents in sample water with a makeup characteristic of water in the region, 6 L of water was collected from a highly contaminated well with fluoride concentrations of 10.7 mg/L as of January 2018 [10]. Full information on the sample water chemistry is provided in appendix C 1.1.

This well water was diluted with DI to bring fluoride concentrations down to 8.5 ± 0.5 mg/L. This concentration is greater than 97 % of that found in water from the sample points shown in figure 1.2.3, and can therefore guarantee the treatment objective would be met for these if it were met at this concentration. Sample water fluoride concentration was tested using both colourimetry and fluoride ion selective electrode probe. Sample water arsenic concentration, pH and TDS was also determined.

### 4.2.3  Batch Test Procedure

Each sample was assigned a blinding code in the form of 'LETTER-LETTER-DIGIT-DIGIT' (e.g. AH65) to ensure there was no distinguishing between adsorbent type, dose, or duplicate number.

Sample beakers were then filled with 90 mL of sample water, and corresponding adsorbent doses were added to this – the order in which adsorbent doses were added to sample water beakers was the order in which they were filtered out of treated water post-batch testing – ensuring immersion times were as homogenous as possible across all batch samples.

#### *4.2.3.1      Batch Parameters*

Table 4.2.3.1.1 - Batch test 1 parameters

| Parameter | Specification |
| --- | --- |
| Adsorbent types | RBC, CABC, $H_2SO_4$ CAB, $H_3PO_4$ CAB, KOH CAB, NaOH CAB |
| Adsorbent dose [ g ] | 0.05, 0.10, 0.20, 0.50, 1.00 * |
| Sample water volume [ mL ] | 90 |
| Adsorbent concentration [ g/L ] | 0.56, 1.11, 2.22, 5.56, 11.11 |
| Replicate number | 2 |
| Control samples | 2 |
| Total samples tested | 56 ** |
| Batch tumbling time [ h ] | 24 |
| Batch tumbling speed [ rpm ] | 30 |

*\* Due to low synthesis yields, KOH and NaOH duplicate doses tested were only up to 0.20 and 0.50 g respectively*

*\*\* Samples tested in two 24-hour batches containing 28 samples on tumbler wheel*

### 4.2.4 Treated Sample Testing

Treated batch samples were filtered to remove saturated adsorbent using the Whatman™ glass microfiber filtration procedure described in appendix B 4. Sample water fluoride concentrations were determined by colourimetry and fluoride ion selective electrode probe. Sample fluoride concentration differences greater than 0.2 mg/L between the colourimeter and ion selective electrode probe were re-tested to ensure no experimental error was made.

## 4.3    Adsorbent Synthesis and Batch Test 2

Following the results of batch test 1 described in section 5.1.1, a second batch test was undertaken, this time to assess the following objectives:

- If acid and base treatment of CdA BC could increase the adsorption capacity of this
- Whether simply burning one 200 L biomass retort in the CdA BC production procedure outlined in section 3.1.1 would be sufficient to achieve effective pyrolysis of cow bone
- Whether separating the CdA BC into the harder, more mineralised outer shell and softer inner core would produce significant differences in fluoride adsorption capacity
- If commercially produced BC imported from Brazil would have any significant difference in adsorption capacity than CdA BC
- The production yields of the adsorbents were again determined for subsequent cost estimation

## 4.3.1 Synthesis Methodology

The following adsorbents were synthesised for the batch test:

Table 4.3.1.1 - Batch test 2 adsorbent synthesis methodologies

| Adsorbent | Synthesis Method |
|---|---|
| CdA BC (RBC) | 1. CdA BC produced according to procedure outlined in section 3.1.1<br>2. BC packed into a column and flushed with RO water until inlet and outlet fluoride concentrations are within ± 0.1 mg/L – ensuring that any $PO_4$ groups are flushed from the BC surface<br>3. Flushed samples removed from column and dried in PID oven until there is no mass change<br>4. Dried BC is then crushed, passed through a US 30 mesh sieve, and weighed |
| Single retort burn CdA BC with shorter pyrolysis time (SPT) | 1. CdA BC produced according to procedure outlined in section 3.1.1, with one 200 L biomass retort burned as combustion fuel instead of two<br>2. BC packed into a column and flushed with RO water until inlet and outlet fluoride concentrations are within ± 0.1 mg/L – ensuring that any $PO_4$ groups are flushed from the BC surface<br>3. Flushed samples removed from column and dried in PID oven until there is no mass change<br>4. Dried BC is then crushed, passed through a US 30 mesh sieve, and weighed |
| CdA BC outer shell (BCO)<br><br>CdA BC inner core (BCI) | 1. CdA BC produced according to procedure outlined in section 3.1.1<br>2. Larger, pyrolysed BC chunks are broken apart to separate the harder outer shell from the softer inner cores before being separately ground up and sieved to 8 x 30 US standard mesh<br>3. BC packed into a column and flushed with RO water until inlet and outlet fluoride concentrations are within ± 0.1 mg/L – ensuring that any $PO_4$ groups are flushed from the BC surface<br>4. Flushed samples removed from column and dried in PID oven until there is no mass change<br>5. Dried BC samples are then crushed, passed through a US 30 mesh sieve, and weighed |

Table 4.3.1.1 - Batch test 2 adsorbent synthesis methodologies

| Adsorbent | Synthesis Method |
|---|---|
| Brazilian imported BC (BBC) | 1. BBC granules packed into a column and flushed with RO water until inlet and outlet fluoride concentrations are within ± 0.1 mg/L – ensuring that any $PO_4$ groups are flushed from the BC surface<br>2. Flushed samples removed from column and dried in PID oven until there is no mass change<br>3. Dried BC samples are then crushed, passed through a # 30 US mesh sieve, and weighed |
| $H_2SO_4$ treated BC ($H_2SO_4$ BC) *<br><br>$H_3PO_4$ treated BC ($H_3PO_4$ BC) *<br><br>HCl treated BC (HCl BC) **<br><br>KOH treated BC (KOH BC) ***<br><br>NaOH treated BC (NaOH BC) *** | 1. Five 100 g samples of # 8 x # 30 US standard mesh size CdA BC taken<br>2. 10 g samples of BC added to tumbler beakers containing 50 mL of 0.1 M $H_2SO_4$ (0.97 wt. %), 0.1 M $H_3PO_4$ (0.97 wt. %), 38 wt. % (12.39 M) HCl, 10 wt. % KOH (1.78 M), or 20 wt. % NaOH (4.99 M) solution<br>3. Acid/base submerged BC samples tumbled for 24 h at 40 rpm<br>4. Treated BC samples filtered and rinsed with DI water<br>5. Rinsed samples packed into a column and flushed with RO water until inlet and outlet fluoride concentrations are within ± 0.1 mg/L – ensuring that any $PO_4$ groups are flushed from the treated BC surfaces<br>6. Flushed samples removed from column and dried in PID oven until there is no mass change<br>7. Dried BC samples are then crushed, passed through a size 30 sieve, and weighed |

*0.1 M acid concentrations were used as it was observed that higher concentrations – similar to base concentrations, destroyed the BC*

** *Pure, undiluted muriatic acid (38 wt.% (12.39 M) HCl) was used, as past, non-tumbled, batch investigations undertaken by CdA had shown this not to destroy BC [121]*

*** *Lower base concentrations were used than in batch test 1 (see table 4.2.1.1), as it was impossible to determine if suspended particles in base solutions were impurities or undissolved base, therefore, by precaution, base dissolution was halted upon observation of suspended material*

### 4.3.2  Batch Sample Water Preparation

After batch experiment 1, it was determined that diluting heavily contaminated well water would dilute the concentration of other species present in this too greatly. Therefore, to more realistically obtain a sample of water characteristic of the region, water from the CdA BC and ceramic filter production site well (known to contain fluoride concentrations lower than 8 mg/L) was taken, and spiked to 8 mg/L with NaF. Full information on the sample water chemistry is provided in appendix C 1.2. This concentration is greater than 97 % of that found in water from the sample points shown in figure 1.2.3, and can therefore guarantee the treatment objective would be met for these if it were met at this concentration.

Sample water fluoride concentration was tested using both colourimetry and fluoride ion selective electrode probe. Sample water arsenic concentration, pH and TDS was also determined.

### 4.3.3  Batch Test Procedure

Each sample was assigned a blinding code in the form of 'LETTER-LETTER-DIGIT-DIGIT' (e.g. AH65) to ensure there was no distinguishing between adsorbent type, dose, or duplicate number. Sample beakers were then filled with 90 mL of sample water, and corresponding adsorbent doses were added to this – the order in which adsorbent doses were added to sample water beakers was the order in which they were filtered out of treated water post-batch testing – ensuring immersion times were as homogenous as possible across all batch samples.

### 4.3.3.1 Batch Parameters

Table 4.3.3.1.1 - Batch test 2 parameters

| Parameter | Specification |
| --- | --- |
| Adsorbent types | RBC, SPT, BBC, BCI, BCO, $H_2SO_4$ BC, $H_3PO_4$ BC, HCl BC, NaOH BC, KOH BC |
| Adsorbent dose [ g ] | 0.05, 0.10, 0.20, 0.50, 1.00 * |
| Sample water volume [ mL ] | 90 |
| Adsorbent concentration [ g/L ] | 0.56, 1.11, 2.22, 5.56, 11.11 |
| Replicate number | 2 |
| Control samples | 2 |
| Total samples tested | 101 ** |
| Batch tumbling time [ h ] | 24 |
| Batch tumbling speed [ rpm ] | 50 |

*Due to low synthesis yields, the second replicate 1.00 g HCl dose could not be tested*
*** Samples tested in three 24-hour batches containing 33, 33 and 35 samples respectively on tumbler wheel*

## 4.3.4 Treated Sample Testing

Treated batch samples were filtered to remove adsorbent using the Whatman™ glass microfilter procedure described in appendix B 4. Sample water fluoride concentrations were determined by colourimetry and fluoride ion selective electrode probe.

## 4.4 RSSCT

The treated BC with the highest adsorption capacity from batch test 2, $H_3PO_4$ BC, was subjected to RSSCT, along with RBC, to compare the breakthrough behaviour of these. The full PD model and column parameters are given in appendix C 2.0.

## 4.4.1 RSSCT Sample Water Preparation

The sample water preparation was prepared using the same methodology outlined in section 4.3.2.

### 4.4.2 RSSCT Methodology

1. Adsorbents sieved to US standard mesh # 100 x # 200 (0.075 mm < x < 0.150 mm)

2. Adsorbent powder submerged in DI water and stirred for 24 h to ensure all pores are saturated with water

3. Saturated adsorbent powder packed into RSSCT column with pipette

4. Chromatography pump started up and DI water pumped through column

5. When desired flowrate reached, DI water switched out to sample water

6. Outlet samples taken hourly *, and sample fluoride concentration measured with colourimeter and fluoride ion selective electrode probe

7. As concentrations approach breakthrough, or when estimated breakthrough bed volume number approaching, samples taken at 15-minute intervals

* Samples take 15 minutes to fill, so concentrations represent the average over the 15-minute period

### 4.4.3 RSSCT Parameters

The PD-RSSCT was designed based on a pilot column comprised of a glass chromatography column with properties listed in table 4.4.3.1 along with the small column properties. The full RSSCT PD model parameters can be found in appendix C 2.0.

Table 4.4.3.1 - RSSCT column parameters

| Parameter | Large Column | Small Column |
|---|---|---|
| Column internal diameter ($d_{i,LC}$) [ cm ] | 2.54 | 0.48 |
| Adsorbent bed depth ($L_{LC}$) [ cm ] | 18 | 18 |
| Flowrate ($Q_{LC}$) [ mL/s ] | 0.0507 | 0.0212 |
| Mean particle size ($d_{p,LC}$) [ cm ] | 0.1285 | 0.0108 |
| Empty bed contact time ($EBCT_{LC}$) [ s ] | 1800 | 151.8 |
| Hydraulic loading rate ($v_{f,LC}$) [ cm/s ] | 0.010 | 0.119 |

### 4.4.4 RSSCT Sample Testing

Fluoride concentration of RSSCT treated samples were tested using colourimetry.

# 5.0 Results

## 5.1 Batch Test Results

Fluoride concentration of samples after 24 h batch tests were measured using colourimetry and fluoride ion selective electrode probe for all doses and their duplicates. Results were averaged across the four measured concentration values (colourimetry and fluoride ion selective electrode probe measures in duplicate). The positive and negative absolute errors were simply determined by finding the magnitude of the difference between the average and the largest and smallest readings respectively.

Despite flushing of samples with RO treated water until colourimetry inlet and outlet readings were consistent, there is a possibility that some phosphate species may have leached after being tumbled and exposed to water for a 24-hour period, this is particularly true for treated samples.

Error bars for equilibrium fluoride concentration were made by accounting for variation in duplicate readings and reported accuracy of the probe as stated by the manufacturers. Positive and negative errors are not equal as the average of the four total colourimeter and fluoride ion selective electrode probe readings was not equidistant from the largest and the smallest readings. Errors were calculated using standard error propagation methods.

Error bars for dose were not included as these were consistent, at 0.0035 g, insignificant relative to absolute values of dosage. However, error in dosage measurement was incorporated into adsorption capacity error calculations, as well as error in the pipette and volumetric flasks used to measure out the 90 mL water samples, shown in appendix B 2.4.5.

Batch experiment 2 results were split into two: chemically treated chars were compared to BC in one case, and chars with different non-chemical production process variations were compared to BC separately.

Isotherm model parameters for each BC from batch test 2 are given in appendix C 3.0.

## 5.1.1 Batch Test 1



Figure 5.1.1.1 - Sample water equilibrium fluoride concentration after 24-hour batch test 1

Figure 5.1.1.2 - Fluoride adsorption capacity of batch test 1 adsorbents. Vertical green dotted line represents equilibrium fluoride concentration of 1.5 mg/L.

### 5.1.1.1 Dose vs Equilibrium Fluoride Concentration

Figure 5.1.1.1 depicts the equilibrium fluoride concentration ($c_e$) of sample waters treated with the various doses of adsorbents, given in section 4.2.3.1.

RBC had the lowest value of $c_e$ at all doses, indicating its highest performance for fluoride uptake. CABC, KOH CAB and NaOH CAB had similar $c_e$ values, although NaOH CAB and KOH CAB had smaller dose ranges. $H_2SO_4$ CAB and $H_3PO_4$ CAB performed similarly, and worse than other tested samples.

Primary error in $c_e$ arose from variation in colourimeter and fluoride ion selective electrode probe readings. However, these errors were small, and indicate that the proposed uptake ranking of the adsorbents is accurate.

### 5.1.1.2 Isotherm Results

Isotherm graphs from batch test 1, given in figure 5.1.1.2, show that with the exception of RBC and CABC, there was no discernible trend in adsorption capacity for any of the CAB samples. RBC showed a type I isotherm shape, as expected for BCs. CABC had a type II or type III isotherm shape – different from that reported by Chatterjee *et al.* [101]. The CAB samples had clustered, irregular adsorption capacities with no visible trends. NaOH CAB had a constant adsorption capacity at approximately 1.2 mg/g across all equilibrium fluoride concentrations ($c_e$). KOH CAB's adsorption capacity was like that of NaOH CAB. $H_2SO_4$ CAB had an adsorption capacity of almost zero across all values of $c_e$. $H_3PO_4$ CAB's adsorption capacity was calculated to be negative at a $c_e$ value of approximately 8.7 mg/L – a value that has no physical meaning (the area in which this occurs is highlighted in red on figure 5.1.1.2). This is attributed to error in fluoride concentration measurements – the decrease in fluoride concentration for the sample in question was negligible, and the probe and/or colourimeter measured a fluoride concentration higher than the initial sample water, resulting in a negative calculated adsorption capacity. This is accounted for *via* the vertical error bars of the value, which extend above q = 0, and reflect the area at which the real value of the adsorption capacity at the equilibrium fluoride concentration. With the exception of RBC, batch 1 sample equilibrium fluoride concentrations for all adsorbents were too high across all doses to determine the adsorption capacity of these at $c_e$ = 1.5, or apply any known adsorption model to these in order to predict their adsorption capacities at other equilibrium fluoride concentrations.

### 5.1.1.3 CAB Synthesis Yield Results

Due to avoidable yield losses during the NaOH and KOH CAB syntheses, yields were calculated in steps to determine realistic total yield losses under the assumption that future syntheses are carried out with no avoidable losses. Table 5.1.1.3.1 gives the masses of samples throughout different synthesis stages.

Table 9.1.1.3.1 - Sample masses during CAB synthesis steps

| Sample | Initial Bone Meal Mass [ g ] | Pre-treatment Dry Mass [ g ] | Post-treatment Dry Mass [ g ] | Post-flushing Dry Final Mass [ g ] |
|---|---|---|---|---|
| Total | 325.0 | 163.5 (initially 261*) | 111.6 | 53.6 |
| $H_2SO_4$ CAB | | 16.2 | 11.1 | 2.9 |
| $H_3PO_4$ CAB | | 16.3 | 10.9 | 1.4 |
| KOH CAB | | 65.0 | 45.7 | 19.1 |
| NaOH CAB | | 66.0 | 43.9 | 30.2 |

*The initial bone meal mass decreased from 325 g to 261 g after NaOCl soaking and drying, however only 163.5 g of this was effectively used in syntheses.*

Yield losses from the post-treatment dry stage to the final post-flushing dry stage were not considered in yield calculations as in practice, CAB samples would not be flushed for use in continuous adsorption columns.

The initial soaking and drying of bone meal resulted in a 19.7 % yield loss.

Table 5.1.1.3.2 - Yield losses for sample production

| Sample | Pre- to Post-Treatment Yield Loss [ % ] | Total Yield Loss from Initial Bone Meal [ % ] |
|---|---|---|
| $H_2SO_4$ CAB | 29.7 | **43.5** |
| $H_3PO_4$ CAB | 33.5 | **46.6** |
| KOH CAB | 33.1 | **46.3** |
| NaOH CAB | 31.5 | **45.0** |

### 5.1.1.4 CABC Synthesis Yield Results

Table 5.1.1.4.1 gives the masses of samples throughout different synthesis stages.

Table 5.1.1.4.1 - Sample masses during CABC synthesis steps

| Sample | Initial BC Mass [ g ] | Pre-treatment Dry Mass [ g ] | Post-treatment Dry Mass [ g ] | Post-flushing Dry Final Mass [ g ] |
|---|---|---|---|---|
| CABC | 50.2 | 43.1 | 36.2 | 12.0 |

Yield losses from the post-treatment dry stage to the final post-flushing dry stage were not considered in yield calculations as in practice, CABC samples would not be flushed for use in continuous adsorption columns.

The total yield loss for CABC production was 27.9 %.

## 5.1.2  Batch Test 2
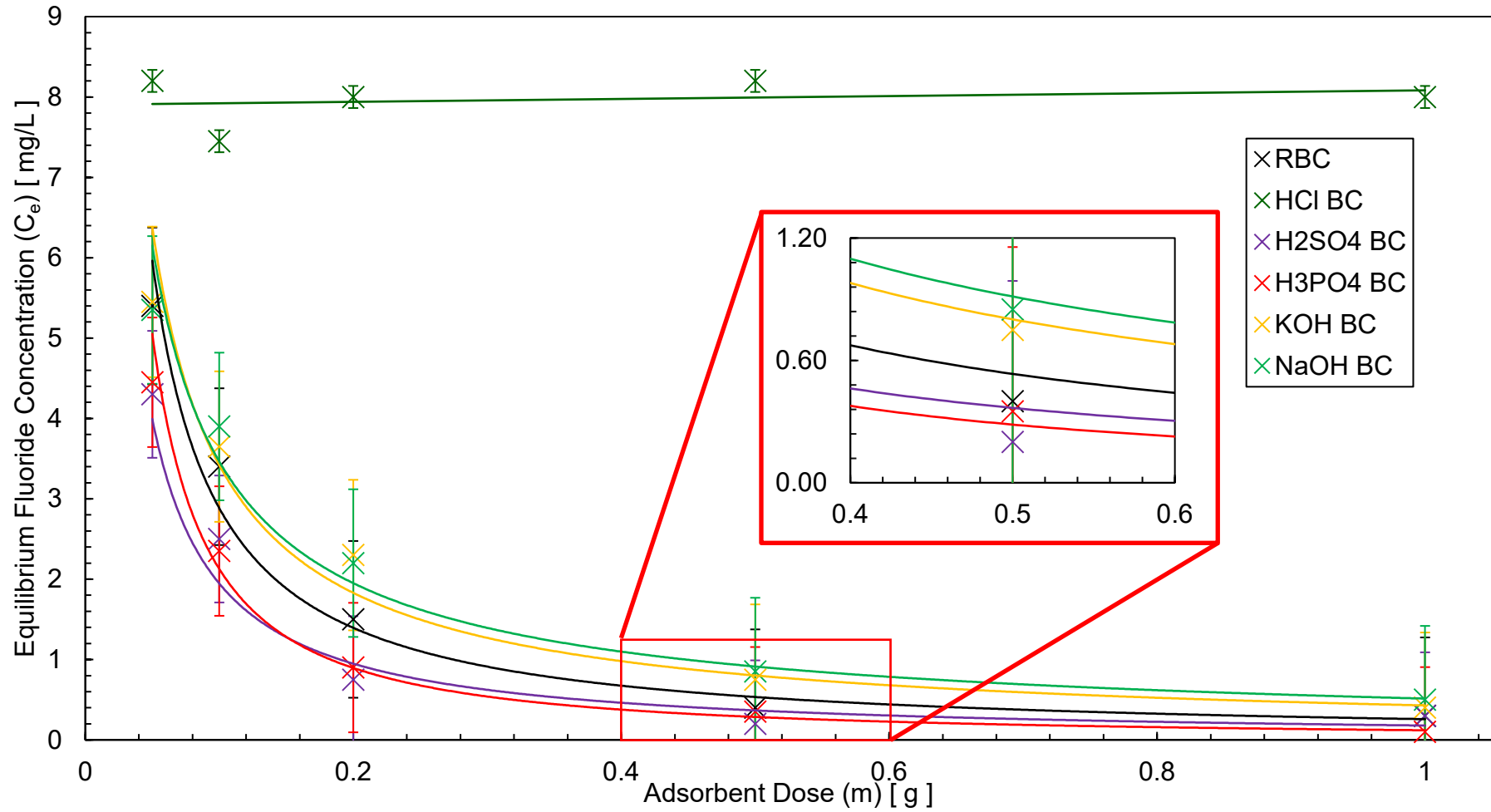


Figure 5.1.2.1 - Sample water equilibrium fluoride concentration after 24-hour batch test 2
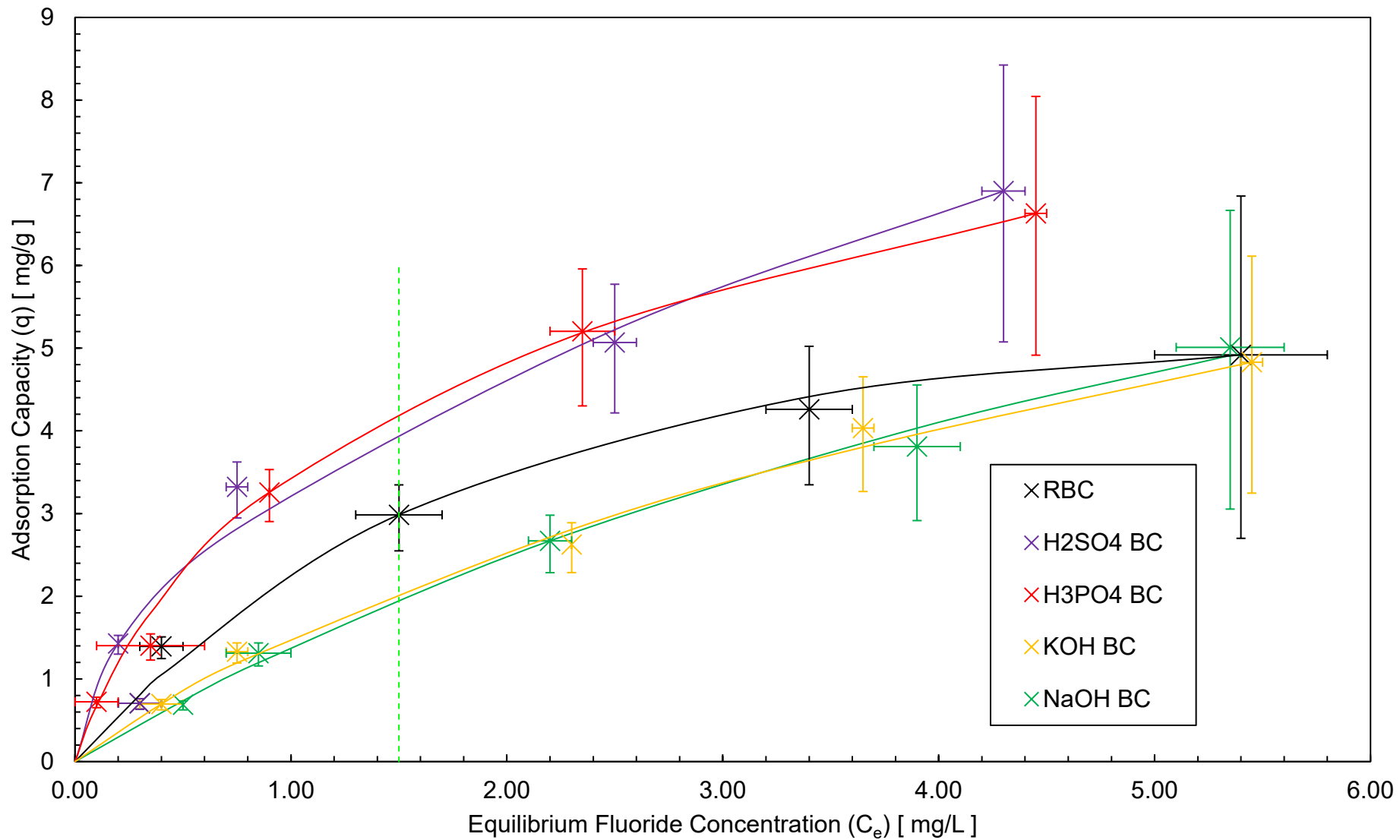
Figure 5.1.2.2 - Fluoride adsorption capacity of batch test 2 adsorbents. Vertical green dotted line represents equilibrium fluoride concentration of 1.5 mg/L.
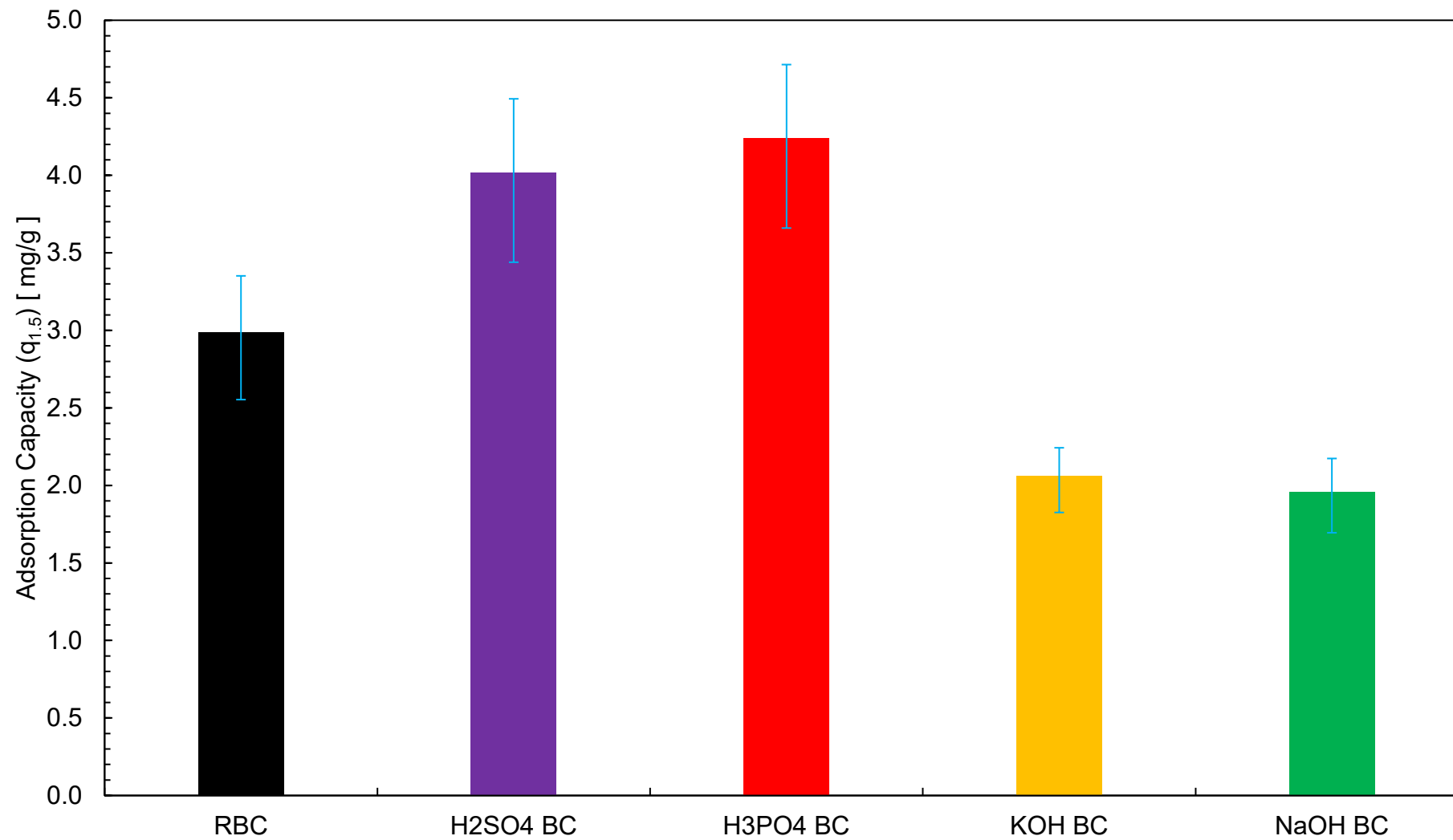
Figure 5.1.2.3 - Isotherm model predicted adsorption capacity of batch test 2 samples
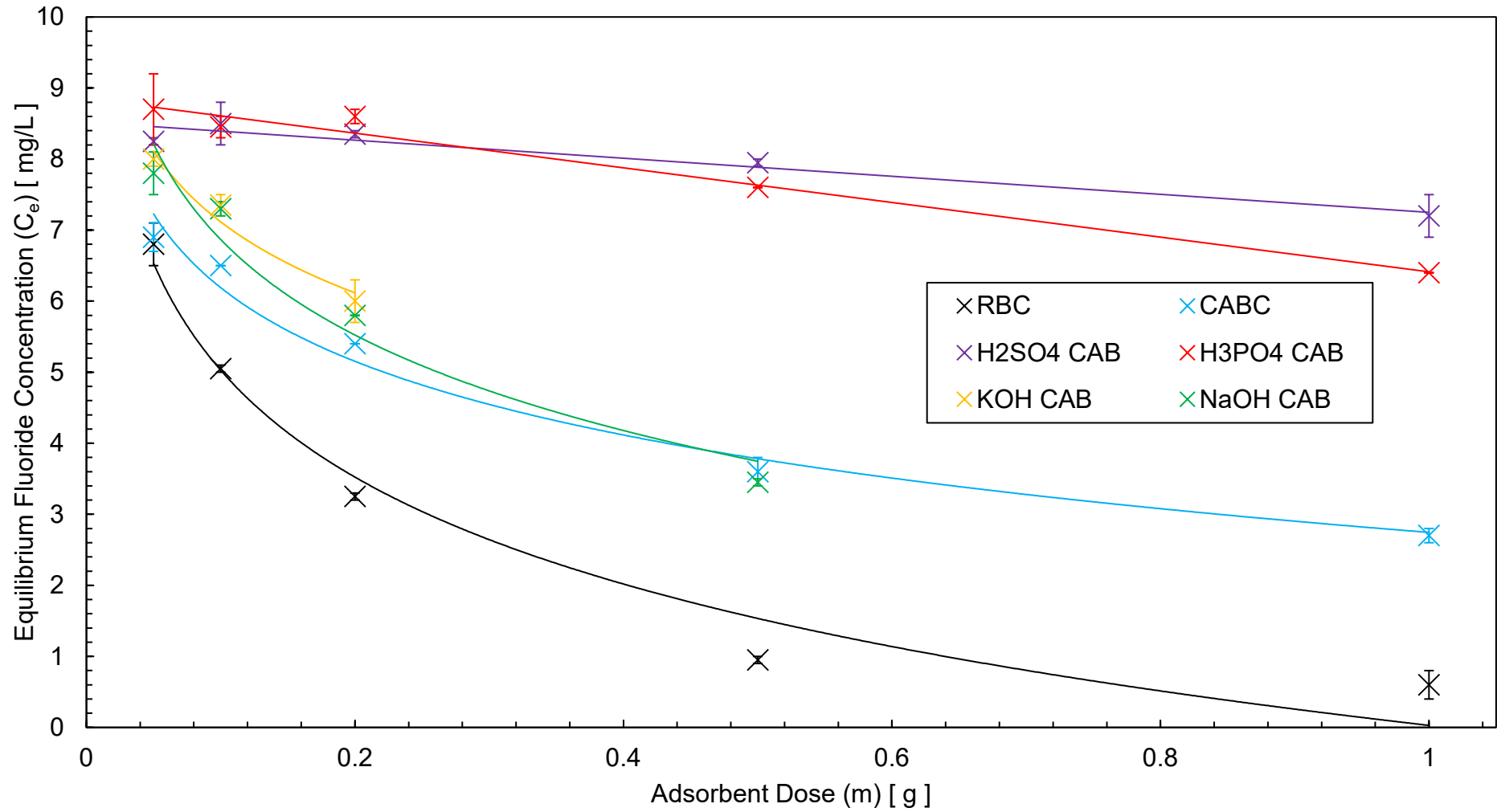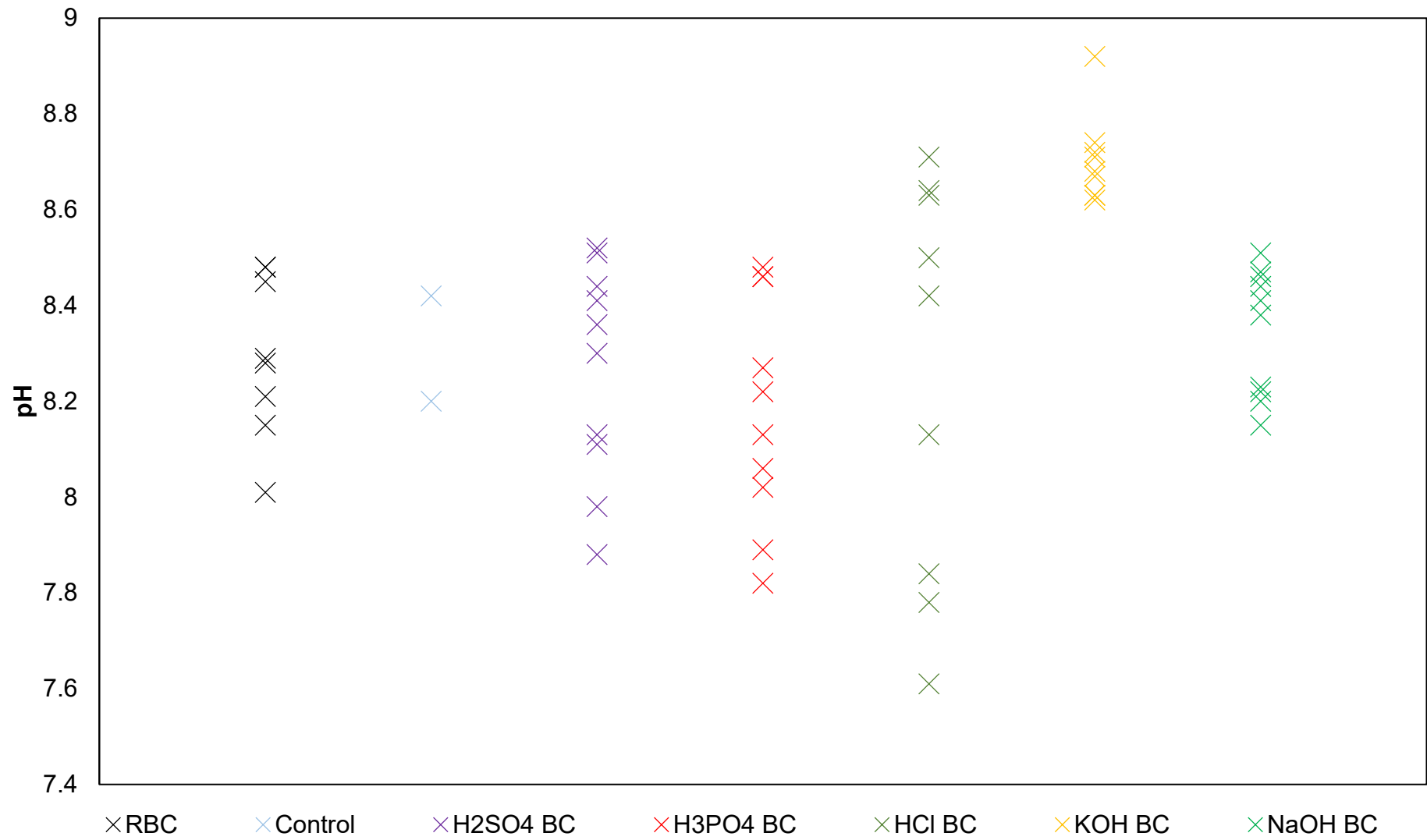
Figure 5.1.2.4 - pH values of batch test 2 samples
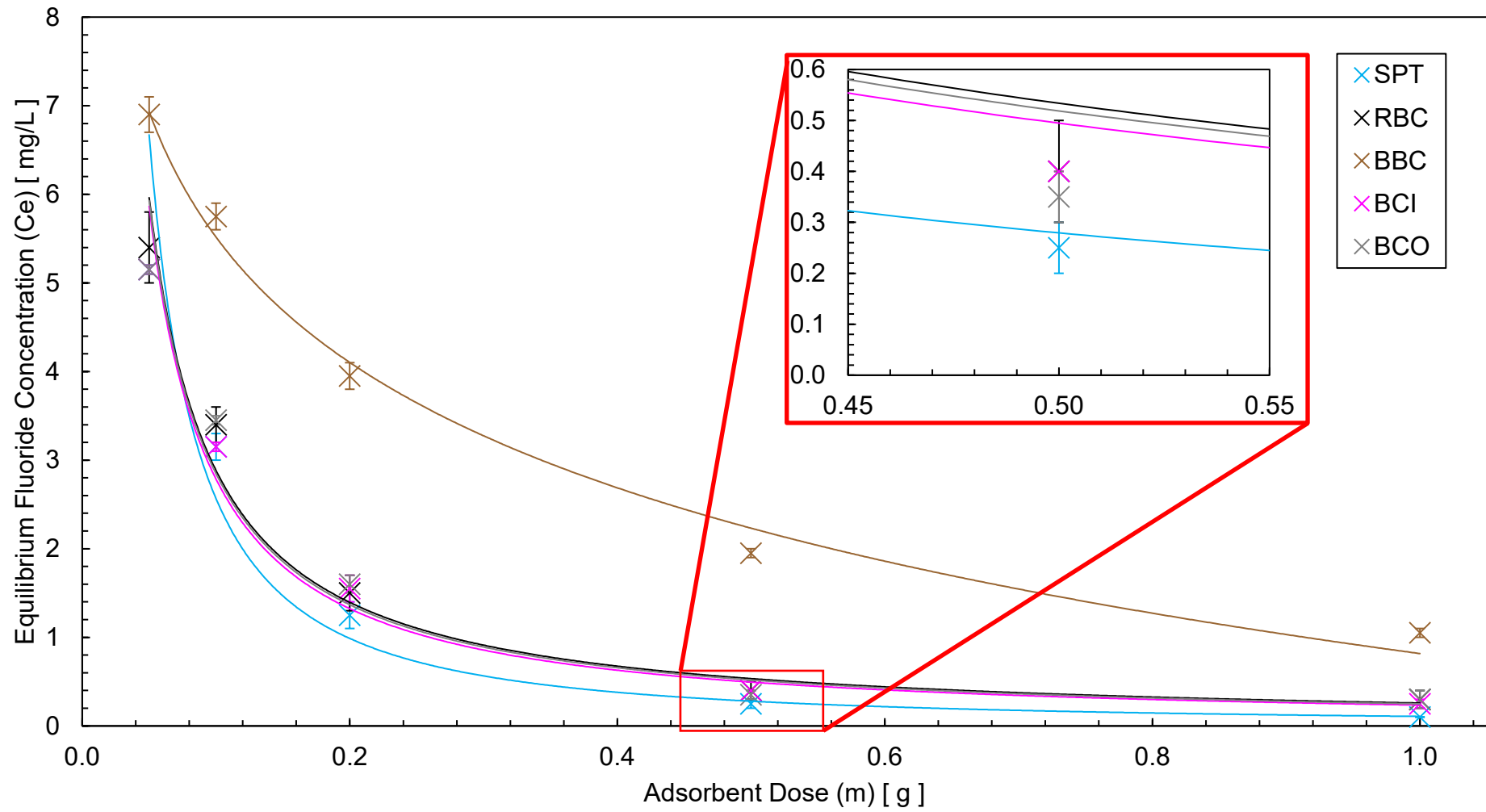
Figure 5.1.2.5 - Sample water equilibrium fluoride concentration after 24-hour batch test 2
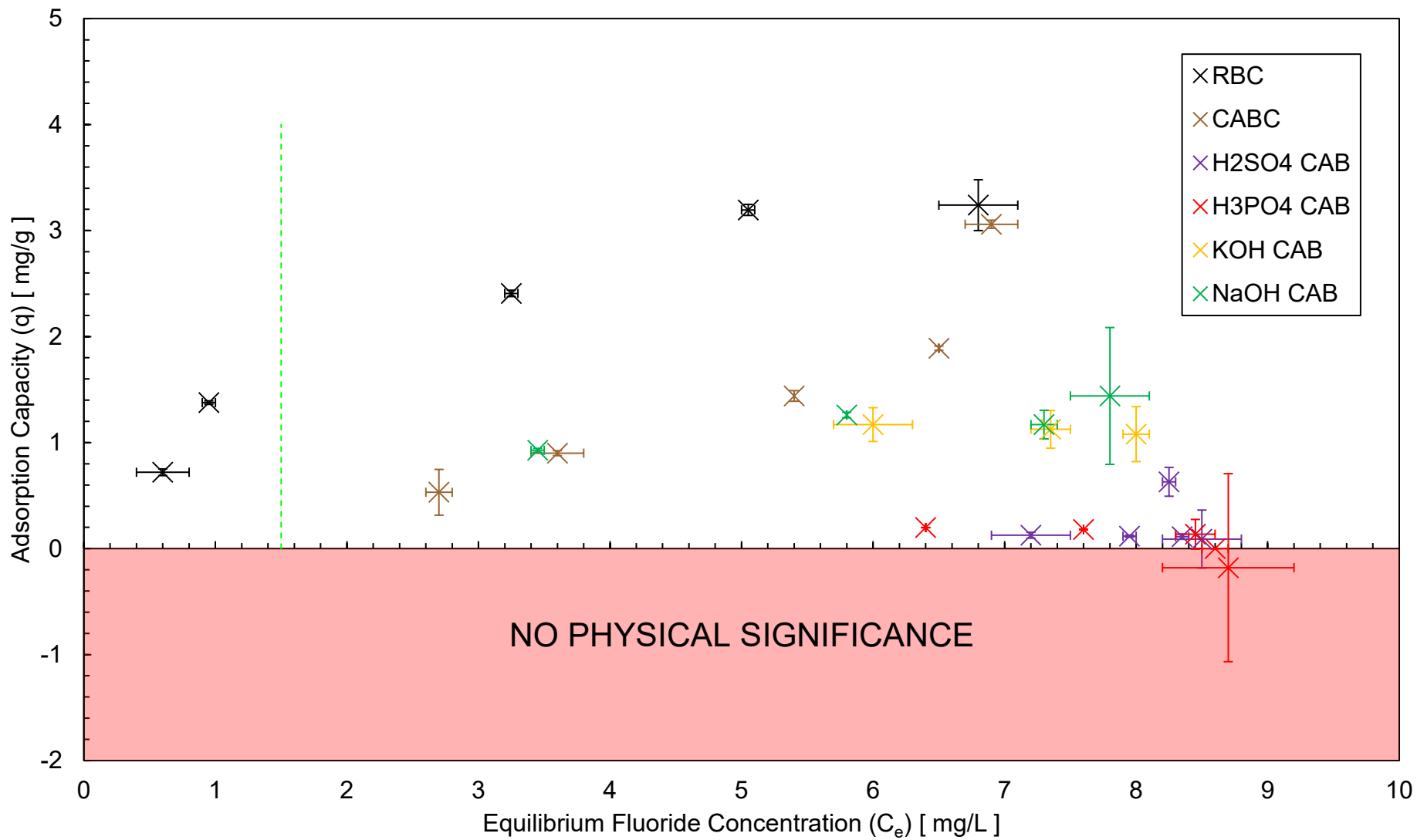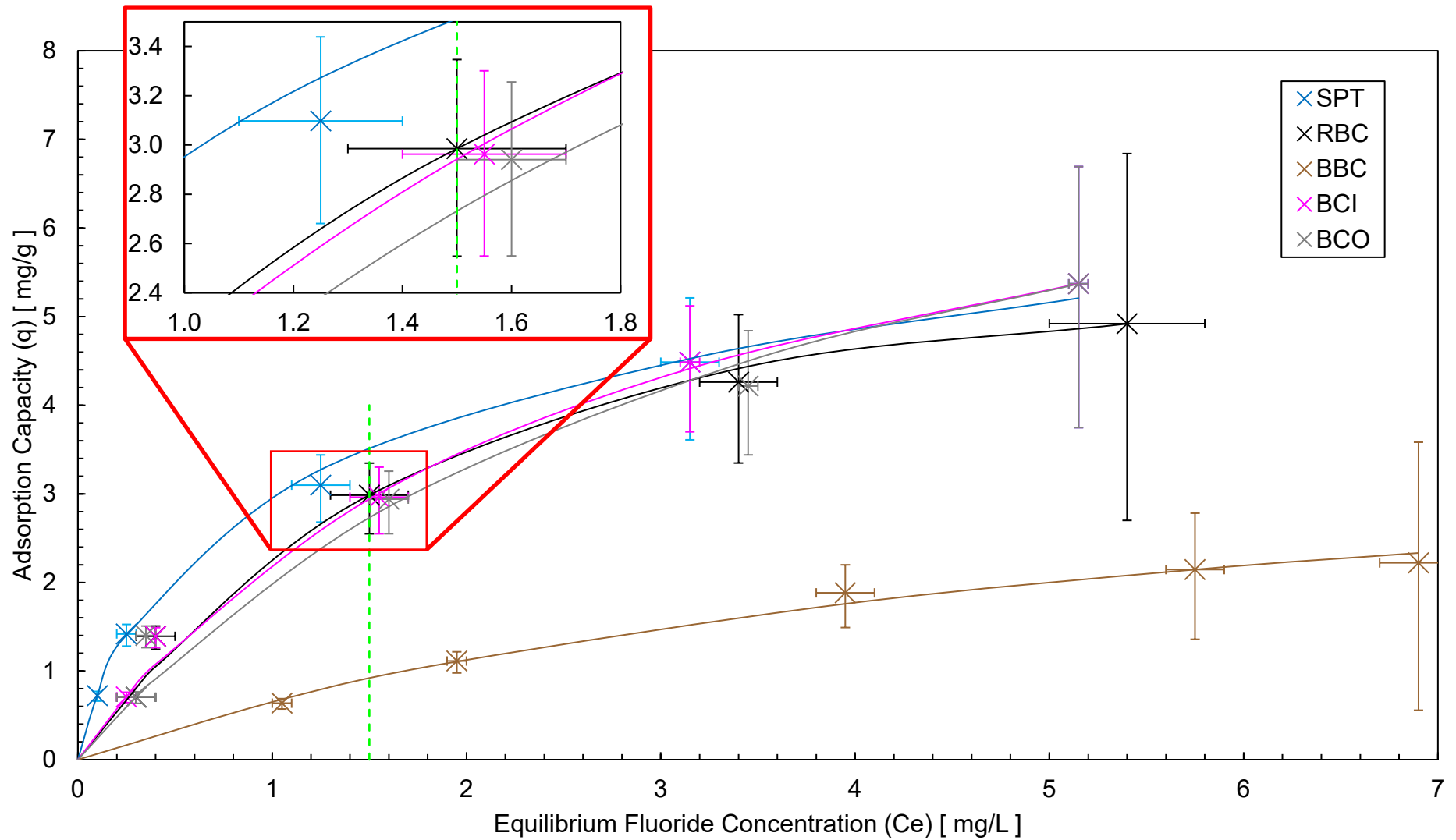
Figure 5.1.2.6 - Fluoride adsorption capacity of batch test 2 adsorbents. Vertical green dotted line represents equilibrium fluoride concentration of 1.5 mg/L.
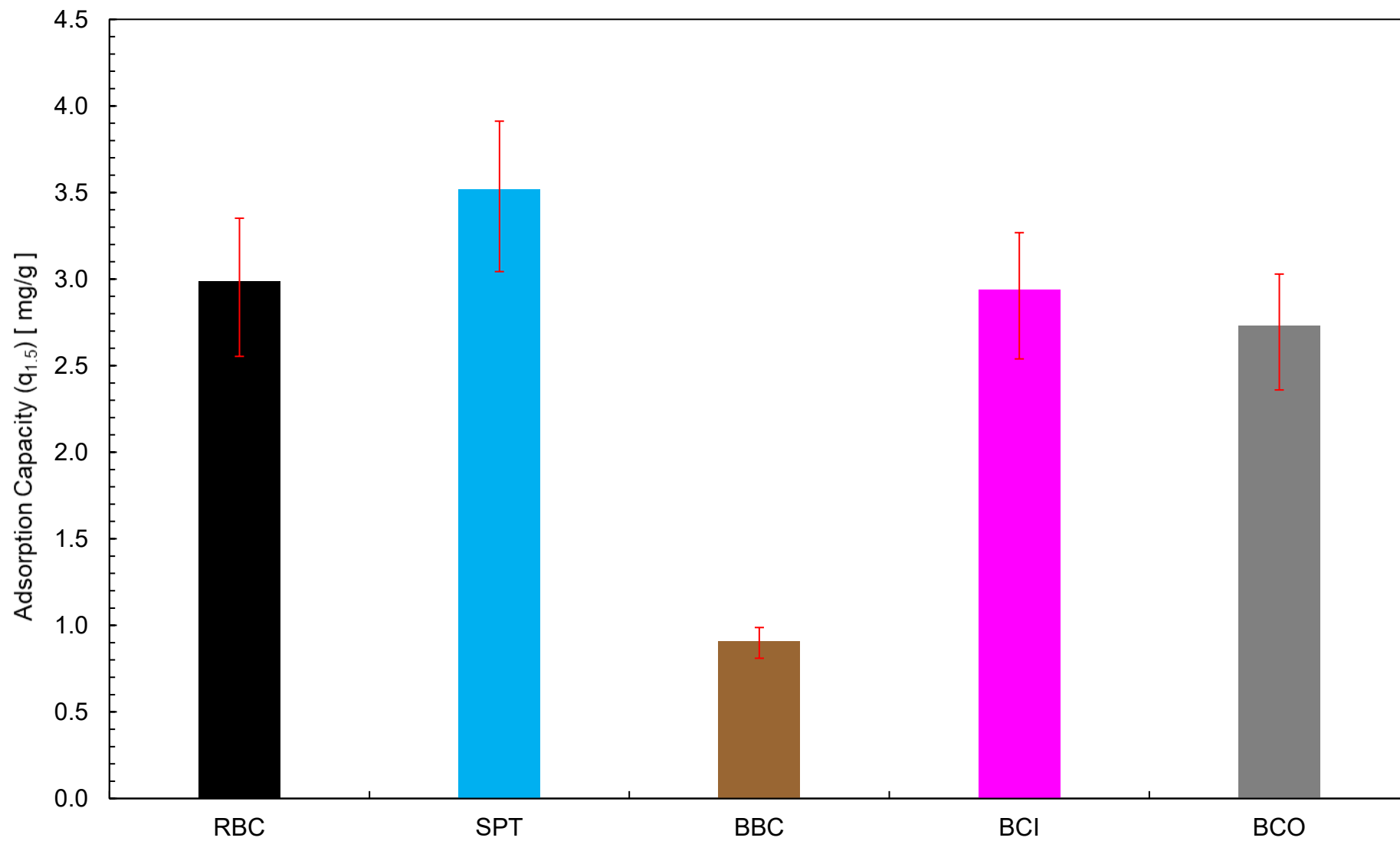
Figure 5.1.2.7 - Isotherm model predicted adsorption capacity of batch test 2 samples
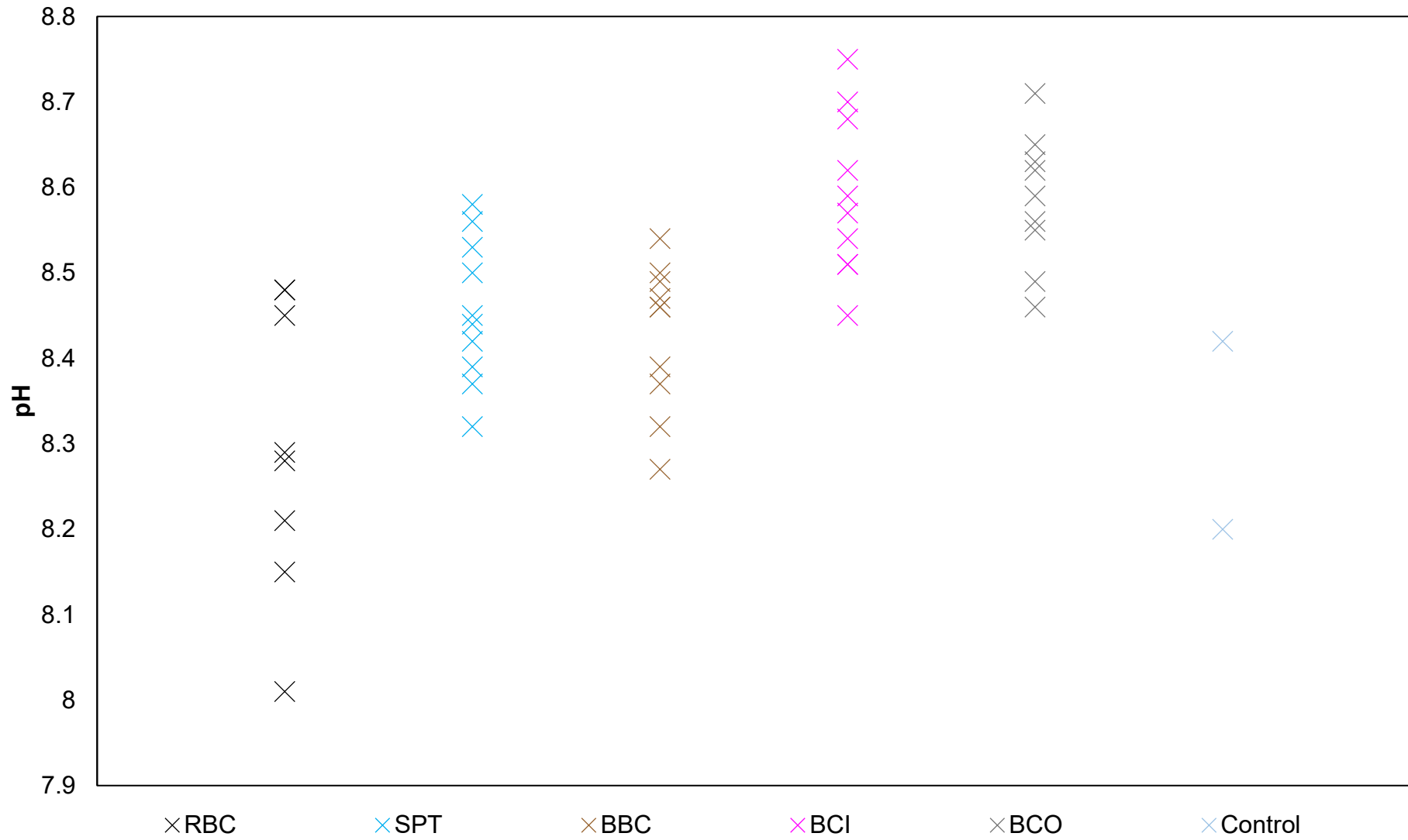
Figure 5.1.2.8 - pH values of batch test 2 samples

All chars tested showed type I isotherm shapes, as seen in figures 5.1.2.2 and 5.1.2.6. Each char type was modelled with three isotherm models: Langmuir, Freundlich and Prausnitz-Radke isotherms. Isotherm constants were determined by minimising the average relative error of the adsorption capacity predicted by the isotherm models compared to experimental data obtained, using the function developed by Marquardt [49], a method employed by several authors when modelling isotherms of BCs [35, 36, 49, 93, 110].

The average relative error was minimised by nonlinear optimisation using the generalised reduced gradient (GRG) method developed by Lasdon et al. [122]. GRG minimised error functions yielding the lowest average relative error for their respective isotherm models were deemed to best fit the data, and are depicted on figures 5.1.2.2 and 5.1.2.6.

### 5.1.2.1 Chemically Treated Bone Char Dose vs Equilibrium Fluoride Concentration

Figure 5.1.2.1 depicts the equilibrium fluoride concentration ($c_e$) of sample waters treated with the various doses of chemically treated BC adsorbents, as well as RBC, given in section 4.3.3.1.

$H_2SO_4$ BC and $H_3PO_4$ BC had similar equilibrium fluoride concentrations ($c_e$) across all adsorbent doses tested, these were the lowest $c_e$ values of all the chars, indicating these were the most effective at fluoride uptake. NaOH BC and KOH BC also had very similar $c_e$ values and performed worse than other BC samples. RBC performance was between acid and base treated samples. HCl BC equilibrium fluoride concentration was essentially constant at 8 mg/L across all doses, indicating no, or insignificant, fluoride uptake across all doses. The error bar width indicates the possibility that sample performance ranking proposed is in fact in a different order $-c_e$ error bars overlap across all samples at all doses tested, with the exception of HCl BC doses.

### 5.1.2.2    Chemically Treated Bone Char Isotherm Results

Table 5.1.2.1.1 gives the isotherm model used, total model relative error, and model predicted adsorption capacity at equilibrium fluoride concentration of 1.5 mg/L ($q_{1.5}$).

Table 5.1.2.1.1 - Adsorbent isotherm model adsorption capacities and model errors

| Adsorbent | Isotherm Model | $q_{1.5}$ [ mg/g ] | Total Model Relative Error [ % ] |
|---|---|---|---|
| RBC | Prausnitz-Radke | 2.99 | 8.50 |
| $H_3PO_4$ BC | Prausnitz-Radke | 4.24 | 7.11 |
| $H_2SO_4$ BC | Freundlich | 4.02 | 4.57 * |
| KOH BC | Prausnitz-Radke | 2.06 | 4.58 |
| NaOH BC | Langmuir | 1.96 | 4.68 |

*The experimental point at equilibrium fluoride concentration ($c_e$) = 0.3 was omitted when applying isotherm models to the data, as the point was deemed anomalous and deviated significantly from the isotherm shapes. Removing the anomalous point reduced the average relative errors by over 20 % across all models.*

HCl isotherm data was not included in figure 5.1.2.2, as data was clustered, with no visible correlation when plotted on a graph, and experimental adsorption capacities close to zero, or slightly negative at all equilibrium fluoride concentrations (which were between 7.45 mg/L to 8.00 mg/L at all doses).

Adsorption capacity error around $c_e$ = 1.5 was relatively low, and there is no overlap between acid treated BC groups, base treated BC groups and RBC, confirming that acid treated chars had the highest fluoride adsorption capacity at $q_{1.5}$. However, there is overlap between $H_2SO_4$ BC and $H_3PO_4$ BC, as well as between KOH and NaOH BC, meaning these cannot be feasibly ranked amongst themselves. Adsorption capacity error is seen to increase as $c_e$ is increased.

Isotherm model predicted adsorption capacities for the chars are shown in figure 5.1.2.3. Error bars were determined by linear interpolation of error magnitude at experimental points either side of $c_e$ = 1.5.

### 5.1.2.3    Chemically Treated Bone Char Treated Water pH

Final pH of water samples treated with all adsorbent types, doses and duplicates are shown in figure 5.1.2.4. Error bars were omitted due to pH probe instrument error being insignificant.

### 5.1.2.4    Chemically Treated Bone Char Yield Results

Table 5.1.2.4.1 gives the masses of BC before treatment and after flushing and drying stages as well as the total yield losses. Although in practice, samples would not be flushed before being added to continuous adsorption columns. The dry, post-treatment masses of treated BC samples was not recorded.

Table 5.1.2.4.1 - Initial and final masses of chemically treated BC samples and total yield losses

| Sample | Initial BC Mass [ g ] | Post-Flushing Dry Mass [ g ] | Total Yield Loss [ % ] |
|---|---|---|---|
| $H_2SO_4$ BC | 100 | 86 | **14** |
| $H_3PO_4$ BC | 100 | 89 | **11** |
| HCl BC | 100 | 5 | **95** |
| KOH BC | 100 | 94 | **6** |
| NaOH BC | 100 | 84 | **26** |

### 5.1.2.5    Production Process Modified Bone Char Dose vs Equilibrium Fluoride Concentration

Figure 5.1.2.5 depicts the equilibrium fluoride concentration ($c_e$) of sample waters treated with the various doses of production process modified BC adsorbents, as well as RBC, given in section 4.3.3.1.

Except for BBC, all BCs tested showed very similar values of $c_e$, therefore fluoride uptake amounts, across all doses. SPT BC had slightly lower value of $c_e$ than the other BCs, although error bar overlaps indicate that this may not be the case. Apart from BBC, equilibrium fluoride concentration error bars overlap for all adsorbents across all doses – this is shown in more detail on the detail zoom shown in figure 5.1.2.5.

### 5.1.2.6 Production Process Modified Bone Char Isotherm Results

Table 5.1.2.6.1 gives the isotherm model used, total model relative error, and model predicted adsorption capacity at equilibrium fluoride concentration of 1.5 mg/L ($q_{1.5}$):

Table 5.1.2.6.1 - Adsorbent isotherm model adsorption capacities and model errors

| Adsorbent | Isotherm Model | $q_{1.5}$ [ mg/g ] | Total Model Relative Error [ % ] |
|:---:|:---:|:---:|:---:|
| RBC | Prausnitz-Radke | 2.99 | 8.50 |
| SPT | Prausnitz-Radke | 3.52 | 2.10 |
| BCI | Prausnitz-Radke | 2.94 | 5.14 |
| BCO | Langmuir | 2.73 | 10.47 |
| BBC | Langmuir | 0.91 | 3.76 |

Despite adsorption capacity error around $c_e$ = 1.5 being relatively low, complete error overlap between RBC, SPT, BCI and BCO at this point makes impossible to rank these. Adsorption capacity error is seen to increase as $c_e$ is increased.

Isotherm model predicted adsorption capacity for the chars is in figure 5.2.1.7. Error bars were determined by linear interpolation of error magnitude at experimental points either side of $c_e$ = 1.5.

### 5.1.2.7 Production Process Modified Bone Chars Treated Water pH

Final pH of water samples treated with all adsorbent types, doses and duplicates are shown in figure 5.1.2.8. Error bars were omitted due to pH probe instrument error being insignificant.

## 5.2    RSSCT Results
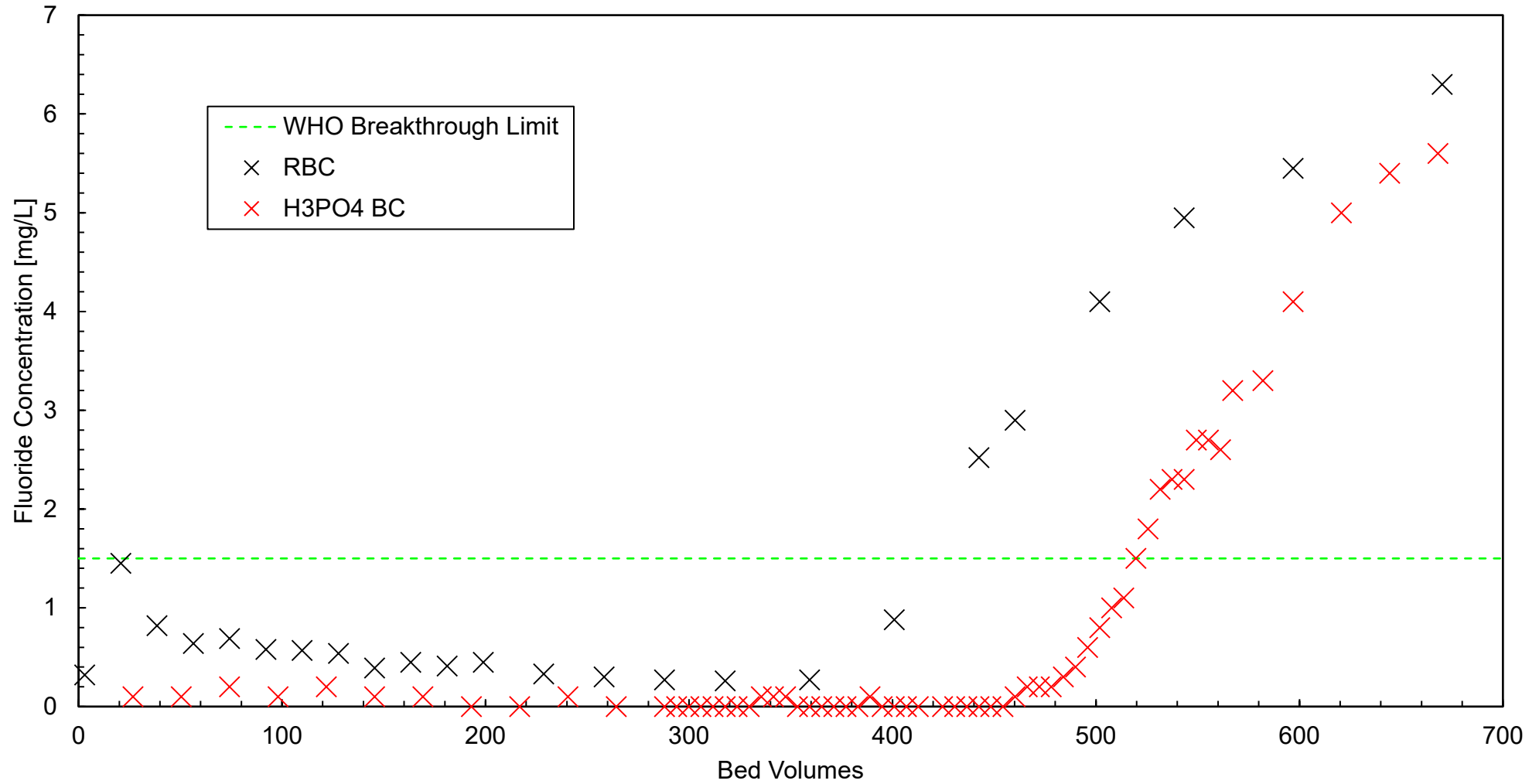


Figure 5.2.1.1 - RSSCT breakthrough curves of $H_3PO_4$ BC and RBC

Figure 5.2.1.1 shows the RSSCT breakthrough curves of $H_3PO_4$ BC and RBC.

Fluoride breakthrough occurred at 520 BV for $H_3PO_4$ BC. Linear interpolation was used to estimate breakthrough BV for RBC at 417 BV.

Error bars are not included as fluoride measurements were taken once per sample, and instrument error of the colourimeter is insignificant. Bed volume error is also insignificant as the chromatography pump used in the RSSCT system was running at a constant pumping speed.

# 6.0  Discussion

The results of the various experiments undertaken during this project are discussed here. It is important to note that CdA's limited resources prevent many forms of laboratory analysis, characterisation and other experiment types typically conducted by authors across literature seeking to learn about fluoride adsorption with BC. However, an attempt to understand the results and contextualise them through theoretical concepts presented in section 2 as well as previous research discussed in section 3 has been made. This section also presents an economic analysis of the treated BC for fluoride removal, to determine whether the objectives of the project have been met, and to which degree.

## 6.1  Batch Test 1

Batch test 1 was undertaken with the aim of replicating the results produced by Yami *et al.* [97] as well as those by Chatterjee *et al.* [101].

### 6.1.1 Method Justification - Yami *et al.*

The chemical treatment proposed by Yami *et al.* [97] was selected as this produced treated bone and BC with the highest adsorption capacity of samples reviewed in literature (see table 3.5.3.2). $H_2SO_4$ and $H_3PO_4$ treated bone performed the best, with treated cow bone followed by a pyrolysis step performing slightly better than non-pyrolysed samples. Pyrolysis however was not undertaken, as the adsorption capacity gains were deemed too small to justify the economic and labour expenses of pyrolysis. Although not explored by Yami *et al.*, NaOH treatment of cow bone was also undertaken, due to its chemical similarities to KOH, cheaper cost, and greater availability.

During the CAB preparations, the raw bone chunks proved to be too difficult to break down with a hammer and the manual crusher. Bone meal was therefore obtained from an external supplier, as a side product from a local abattoir, and used for synthesis. The composition of this bone meal was unknown, and by appearance contained a large proportion of organic matter (e.g. fat). The supplier claimed the bone meal to contain a minimum of 60 wt. % bone, although this was unverifiable.

### 6.1.2 Method Justification - Chatterjee *et al.*

The treatment method proposed by Chatterjee *et al.* [101] was selected due to a seemingly promising presentation of the adsorption capacity results by the authors of the paper. Specifically, the adsorption capacity of the $Al_2(SO_4)_3$/CaO doped BC is given throughout the paper as 150 mg/g; two orders of magnitude greater than the capacities of other bone based adsorbents reported in literature. The doped BC is specifically said to be ideal for applications in removing fluoride for drinking water purposes. The remarkably high adsorption capacity is even compared to other BC adsorbents that report capacities more typical of those found in literature. However, the paper fails to mention in words that this adsorption capacity of 150 mg/g is at a $c_e$ of 1000 mg/L fluoride, as opposed to 1.5 mg/L, the standard usually adhered to when reporting fluoride adsorption capacities in literature. A $c_e$ of 1000 mg/L is also far too high to have any useful applications in drinking water treatment.

After results showing disappointingly low adsorption capacities from batch test 1 for this doped adsorbent, a review of the supplementary information provided by the authors yielded the Langmuir parameters, which were calculated to give the $q_{1.5}$ of the $Al_2(SO_4)_3$/CaO doped BC of 1.27 mg/g.

### 6.1.3 Synthesis Notes - Yami *et al.*

Significant yield reduction occurred during the course of CAB synthesis while following the methodology proposed by Yami *et al.* [97]. The slurry-like bone meal was soaked in 13 wt. %. NaOCl solution for 24 h to remove organic impurities. Figure 6.1.3.1 depicts the resulting slurry after soaking. It is clear from the figure that even after soaking, a significant proportion of organic matter remained.

Figure 6.1.3.1 - Bone meal slurry after soaking for 24 h in 13 wt. % NaOCl. Left: Side view. Right: Top view.

The cake was filtered using a coffee filter and dried for approx. 3 h at 60 ± 20 °C (as depicted in figure 4.1.1.1) after rolling this flat onto an aluminium sheet with a PVC pipe and separated into four batches for treatment. Figure 6.1.3.2 shows the dry bone meal.



Figure 6.1.3.2 - Dry bone meal

Drying the $H_2SO_4$ and $H_3PO_4$ treated bone samples resulted in some filter paper drying with this and sticking to the treated bone meal. These were discarded and resulted in some yield losses. The acid treated CAB samples are depicted in figure 6.1.3.3.

Figure 6.1.3.3 - Left: $H_2SO_4$ CAB. Right: $H_3PO_4$ CAB.

Preparing 50 wt.% KOH and NaOH solutions was impossible, as solid impurities in the KOH pellets and NaOH flakes suspended in their respective solutions made it impossible to determine at which point saturation had occurred. Base addition was therefore halted when solid particles in suspension were observed, resulting in KOH and NaOH solutions of 34.3 wt. % and 31.8 wt. % respectively.

The NaOH treated CAB was left to dry on aluminium foil after rinsing with DI water. The remaining NaOH that was not rinsed away by DI water subsequently reacted with the surface of the aluminium foil with the following series of reactions:

$$2\,Al + 6\,H_2O \rightarrow 2\,Al(OH)_3 + 3\,H_2 \qquad (6.1.3.1a)$$

$$Al(OH)_3 + NaOH \rightarrow Na^+ + [Al(OH)_4]^- \qquad (6.1.3.1b)$$

$$Al_2O_3 + NaOH + 3\,H_2O \rightarrow 2\,Na^+ + 2\,[Al(OH)_4]^- \qquad (6.1.3.1c)$$
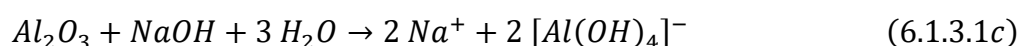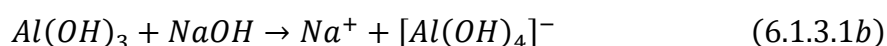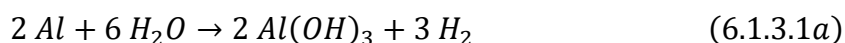
These reactions describe the formation of free sodium ions, which attack the aluminium foil and corrode this. The initial NaOH CAB batch was therefore discarded, and the dry bone meal reserved for KOH treatment was split in two, for both NaOH and KOH treatments.

The KOH CAB batch was spread onto baking paper purchased from a local store in order to prevent the basic attack on aluminium that had occurred with the NaOH CAB. However, upon oven drying, the waxy surface layer of the baking paper melted into sample (depicted in figure 6.1.3.4), which was then discarded.

Figure 6.1.3.4 - Wax melted into KOH CAB sample.

A glass Pyrex dish was therefore obtained to dry both base treated CAB samples. Figure 6.1.3.5 shows the dry base treated CAB samples.



Figure 6.1.3.5 - Left: Dry KOH CABC. Right: Dry NaOH CABC.

Recovering and drying CAB samples after flushing resulted in more significant yield losses, resulting in KOH and NaOH CAB samples not having sufficient adsorbent material to carry out the full range of doses planned in batch test 1 (see table 4.3.2.1.1). Figure 6.1.3.6 shows the dry, flushed and sieved CAB samples that were subsequently used in batch test 1.

Figure 6.1.3.6 - Top left: H2SO4 CAB. Top right: H3PO4 CAB. Bottom left: KOH CAB. Bottom right: NaOH CAB.

## 6.1.4  Synthesis Notes - Chatterjee *et al.*

The CABC synthesis was undertaken with no complications, and yielded a solid grey cake as shown in figure 6.1.4.1.



Figure 6.1.4.1 - Left: dry CABC cake on filter paper. Right: Close-up of CABC cake piece.

The cake was pulverised with a mortar and pestle for use in batch test 1.

### 6.1.5  Experimental Results - Yami *et al.*

The poor performance and unexpected isotherm behaviour of the CAB adsorbents seen in figures 5.1.1.1 and 5.1.1.2 indicate that either:

1. The synthesis of the adsorbents was undertaken incorrectly
2. There was little control over the composition and therefore performance predictability of the synthesised adsorbents due the unknown bone vs organic matter ratio
3. The batch test was undertaken incorrectly
4. The interferences measured by the colourimeter and/or fluoride ion selective electrode probe gave inaccurate results
5. A combination of the above

Given the experimental limitations that were encountered during the CAB syntheses, several factors prevented the experiment from being replicated faithfully including:

1. The apparent saturation of KOH and NaOH solutions before reaching 50 wt. %
2. The unavailability of a hot plate to heat solutions to 50 °C while stirring these as was done by the original authors [97]
3. The thickening of the slurries during the soaking, preventing adequate stirring

It is therefore possible that the incorrect synthesis of the CAB samples had a part to play in the results observed.

Due to the fact that the starting material was a bone meal with a reported, but unconfirmed bone content of 60 wt. % and an unknown true composition, it is likely that there was little control over the behaviour of this whilst following synthetic steps outlined by Yami *et al.*, and that the final treated bone content was unknown. This makes this very likely to have caused the poor performance and unpredictable isotherm behaviour.

The RBC behaved predictably, displaying an isotherm shape very similar to the Freundlich isotherm observed by Yami *et al.*, as well as having a $q_{1.5}$ within the range of BCs tested by the authors. This rules out the possibility that the batch test itself was undertaken incorrectly, making it highly unlikely for this to explain the phenomena observed.

The only possible interference that could be experienced by the fluoride ion selective electrode probe arises from the presence of free $Al^{3+}$ ions in solution leached from the CABC. The colourmieter will however experience interference from leached $PO_4^{3-}$ groups. However as mentioned in section 4.2.4, quantitative results deviating by more than 0.2 mg/L were re-tested, ruling out the possibility of any instrument interferences from the CAB adsorbents.

### 6.1.6 Experimental Results - Chatterjee *et al.*

The isotherm shape of the CABC synthesised (seen in figure 5.1.1.2) indicated type II or type III adsorption, as shown in figure 2.6.1.

A type II isotherm behaviour is typical of a non-porous or macro-porous adsorbent, and represents monolayer-multilayer adsorption [123].
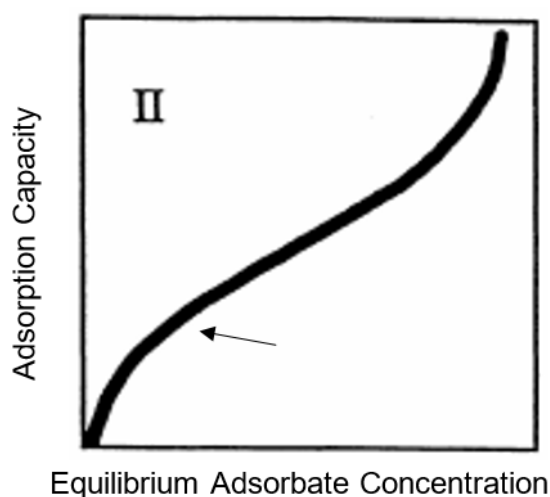


*Figure 6.1.6.1 - IUPAC type II isotherm shape. The arrow at the beginning of the pseudo-linear section represents the point at which monolayer coverage is complete, and multilayer adsorption is about to begin. [44]*

If the CABC isotherm is of type II, a possible reason for this is the destruction or enlargement of existing pores on the BC during the doping process, which would result in the adsorbent becoming non-porous or macro-porous respectively.

Type III isotherms indicate unrestricted multilayer adsorption which forms because lateral adsorbate-adsorbate interactions are comparatively stronger than adsorbent-adsorbate interactions [123]. This is a highly unlikely scenario, as fluoride ions will naturally repel each other due to their overall negative charges.

99

It is likely that although the synthesis was conducted according to the methodology laid out by Chatterjee *et al.*, the BC pores were either enlarged or destroyed during the synthesis. This would explain both the type II isotherm shape of the CABC observed in figure 5.1.1.2, as well as the fact that by visual inspection, $q_{1.5}$ is smaller than the 1.27 mg/g calculated using the Langmuir parameters provided by the authors.

## 6.2 Batch Test 2

Batch test 2 was undertaken with the aims outlined in section 4.3.

### 6.2.1 BC Chemical Treatment Method Justification

Following the results from batch test 1, it was hypothesised that the poor results observed were primarily due to the unknown composition of the bone meal used to synthesise the CAB. It was therefore decided to base the syntheses again on the method proposed by Yami *et al.* [97]. However, due to the difficulty in crushing and processing cow bone, it was decided to reverse the chemical treatment and pyrolysis steps undertaken by the authors, and treat BC with acids and bases.

HCl was added as another acid for treatment due to its chemical similarity to $H_2SO_4$ and $H_3PO_4$ as well as its low price and high availability, the same reasons NaOH was added as another base.

### 6.2.2 BC Production Process Modification Method Justification

The shorter pyrolysis time (SPT) BC was investigated to determine if it would be possible to produce a viable BC adsorbent by burning only one wood pellet retort, saving on fuel costs, production time, and labour costs.

The commercial Brazilian bone char (BBC) was included in batch experiment 2 to determine if purchasing a commercial BC has any economic advantage over producing BC *in situ*, as is currently done by CdA.

The inner and outer BC material (BCI and BCO respectively) were also selected as adsorbents in batch test 2 in an attempt to determine if the softer, more easily pulverised inner core was in fact composed of a greater proportion of non-HAP material, such as organic matter, than the harder outer 'shell'. This was done to see if these had any significant difference in adsorption capacity, with the potential of harnessing these differences in future.

## 6.2.3  Synthesis Notes - Chemically Treated BC

The initial aims of this experiment were to apply a modified methodology based on the work conducted by Yami *et al.* [97]. However, it was also initially decided to push the acid and base concentration as high as possible, to see if this could produce any positive effect on the adsorption capacity of the BC, as a proof of concept of sorts.

The addition of 98 wt. % $H_2SO_4$ to BC led to the immediate vigorous bubbling of the solution, a rapid temperature rise and the emission of a choking, unpleasant smelling vapour, requiring the evacuation of the laboratory. The remaining sludge was inspected after emissions ceased, and it was observed that the acid had completely dissolved the BC. A 2:1 mass ratio of 85 wt. % $H_3PO_4$ solution to BC left behind a thick, almost solid sludge. This ratio was increased to 5:1, however the BC was observed to dissolve.

At the advice of Dr Joshua Kearns (personal communication, May 2018), the $H_2SO_4$ and $H_3PO_4$ concentrations were decreased to 0.1 M (0.98 wt. % for both acids).

Undiluted muriatic acid (38 wt. % HCl solution) was used to treat BC. Although not appearing to dissolve the BC initially, significant yield losses of 95 % were observed by the end of the full treatment (post-RO flushing).

10 wt. % KOH and 20 wt. % NaOH solutions were used to treat BC. These were chosen to ensure no suspended solids would be observed in these solutions, therefore guaranteeing complete dissolution of the solid bases.

After treatment, flushing, drying and sieving synthesis stages, all the adsorbents had the same, black granular appearance of untreated BC, as shown in figure 6.2.3.1:



*Figure 6.2.3.1 - Dry RBC sieved through US standard # 30 mesh for use in batch test 2*

## 6.2.4  Preparation Notes - Production Process Modified BC

All BCs were prepared according to the procedure outlined in section 4.3.1. The detailed procedure can be found in appendix B 2.4.3.

The BCI had a distinctly shinier appearance than the BCO after pyrolysis, separation, and crushing. This is shown in figure 6.2.3.2.



*Figure 6.2.3.2 - Left: Crushed BCI. Right: Crushed BCO.*

During RO flushing, the SPT outlet water was yellow in colour and had a distinct 'burnt' smell to it. It was decided to continue flushing this until outlet water was clear and odourless. Figure 6.2.3.3 shows the yellow coloured SPT RO flush outlet water.



*Figure 6.2.3.3 – SPT RO flush yellow outlet water*

### 6.2.5 Experimental Results - Chemically Treated BC

The HCl BC dose vs equilibrium fluoride concentration curve given in figure 5.1.2.1 shows essentially no fluoride removal at any of the doses tested, with the exception of the likely anomalous result at the 0.1 g dose, which shows approximately 0.5 mg/L fluoride removal. The reason this BC showed no adsorption is most likely because the concentrated HCl solution used to synthesise the BC destroyed any pores on the adsorbent *via* strong acidic corrosion, drastically reducing its overall surface area. This is corroborated by the significant yield losses of 95 % observed during the synthesis of this BC. It is possible that the PZC of the adsorbent was also lowered, thereby reducing the adsorption capacity of this. This is evidenced in figure 5.1.2.4, which shows a reduction in solution pH following adsorption related to the dose of adsorbent added. This solution pH reduction effect is greater than with the other chemically treated BC samples tested. This indicates a release of protons from the surface of the BC into solution, reducing the number of positively charged sites on the surface to attract fluoride anions and/or reducing the overall magnitude of positive charge on the BC surface.

The isotherm graph given in figure 5.1.2.2 shows very clear type I isotherm shapes for all of the adsorbents tested. $H_2SO_4$ BC and $H_3PO_4$ BC increased the adsorption capacity of the RBC by 25.6 % (error: + 51.9 % / - 23.8 %) and 29.5 % (error: + 56.7 % / - 20.6 %) respectively. The mechanism behind this increase could be explained by that proposed by Medellin-Castillo *et al.* [93]. The authors found that the addition of 0.5 M nitric acid (an acid chemically similar to $H_2SO_4$ and $H_3PO_4$, as well as at a concentration of similar magnitude to those used the synthesis of the BCs) caused the HAP crystallinity to increase. It is unlikely that some or all of the HAP in the BC was converted to monetite, as Medellin-Castillo *et al.* found that at a treatment $HNO_3$ concentration of 0.5 M, no HAP was converted to monetite, whereas at 1.5 M $HNO_3$ concentration, complete conversion of HAP to monetite had occurred. This implies increasing acidic strength will increase the HAP to monetite conversion. Due to the fact that is a $H_3PO_4$ weaker acid than $HNO_3$, and used at a concentration of 0.1 M, it is highly unlikely the acid was able to convert any HAP to monetite. Although $H_2SO_4$ is a stronger acid than $HNO_3$, its low concentration of 0.1 M would indicate little to no conversion to monetite.

The adsorption mechanisms for these chars would therefore occur as follows:

$$Ca_{10}(PO_4)_6(OH)_2 + 20\ F^- \rightarrow 10\ \equiv CaF_2 + 3\ PO_4{}^{3-} + 2\ OH^- \qquad (3.5.3.4a)$$

$$Ca_{10}(PO_4)_6(OH)_2 + 2\ F^- \rightarrow\ \equiv Ca_{10}(PO_4)_6F_2 + 2\ OH^- \qquad (3.5.3.4b)$$
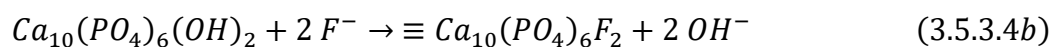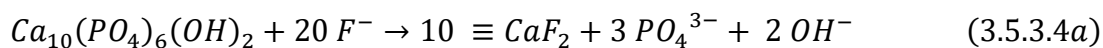
Forming fluorite and FHAP *via* reactions 3.5.3.4a and 3.5.3.4b respectively. XPS analysis of the acid treated BCs would reveal if there has been any change in crystallinity or crystal phase of the samples, and to what extent this has happened.

The mechanism proposed by Yami *et al.* [97], where ion exchange mechanisms between fluoride ions and OH$^-$, as well as SO$_4{}^{2-}$ and PO$_4{}^{3-}$ species formed from the crystal phase change of HAP to bassanite and monetite respectively, increase the uptake capacity of treated cow bone is unlikely to be occurring here. This is perhaps due to the fact that the bone was pyrolysed prior to acid treatment in this work. In addition, the work by Medellin-Castillo *et al.* has shown that these phase changes are unlikely to have occurred during the synthesis of the H$_2$SO$_4$ BC and H$_3$PO$_4$ BC.

KOH BC and NaOH BC decreased the adsorption capacity of the RBC by 31.1 % (error: + 15.0 % / - 20.0 %) and 34.4 % (error: + 15.3 % / - 20.6 %) respectively. Yami *et al.* found that KOH treated cow bone increased the SSA of this by a greater amount than H$_2$SO$_4$ treated bone, but found no correlation between SSA and adsorption capacity. The authors also pointed out that the PZC of the base treated bone was higher than the acid treated bone, but again saw no correlation of this with fluoride uptake capacity. The authors did however find that the base treated bone increased the adsorption capacity when compared to regular, untreated BC. These findings go against what was observed in this work. A reason for this may be that the relatively high concentrations of bases on the BC caused some degree of basic corrosion, and either enlarging or destroying existing pores in the BC, thereby significantly reducing the SSA of the BC. SEM analysis along with N$_2$-BET of the treated BC would reveal whether this is indeed the case or not.

In three of five cases, the Prausnitz-Radke isotherm model best fitted the experimental adsorption data, this is in agreement with work by Medellin-Castillo *et al.*, who commented that the three-parameter nature of the model makes it a strong fit for type I BC adsorption model isotherms.

## 6.2.6 Experimental Results - Production Process Modified BC

The BBC adsorption capacity was 69.6 % (error: + 6.3 % / - 8.3 %) worse than the RBC capacity. The BBC performed more closely along the lines of BC values reported across literature (albeit slightly worse), as can be seen in table 3.5.3.1. The CdA produced RBC has undergone several generations of optimisation prior to the work presented here, including iterations on pyrolysis temperature, method, time, etc. For these reasons, the RBC has a noticeably greater adsorption capacity than typically produced BC, due to its optimisation for the very purpose of fluoride adsorption from groundwater. It is also possible that the BC has been (inadvertently) optimised to specifically perform highly when exposed to the chemical composition of the groundwater from the Independencia Basin.

The BBC may have also been produced with other applications in mind. Commercial BCs have a wide variety of applications, including for soil amendment, as a fertiliser, or even as a pigment in dye manufacture [124].

When taking into account absolute errors, the RBC, SPT, BCI and BCO were indistinguishable in terms of adsorption capacity, their respective error bars all overlapped. This provides strong evidence to indicate that the composition and adsorption mechanism of these is the same. Sections 3.2 and 3.4.1 discuss the composition and possible mechanisms of fluoride adsorption of BC in depth respectively. These results show that there is no advantage to separating the harder BCI from the BCO. The results also indicate that there may be an economic advantage to conducting pyrolysis using only a single retort of wood pellet fuel. However, the SPT treated water samples after batch test 2 were mostly yellow in colour, and had a distinctly 'burnt' odour, rendering this char inappropriate for domestic use. The volume of water required to clear the colour and odour of a single filter cartridge of char containing 350 g of SPT was over 100 L - equivalent to over four days of water flow for a domestic, family sized column [100], ruling out SPT as a viable option for fluoride removal.

In three of five cases, the Prausnitz-Radke isotherm model best described the adsorption behaviour of the BC samples, confirming the three-parameter model's superiority over other models, as explained in section 6.2.5.

## 6.3 RSSCT

The BC with the highest adsorption capacity from batch test 2 - $H_3PO_4$ BC, was subjected to RSSCT along with RBC to compare their respective breakthrough behaviours.

### 6.3.1 Method Justification

The RSSCT was undertaken, as this would give a more realistic comparison for adsorbent performance than a batch test, due to real world fluoride adsorption from groundwater being done *via* continuous adsorption using fixed bed columns, the underlying theory of which is detailed in section 2.9.2.

### 6.3.2 Experimental Results

The $H_3PO_4$ BC treated 520 BV, 103 more BV than the RBC before breaking through, corresponding to a 24.7 % increase in performance. This value is slightly smaller than the 29.5 % adsorption capacity increase observed by the $H_3PO_4$ BC in batch test 2. The similarity in values indicates that the PD model used to model the breakthrough behaviour was appropriate to produce an accurate breakthrough curve.

## 6.4 Economic Analysis

As explained in section 1.4.1, the overall driving objective of the project was to optimise the BC fluoride adsorbent to reduce the overall frequency of replacement, and hence cost of this for end users. An economic analysis was therefore undertaken using the RSSCT results to compare the current costs of the RBC to the new theorised costs of the improved $H_3PO_4$ BC.

Costings were calculated using internal data at CdA for the total production cost of RBC, and incorporating the added cost of $H_3PO_4$ solution required for treatment. Costs of DI water used in synthesis, other equipment and materials as well as labour were neglected. Costing was done in Mexican Pesos (MXN), and converted to an overall percentage cost saving.

The parameters used for the calculations are given in table 6.4.1.

Table 6.4.1 - Costing parameters for optimised BC

| Parameter | Value |
|---|---|
| RBC Cost [ MXN/L ] | 32 |
| RBC Density [ kg/L ] | 0.66 |
| RBC Cost [ MXN/kg ] | 48.5 |
| RBC Treatment Capacity [ L/kg ] | 198.6 |
| RBC Water Treatment Cost [ MXN/L ] | 0.244 |
| 85 wt. % $H_3PO_4$ Solution Cost [ MXN/L ] | 76 * |
| 0.1 M $H_3PO_4$ Solution Cost [ MXN/L ] | 0.9 |
| Cost per kg BC Treated [ MXN/kg ] | 50.2 |
| Treatment Yield Loss [ % ] | 11 |
| Yield Loss Adjusted Cost per kg BC Treated [ MXN/kg ] | 55.8 |
| $H_3PO_4$ BC Treatment Capacity [ L/kg ] | 247.6 |
| $H_3PO_4$ BC Water Treatment Cost [ MXN/L ] | 0.225 |
| Percentage Cost Saving [ % ] | **7.8** |

*Data obtained from Mercado Libre* [125]

It can be seen from table 6.4.1 that chemical treatment of BC with 0.1 M $H_3PO_4$ could result in end user cost savings of almost 8 %.

## 6.5   Recommendations for Future Investigations

The chemical treatment of BC proved effective at increasing the adsorption capacity of this and thereby reducing overall adsorbent costs. With the recent installation of RSSCT equipment at the CdA laboratory, it is now possible to screen potential adsorbents in a significantly reduced amount of time when compared to pilot-scale column tests.

Low dosage (0.1 M) acid treatment of the BC has been shown to increase fluoride uptake. A follow up experiment should investigate the low dosage treatment of BC using a range of acids and bases (e.g. HCl, $HNO_3$, KOH and NaOH) in a batch experiment to compare the performance of these with $H_2SO_4$ BC and $H_3PO_4$ BC.

After determination of the most effective chemical treating agent, a second batch experiment should explore a range of treatment dosages (e.g. 0.01 M, 0.05 M, 0.1 M, 0.5 M, 1 M, 5 M) of this treating agent in another batch experiment, to determine how to optimise the adsorption capacity following treatment.

When the optimal chemical treatment has been found, RSSCT should be undertaken to determine the breakthrough behaviour of the treated BC. The sample should be taken to total saturation, followed by desorption with DI water. The cycle of saturation/desorption should be repeated numerous times to investigate the regenerative efficiency of this treated BC. Adsorbent regeneration is an avenue of investigation which could be undertaken by CdA in future.

# 7.0  Conclusion

Following a review on the state of the art of chemical treatment of bone and BC, a batch test was undertaken with the aims of replicating the results of the two most promising experiments presented in literature, by Yami *et al.* [97] as well as Chatterjee *et al.* [101]. Raw bone meal was treated with either 30 wt. % $H_3PO_4$, 30 wt. % $H_2SO_4$, 40 wt. % KOH or 32 wt. % NaOH. BC was doped with a combination of CaO and $Al_2(SO_4)_3$. These synthesised adsorbents were subjected to a 24-hour batch test at various doses, along with RBC produced by CdA. The results were unexpected and disappointing. None of the synthesised adsorbents with the exception of the $CaO/Al_2(SO_4)_3$ doped BC yielded predictable or meaningful isotherm shapes. This was attributed to the unknown composition of the raw bone meal, of which the bone to organic matter ratio could not be determined or controlled. The $CaO/Al_2(SO_4)_3$ doped BC showed a $q_{1.5}$ far smaller than that expected from the results presented by Chatterjee *et al.*, results which upon further investigation were found to be in fact showing $q_{1000}$. The $CaO/Al_2(SO_4)_3$ doped BC was also determined to express a type II isotherm shape, indicating unrestricted multilayer adsorption of a macro-porous or non-porous adsorbent. It was determined that this behaviour could be explained by the enlarging or destruction of the BC pores during the synthesis. This also provides a reason as to why the $q_{1.5}$ of the adsorbent was even lower than the $q_{1.5}$ of the adsorbent synthesised by the authors.

A second batch test was undertaken to investigate the acid and base treatment of BC, loosely basing the methodology on the work of Yami *et al.*, whilst attempting to confirm if the chemical treatment of BC could in any way increase the adsorption capacity of this. BC was treated with 0.1 M $H_2SO_4$ (0.97 wt. %), 0.1 M $H_3PO_4$ (0.97 wt. %), 38 wt. % (12.39 M) HCl, 10 wt. % KOH (1.78 M), and 20 wt. % NaOH (4.99 M). The $H_2SO_4$ and $H_3PO_4$ increased the adsorption capacity of the BC by 25.6 % (error: + 51.9 % / - 23.8 %) and 29.5 % (error: + 56.7 % / - 20.6 %) respectively. This was attributed to an increased HAP crystallinity from the acid treatment, resulting in the formation of fluorite and FHAP upon exposure to fluoride ions from the batch test.The HCl caused a drastic yield loss of 95 %, and subsequently showing no fluoride adsorption after batch testing. This was explained by the concentrated nature of the HCl used for treatment, which caused acid corrosion, destroying the BC surface and pores.

The KOH and NaOH decreased the adsorption capacity by 31.1 % (error: + 15.0 % / - 20.0 %) and 34.4 % (error: + 15.3 % / - 20.6 %) respectively. This was attributed to the potential basic corrosion of the porous structure of the BC, decreasing the surface area of this by enlarging or destroying some pores.

BCs with a modified production process were also investigated, including BC produced with a shorter pyrolysis time using less wood fuel, a commercial BC from Brazil, and BC with the harder outer shell and inner softer core separated. With the exception of the Brazilian BC, the performance of all of the other BCs was indistinguishable, with their errors all overlapping each other. This showed that a shorter pyrolysis time could in fact produce a BC as effective as the RBC currently used by CdA. However, the outlet water exposed to this BC had a burnt odour and a yellow colour, rendering it unusable in a domestic setting. This result also showed that there is no significant difference in the composition or adsorption performance of the different parts of BC, making it unnecessary to investigate initial screening of raw cow bone for 'better' pieces. The commercial Brazilian BC performed 69.6 % (error: + 6.3 % / - 8.3 %) worse than the RBC, and more in line with other BCs reported in literature. This was in part attributed to the fact that the RBC used by CdA has undergone several rounds of production process optimisation to maximise its adsorption capacity, making it an extremely effective BC compared to others. Also, the designed application of the Brazilian BC may have been for other industrial or agricultural purposes.

Finally, the best performing BC, $H_3PO_4$ BC, was subjected to RSSCT along with CdA produced RBC, to compare their respective breakthrough performances. RBC achieved breakthrough at 417 BV, whereas $H_3PO_4$ BC broke through at 520 BV, corresponding to a 24.7 % increase in performance, and therefore a 7.8 % cost reduction for domestic users.

# 8.0 References

1. Conagua, *Statistics on Water in Mexico , 2010 edition Statistics on Water in Mexico , 2010 edition National Water Commission of Mexico.* Statistics, 2010: p. 1-258.
2. Conagua, *Estadísticas del Agua Síntesis Edición 2005.* 2005.
3. Góngora-Ortega, J., et al., *Prevalencia de enfermedad renal crónica en niños de Aguascalientes, México.* Salud pública de México, 2008. **50**(6): p. 436-437.
4. Pérez, J.G., *Prevalencia de fluorosis y caries dental en poblaciones infantiles con diferentes niveles de exposición a hidruros.* 2004, tesis de maestría in Toxicología dirigida por J. Llamas, Aguascalientes ….
5. Rahman, M.M., J.C. Ng, and R. Naidu, *Chronic exposure of arsenic via drinking water and its adverse health impacts on humans.* Environmental geochemistry and health, 2009. **31**(1): p. 189-200.
6. Instituto Nacional de, S., *Principales resultados de la Encuesta Intercensal 2015 Guanajuato.* Inegi, 2015.
7. Conagua, *Statistics on Water in Mexico , 2017 edition Statistics on Water in Mexico , 2017 edition National Water Commission of Mexico.* 2017.
8. Internal, C., *Mexico Today - Presentation.*
9. Adrián Ortega-Guerrero, M., *Presencia, distribución, hidrogeoquímica y origen de arsénico, fluoruro y otros elementos traza disueltos en agua subterránea, a escala de cuenca hidrológica tributaria de Lerma-Chapala, México.* Revista Mexicana de Ciencias Geologicas, 2009. **26**(1): p. 143-161.
10. CdA, *CdA-Public-Database-v1-2018-05-15.*
11. World Health, O., *Fluoride in Drinking-water Back ground Document for development of WHO Guidelines for Drinking-water Quality.* Guidelines for drinking-water quality, 2006: p. 1-9.
12. Organisation, W.H., *Arsenic in Drinking-water Back ground Document for development of WHO Guidelines for Drinking-water Quality.* 2006.
13. World Health, O., *Environmental health criteria 224: arsenic and arsenic compounds.* World Health Organization, Geneva, 2001: p. 1-108.
14. Fejerskov, O. and E. Kidd, *Dental Caries: The Disease and its Clinical Management second edition.* 2008. 27-32.
15. Buzalaf, M.A.R., et al., *Mechanisms of Action of Fluoride for Caries Control.* Monogr Oral Sci., 2011. **22**: p. 97-114.
16. Fejerskov, O., A. Thylstrup, and M.J. Larsen, *Clinical and structural features and possible pathogenic mechanisms of dental fluorosis.* European Journal of Oral Sciences, 1977. **85**(7): p. 510-534.
17. Thylstrup, A. and O. Fejerskov, *Clinical appearance of dental fluorosis in permanent teeth in relation to histologic changes.* Community Dentistry and Oral Epidemiology, 1978. **6**(6): p. 315-328.
18. Ramya, R., C.G. Ajithkrishnan, and K. Thanveer, *Development and psychometric testing of a visual analog scale for dental fluorosis.* Journal of Indian Association of Public Health Dentistry, 2014. **12**(1): p. 4-4.
19. del Carmen, A.-D., d.l.F.-H. Javier, and C.-V. Aline, *Dental fluorosis, fluoride in urine, and nutritional status in adolescent students living in the rural areas of Guanajuato, Mexico.* Journal of International Society of Preventive and Community Dentistry, 2016. **6**(6): p. 517-517.
20. Agua, C.d. *How We Work.* 2019.

21. Mohapatra, M., et al., *Review of fluoride removal from drinking water.* Journal of Environmental Management, 2009. **91**(1): p. 67-77.
22. Chibi, C. and J. Haarhoff, *A Promising Approach to Fluoride Removal in Rural Drinking Water Supplies.* Presented at WISA 2000 Biennial Conference, Sun City, South Africa, 2000(28 May-1 June 2000): p. 1-11.
23. Benefield, L.D., J.F. Judkins, and B.L. Weand, *Process chemistry for water and wastewater treatment.* 1982: Prentice Hall Inc.
24. Shen, J. and A. Schäfer, *Removal of fluoride and uranium by nanofiltration and reverse osmosis: a review.* Chemosphere, 2014. **117**: p. 679-691.
25. Boruff, C.S., *Removal of fluorides from drinking waters.* Industrial & Engineering Chemistry, 1934. **26**(1): p. 69-71.
26. Maier, F.J., *Methods of removing fluorides from water.* American Journal of Public Health and the Nations Health, 1947. **37**(12): p. 1559-1566.
27. Parthasarathy, N., J. Buffle, and W. Haerdi, *Combined use of calcium salts and polymeric aluminium hydroxide for defluoridation of waste waters.* Water Research, 1986. **20**(4): p. 443-448.
28. Sorg, T.J. and G.S. Logsdon, *Treatment technology to meet the interim primary drinking water regulations for inorganics: Part 2.* Journal-American Water Works Association, 1978. **70**(7): p. 379-393.
29. Culp, R.L. and H.A. Stoltenberg, *Fluoride reduction at la crosse, kan.* Journal (American Water Works Association), 1958. **50**(3): p. 423-431.
30. Schoeman, H., *The effect of particle size and interfering ions on fluoride removal by activated alumina.* Water SA, 1987. **13**(4): p. 229-234.
31. Rubel Jr, F. and R.D. Woosley, *The removal of excess fluoride from drinking water by activated alumina.* Journal-American Water Works Association, 1979. **71**(1): p. 45-45.
32. The, B. and E.P.A. Land Revitalization Technology Support Center, *Glossary*.
33. Ruthven, D.M., *Principles of Adsorption and Adsorption Processes*.
34. Bennett, G.F., *Partition and Adsorption of Organic Contaminants in Environmental Systems*. Vol. 98. 2003. 321-322.
35. Medellin-Castillo, N.A., et al., *Adsorption of fluoride from water solution on bone char.* Industrial and Engineering Chemistry Research, 2007. **46**(26): p. 9205-9212.
36. Medellin-Castillo, N.A., et al., *Adsorption capacity of bone char for removing fluoride from water solution. Role of hydroxyapatite content, adsorption mechanism and competing anions.* Journal of Industrial and Engineering Chemistry, 2014. **20**(6): p. 4014-4021.
37. Atkins, P. and J. de Paula, *Physical Chemistry for the Life Sciences*. Vol. 91. 2017. 399-404.
38. Generalic, E., *Lennard-Jones potential*. 2018.
39. Kosmulski, M., *Surface Charging and Points of Zero Charge, Surfactant Science Series*. 2009.
40. Lawrence, A.S.C., *Colloidal Dispersions*. Vol. 171. 1953. 142-142.
41. Mahlknecht, J., et al., *Geochemical and isotopic investigations on groundwater residence time and flow in the Independence Basin, Mexico.* Journal of Hydrology, 2006. **324**(1-4): p. 283-300.
42. Mahlknecht, J., B. Steinich, and I. Navarro De León, *Groundwater chemistry and mass transfers in the Independence aquifer, central Mexico, by using multivariate statistics and mass-balance models.* Environmental Geology, 2004. **45**(6): p. 781-795.

43.    Brunauer, S., et al., *On a Theory of the van der Waals Adsorption of Gases.* Journal of the American Chemical Society, 1940. **62**(7): p. 1723-1732.

44.    Donohue, M.D. and G.L. Aranovich, *Classification of Gibbs adsorption isotherms.* Advances in Colloid and Interface Science, 1998. **76**: p. 137-152.

45.    Sing, K.S.W., et al., *REPORTING PHYSISORPTION DATA FOR GAS/SOLID SYSTEMS with Special Reference to the Determination of Surface Area and Porosity.* Dissertation, 2009. **57**(4): p. 603-619.

46.    Abe, I., et al., *Adsorption of fluoride ions onto carbonaceous materials.* Journal of Colloid and Interface Science, 2004. **275**(1): p. 35-39.

47.    Freundlich, H., *Kapillarchemie, eine Darstellung der Chemie der Kolloide und verwandter Gebiete, von Dr. Herbert Freundlich.* 1909: akademische Verlagsgesellschaft.

48.    Van Bladel, R. and A. Moreale, *Adsorption of herbicide‐derived p‐chloroaniline residues in soils: a predictive equation.* Journal of Soil Science, 1977. **28**(1): p. 93-102.

49.    Ayawei, N., A.N. Ebelegi, and D. Wankasi, *Modelling and Interpretation of Adsorption Isotherms.* Journal of Chemistry, 2017. **2017**: p. 1-11.

50.    Nimibofa, A., W. Donbebe, and E.D. Dikio, *Adsorption of Congo Red by Ni / Al-CO3 : Equilibrium , Thermodynamic and Kinetic Studies Adsorption of Congo Red by Ni / Al-CO 3 : Equilibrium , Thermodynamic and Kinetic Studies.* 2015(September).

51.    Vijayaraghavan, K., et al., *Biosorption of nickel(II) ions onto Sargassum wightii: Application of two-parameter and three-parameter isotherm models.* Journal of Hazardous Materials, 2006. **133**(1-3): p. 304-308.

52.    Sparks, D.L., *5 - Sorption Phenomena on Soils*, D.L.B.T.E.S.C. Sparks, Editor. 2003, Academic Press: Burlington. p. 133-186.

53.    Henry, W., *III. Experiments on the quantity of gases absorbed by water, at different temperatures, and under different pressures.* Philosophical Transactions of the Royal Society of London, 1803(93): p. 29-274.

54.    Van't Hoff, J.H., *Etudes de dynamique chimique.* Vol. 1. 1884: Muller.

55.    Clapeyron, É., *Mémoire sur la puissance motrice de la chaleur.* Journal de l'École polytechnique, 1834. **14**: p. 153-190.

56.    Clausius, R., *Über die bewegende Kraft der Wärme und die Gesetze, welche sich daraus für die Wärmelehre selbst ableiten lassen.* Annalen der Physik, 1850. **155**(3): p. 368-397.

57.    Radke, C. and J. Prausnitz, *Adsorption of organic solutes from dilute aqueous solution of activated carbon.* Industrial & Engineering Chemistry Fundamentals, 1972. **11**(4): p. 445-451.

58.    Nadu, T., *Adsorption Isotherm Modeling of Phenol Onto Natural soils – Applicability of Various Isotherm Models.* International Journal of Environmental Research, 2012. **6**(1): p. 265-276.

59.    Aarden, F.B., *Adsorption onto Heterogeneous Porous Materials : Equilibria and Kinetics.* 2001. 129-129.

60.    Fick, A., *Ueber diffusion.* Annalen der Physik, 1855. **170**(1): p. 59-86.

61.    Perry, J.H., *Chemical engineers' handbook.* 1950, ACS Publications.

62.    Dullien, F.A.L., *Porous Media - Fluid Transport and Pore Structure.*

63.    Mackie, J.S. and P. Meares, *The diffusion of electrolytes in a cation-exchange resin membrane I. Theoretical.* Proceedings of the Royal Society of London. Series A. Mathematical and Physical Sciences, 1955. **232**(1191): p. 498-509.

64. Suzuki, M. and J.M. Smith, *Axial dispersion in beds of small particles.* The Chemical Engineering Journal, 1972. **3**: p. 256-264.

65. Wakao, N. and J.M. Smith, *Diffusion in catalyst pellets.* Chemical Engineering Science, 1962. **17**(11): p. 825-834.

66. Satterfield, N., *Mass Transfer in Heterogeneous Catalysis Review.* **76**(3): p. 509-510.

67. Pagitsas, M., A. Nadim, and H. Brenner, *Projection operator analysis of macrotransport processes.* The Journal of chemical physics, 1986. **84**(5): p. 2801-2807.

68. Kirby, B.J., *Micro- and Nanoscale Fluid Mechanics*. Vol. 91. 2017. 399-404.

69. Wakao, N. and T. Funazkri, *Effect of fluid dispersion coefficients on particle-to-fluid mass transfer coefficients in packed beds: correlation of Sherwood numbers.* Chemical Engineering Science, 1978. **33**(10): p. 1375-1384.

70. Wilson, E.J. and C.J. Geankoplis, *Liquid mass transfer at very low reynolds numbers in packed beds.* Industrial and Engineering Chemistry Fundamentals, 1966. **5**(1): p. 9-14.

71. Hu, J., et al., *Adsorption kinetics of fluoride on bone char and its regeneration.* Environment Protection Engineering, 2017. **43**(3): p. 93-112.

72. Leyva-Ramos, R., et al., *Intraparticle diffusion of cadmium and zinc ions during adsorption from aqueous solution on activated carbon.* Journal of Chemical Technology & Biotechnology: International Research in Process, Environmental & Clean Technology, 2005. **80**(8): p. 924-933.

73. Liu, Y. and Y.J. Liu, *Biosorption isotherms, kinetics and thermodynamics.* Separation and Purification Technology, 2008. **61**(3): p. 229-242.

74. Crittenden, B. and W.J. Thomas, *Adsorption technology and design*. 1998: Elsevier.

75. Loebenstein, W.V., *Batch adsorption from solution.* Journal of Research of the National Bureau of Standards Section A: Physics and Chemistry, 1962. **66A**(6): p. 503-503.

76. Faust, S.D. and O.M. Aly, *Adsorption processes for water treatment*. 2013: Elsevier.

77. Ergun, S., *Fluid flow through packed columns.* Chem. Eng. Prog., 1952. **48**: p. 89-94.

78. Chilton, T.H. and A.P. Colburn, *II—pressure drop in packed tubes1.* Industrial & Engineering Chemistry, 1931. **23**(8): p. 913-919.

79. LeVan, M.D., *Thermal swing adsorption: regeneration, cyclic behavior, and optimization*. 1989, Springer. p. 339-355.

80. Crittenden, J.C., et al., *Design considerations for GAC treatment of organic chemicals.* Journal-American Water Works Association, 1987. **79**(1): p. 74-82.

81. Denning, P.C. and B.I. Dvorak, *Maximizing Sorbent Life: Comparison of Columns in Parallel, Lead-Lag Series, and with Bypass Blending.* Water Environment Research, 2009. **81**(2): p. 206-216.

82. Narbaitz, R.M. and A. Benedek, *Least cost process design carbon adsorbers.* 2016. **55**(10): p. 1244-1251.

83. Kearns, J., et al., *Lead-lag series and staged parallel operational strategies improve the performance and cost-effectiveness of bonechar for control of fluoride in groundwater.* Journal of Water, Sanitation and Hygiene for Development, 2018(October): p. 1-8.

84. CdA, *Optimizing fluoride adsorption and removal using bone char in a lead- lag column configuration.*

85. Crittenden, J.C., J.K. Berrigan, and D.W. Hand, *Design of rapid small-scale adsorption tests for a constant diffusivity.* J. Water Pollut. Control Fed., 1986. **58**(4): p. 312-319.

86. Poddar, M., *A Review on the use of rapid small scale column test (RSSCT) on predicting adsorption of various contaminants.* IOSR Journal of Environmental Science, Toxicology and Food Technology, 2013. **3**(1): p. 77-85.

87. Mastropole, A.J., *Evaluation of Available Scale-Up Approaches for the Design of GAC Contactors.* 2017. **91**(1): p. 399-404.

88. Badruzzaman, M., P. Westerhoff, and D.R.U. Knappe, *Intraparticle diffusion and adsorption of arsenate onto granular ferric hydroxide (GFH).* Water Research, 2004. **38**(18): p. 4002-4012.

89. Westerhoff, P., et al., *Rapid Small-Scale Column Tests for Arsenate Removal in Iron Oxide Packed Bed Columns.* Journal of Environmental Engineering, 2005. **131**(2): p. 262-271.

90. Kearns, J. and CdA, *bonechar CD RSSCT.* 2018.

91. Kearns, J. and CdA, *bonechar PD RSSCT.* 2018.

92. Jones, J.A., *EQUILIBRIUM AND KINETIC ANALYSIS OF FLUORIDE ADSORPTION ON BONE CHARCOAL.* 2012.

93. Medellin-Castillo, N.A., et al., *Removal of fluoride from aqueous solution using acid and thermally treated bone char.* Adsorption, 2016. **22**(7): p. 951-961.

94. Patel, S., et al., *Synthesis and characterisation of mesoporous bone char obtained by pyrolysis of animal bones, for environmental application.* Journal of Environmental Chemical Engineering, 2015. **3**(4): p. 2368-2377.

95. Shahid, M.K., J.Y. Kim, and Y.-G. Choi, *Synthesis of bone char from cattle bones and its application for fluoride removal from the contaminated water.* Groundwater for Sustainable Development, 2019. **8**(December 2018): p. 324-331.

96. Wang, L., et al., *Insight into mechanisms of fluoride removal from contaminated groundwater using lanthanum-modified bone waste.* RSC Advances, 2017. **7**(85): p. 54291-54305.

97. Yami, T.L., E.C. Butler, and D.A. Sabatini, *Chemically activated cow bone for increased fluoride removal from drinking water.* Journal of Water, Sanitation and Hygiene for Development, 2016. **6**(2): p. 215-223.

98. Brunson, L.R. and D.A. Sabatini, *An Evaluation of Fish Bone Char as an Appropriate Arsenic and Fluoride Removal Technology for Emerging Regions.* Environmental Engineering Science, 2009. **26**(12): p. 1777-1784.

99. Solutions, A. and J. Kearns, *E-Z Adsorption Char Drum Oven.*

100. Dossi, S., *Developing Adsorption Filters for Fluoride and Arsenic Removal from Water.* 2018.

101. Chatterjee, S., M. Mukherjee, and S. De, *Defluoridation using novel chemically treated carbonized bone meal: batch and dynamic performance with scale-up studies.* Environmental Science and Pollution Research, 2018. **25**(18): p. 18161-18178.

102. Wilson, J.A., I.D. Pulford, and S. Thomas, *Sorption of Cu and Zn by bone charcoal.* Environmental Geochemistry and Health, 2003. **25**(1): p. 51-56.

103. Wingenfelder, U., et al., *Removal of heavy metals from mine waters by natural zeolites.* Environmental Science and Technology, 2005. **39**(12): p. 4606-4613.

104. Elliott, J.C., *Structure and chemistry of the apatites and other calcium orthophosphates.* Vol. 18. 2013: Elsevier.

105. Delgadillo-Velasco, L., et al., *Bone char with antibacterial properties for fluoride removal: Preparation, characterization and water treatment.* Journal of Environmental Management, 2017. **201**: p. 277-285.

106. Granados-Correa, F., et al., *Adsorption Behaviour of La ( III ) and Eu ( III ) Ions from Aqueous Solutions by Hydroxyapatite : Kinetic , Isotherm , and Thermodynamic Studies.* 2013. **2013**.

107. Rouquerol, F., J. Rouquerol, and K. Sing, *Adsorption by Powders and Porous Solids: Principles, Methodology and Applications.* 1998: Academic Press.

108. McNaught, A.D. and A.D. McNaught, *Compendium of chemical terminology.* Vol. 1669. 1997: Blackwell Science Oxford.

109. Babić, B.M., et al., *Point of zero charge and intrinsic equilibrium constants of activated carbon cloth.* Carbon, 1999. **37**(3): p. 477-481.

110. Leyva-Ramos, R., et al., *Kinetic modeling of fluoride adsorption from aqueous solution onto bone char.* Chemical Engineering Journal, 2010. **158**(3): p. 458-467.

111. He, J., et al., *Performance of novel hydroxyapatite nanowires in treatment of fluoride contaminated water.* Journal of hazardous materials, 2016. **303**: p. 119-130.

112. Tapia-Picazo, J.C., et al., *Fluoride adsorption properties of cerium-containing bone char.* Journal of Fluorine Chemistry, 2017. **197**: p. 63-73.

113. Roy, R.K., *A primer on the Taguchi method.* 2010: Society of Manufacturing Engineers.

114. Rojas-Mayorga, C.K., et al., *Optimization of pyrolysis conditions and adsorption properties of bone char for fluoride removal from water.* Journal of analytical and applied pyrolysis, 2013. **104**: p. 10-18.

115. Ayoob, S., A.K. Gupta, and V.T. Bhat, *A conceptual overview on sustainable technologies for the defluoridation of drinking water.* Critical Reviews in Environmental Science and Technology, 2008. **38**(6): p. 401-470.

116. Masamba, W.R.L., et al., *Water defluoridation using Malawi's locally sourced gypsum.* Physics and Chemistry of the Earth, Parts A/B/C, 2005. **30**(11-16): p. 846-849.

117. Hach, *DR/890 Portable Colorimeter.*

118. Extech, I., *Extech FL700: Waterproof ExStik® Fluoride Meter.*

119. AliExpress, *JUANJUAN Store.*

120. Industrial Test Systems, I., *Quick Arsenic Econo II.*

121. Caminos de, A., *Acid Treated Bone Char Batch Test.* 2016.

122. Lasdon, L.S., et al., *Design and testing of a generalized reduced gradient code for nonlinear programming.* 1976, STANFORD UNIV CA SYSTEMS OPTIMIZATION LAB.

123. Zhang, P., *Adsorption and Desorption Isotherms*, K.R. Group, Editor. 2016, Dartmouth College.

124. Dimengo, M., *Bone Char Benefits*, in *Acres U.S.A.* 2018.

125. Grodeco. *Acido Fosforico 85% 20 Lt Uso Hidroponico Regulador Ph.* 2018.

# Appendix A: Roles and Responsibilities

During my industrial placement at Caminos de Agua, I worked as a technical fellow on a volunteer basis, individually conducting laboratory experiments designed by myself, under the supervision of Aaron Krupp, Caminos de Agua's Research and Technology Development Coordinator.

My initial responsibility upon arrival at the organisation was to conduct a comprehensive literature review of existing scientific papers in the Caminos de Agua repertoire, as well as finding other papers containing novel research into the application of bone and bone char as a low cost fluoride adsorbent. Following this, I was then tasked with experimental design, following the rigorous criteria and attention to detail demanded by Caminos de Agua, to ensure full documentation of the work conducted, as well as the production of accurate and reliable results. This was done under the guidance of my industrial supervisor, Aaron Krupp. All parts of the experimental syntheses, batch experiments, and the collection of results were undertaken by myself in the Caminos de Agua laboratory, with the exception of the production of the bone char by pyrolysis conducted at the ceramic and bone char production site owned by the organisation.

I was also asked to design and undertake an experiment to firstly troubleshoot the fluoride ion selective electrode probe, and then determine if its readings were sufficiently accurate to be used in experimental settings as well as for water monitoring purposes.

I attended some fundraisers organised by Caminos de Agua, running information stalls to provide guests with information about the state of the Independencia Basin, the organisation's work, as well as answering any questions they may have.

Lastly, I participated in the filming of a submission video to the James Dyson award for the Aguadapt product developed by Aaron Krupp with Caminos de Agua. Aguadapt is a versatile, low cost adaptor that can be used to treat surface water from a variety of containers as well as having the option to adapt other filtration systems for any other contaminants present in water. After the product was shortlisted as a finalist in the Mexico round of the James Dyson award, I accompanied some colleagues to Mexico City to speak with the press in national newspaper and television interviews.

# Appendix B: Experimental Methodologies

## B 1.0 Batch Test 1

### B 1.1 Dependent Variables

1. Equilibrium fluoride concentration (i.e. concentration of fluoride in water after 24-hour batch test).
2. Production yield percentage (i.e. percentage of initial wet (and dry) bone converted to usable adsorption media).

### B 1.2 Independent Variables

*All:*

1. Adsorption media dose: [0.05 g, 0.10 g, 0.20 g, 0.50 g, 1.00 g] i.e. [0.56 g/L, 1.11 g/L, 2.22 g/L, 5.56 g/L, 11.11 g/L]

### B 1.3 Control Variables

*All:*

1. Batch test time: 24 h
2. Batch tumbler speed: 30 - 40 rpm
3. Initial water fluoride concentration: 8.5 mg/L
4. Batch water sample volume: 90 mL

*BC:*

1. Burn time: 1.5 h
2. Burn temperature: 400 - 600 °C
3. Particle size: < # 30 US standard mesh (< 0.6 mm)

*CAB:*

1. NaOCl solution soaking time: 24 h
2. Bone drying time: 1.5 h
3. Bone drying temperature: 100 °C
4. Particle size: < # 30 US standard mesh (< 0.6 mm)
5. Fines drying time: 1.5 h
6. Fines drying temperature: 100 °C
7. $H_3PO_4$ activating agent concentration: 30 wt. %
8. $H_2SO_4$ activating agent concentration: 30 wt. %
9. NaOH activating agent concentration: 29.5 wt. %
10. KOH activating agent concentration: 34.3 wt. %
11. Activating agent soaking time: 4 h
12. Stirrer speed: 150 rpm
13. Media to activating agent ratio: 1:1 wt. %
14. Activated media drying time: 1.5 h
15. Activated media drying temperature: 70 °C

*CABC:*

1. Mass BC per litre water: 100 g
2. $Al_2(SO_4)_3$ activating agent preparation medium dosage: 500 g/L
3. CaO activating agent preparation medium dosage: 15 g/L
4. CaO soak time: 2 h
5. $Al_2(SO_4)_3$ soak time: 4 h (post addition of CaO)
6. Stirrer speed: 150 rpm
7. Activated media drying time: 1.5 h
8. Activated media drying temperature: 70 °C
9. Particle size: < # 30 US standard mesh (< 0.6 mm)

## B 1.4 Procedure

### B 1.4.1     Notes

1. Batch experiments were conducted blindly and in duplicate.
2. CAB solution preparation parameters were calculated using Excel.

### B 1.4.2     Materials

1. Raw bone meal (minimum 200 g)
2. CdA produced BC (minimum 100 g)
3. 13 wt. % NaOCl solution (minimum 0.3 L)
4. 85 wt. % $H_3PO_4$ (minimum 10 mL)
5. 98 wt. % $H_2SO_4$ (minimum 20 mL)
6. 99 wt. % NaOH (minimum 40 g)
7. 80 wt. % KOH (minimum 15 g)
8. 100 wt. % $Al_2(SO_4)_3$ (minimum 100 g)
9. 100 wt. % CaO (minimum 3 g)
10. Sample water (minimum 3 L)
11. DI water (minimum 10 L)

*Note:* Amounts specified above are for a single batch experiment run. Amounts were multiplied by 2 for duplicate quantity requirements.

### B 1.4.3     Preparation

### B 1.4.3.1     RBC

1. A representative sample (approx. 50 g) of BC that was subjected to a burn temperature 400 - 600 °C for 1.5 h was taken, it was ensured that this was dry. The sample was weighed and the value recorded.
2. The BC was placed in a toaster oven and dried at 70 °C. The temperature was monitored with a thermocouple. The sample was then weighed and the value recorded.
3. A # 30 US standard mesh sieve was brushed with a toothbrush to ensure there were no residuals in the sieve. The sieve was kept dry.
4. A Ziploc bag of uncrushed BC pieces was placed on a flat surface and rolled over with a section of PVC tubing until the BC pieces were crushed.
5. The crushed BC was placed in the # 30 US standard mesh sieve.
6. The sieve was shaken above a collection bucket until all small particles have passed through the mesh.
7. Any BC too big for the mesh was re-crushed by repeating steps 4 - 6. This was repeated until all BC had been crushed and sieved.
8. The char that passed through the # 30 US standard mesh sieve was weighed and the value recorded.

### B 1.4.3.2     CAB

1. The raw cow bone meal was weighed and the value recorded.
2. The bone meal was submerged 13 wt.% NaOCl solutions for 24 h to remove impurities.
3. The resulting slurry was filtered using a coffee filter and rinsed with DI water.
4. The filtered bone meal was placed in a toaster oven and dried at 70 °C for 1.5 h, while the temperature was monitored with a thermocouple.
5. 50 mL of activating agent solutions of $H_3PO_4$, $H_2SO_4$, NaOH and KOH were prepared with concentrations as specified by the control variable list by diluting purchased solutions or dissolving solids appropriately using DI water.
6. Four samples of the bone meal were taken. Their exact weights were recorded.
7. A corresponding amount of each solution for each of the bone meal samples was added in order to have a 1 : 1 ratio by weight of solution and bone meal.
8. The bone meal samples were submerged in their corresponding solutions and stirred for 4 h with stirrer speed approx. 150 rpm (lowest setting of Thermo Scientific Magnetic Stirrer RT Basic-12, to prevent further crushing of bone) at room temperature.
9. The activated samples were filtered using a coffee filter, and rinsed with DI water.
10. One sample of wet CAB was packed inside the inner column cartridge.
11. The outer column cartridge was closed around the inner cartridge.
12. The inlet tube of column system was attached to the RO tap.
13. The outlet tube was placed in an empty waste container.

14. The RO flow was started.
15. The inlet and outlet water was sampled using sample containers at time 0 hours and each time the waste container was filled until the fluoride concentration at the inlet was within ± 0.1 mg/L of the outlet. This was done to ensure there was no leached $PO_4$ interfering with fluoride colourimeter readings. Note: All RO flush outlet samples were filtered using the Whatman™ glass microfiber filtering method given in appendix B 4.0 before measuring using the colourimeter and FL700 probe. This was not done for the acid treated bone in the original experimental run.
16. The flushed adsorbent was removed from the column.
17. Steps 18 – 24 were repeated for the other three samples.
18. Retained samples were dried in a toaster oven for 1.5 h at 100 °C.
19. The remaining samples were weighed and the values recorded.
20. A # 30 US standard mesh sieve was brushed with a toothbrush to ensure there were no residuals in the sieve. The sieve was kept dry.
21. A Ziploc bag containing one of the CAB samples was placed on a flat surface and rolled over with a piece of PVC tubing to crush the CAB.
22. The crushed CAB was placed in a # 30 US standard mesh sieve.
23. The sieve was shaken above a collection bucket until all small particles passed through the mesh.
24. Any CAB that was too big to pass through the mesh was crushed by repeating steps 21 - 23. This was repeated this until all the CAB had been crushed and sieved.
25. The CAB that passed through the mesh was weighed and the value recorded.
26. Steps 10 – 25 were repeated for the other three samples.

### B 1.4.3.3    CABC

1. A representative sample (approx. 50 g) of uncrushed BC was taken. Its exact weight was recorded.
2. The BC was placed in a Ziploc bag and break up into smaller pieces with hammer.
3. A # 8 and # 30 US standard mesh sieve were brushed with a toothbrush to ensure there were no residuals in the. The sieves were kept dry.
4. The # 8 sieve was placed on top of the # 30 sieve.
5. A Ziploc bag of uncrushed BC pieces was placed on a flat surface and rolled over with a section of PVC tubing until the BC pieces were crushed.
6.  The crushed BC was placed in the # 8 US standard mesh sieve.
7. The sieves were shaken above a collection bucket until all small particles passed through the # 8 mesh.
8. Any BC pieces too big for the # 8 sieve were re-crushed by repeating steps 5 - 7.
9. The BC that passed through the # 8 sieve but were too big to pass through the # 30 sieve were weighed and the value recorded.

10. Exactly 20 g of the BC that passed through # 8 sieve but was too big to pass through # 30 sieve was retained.
11. 200 g of DI water was taken and the BC added to this.
12. 3 g of CaO was added to this. This was to ensure a 15 g/L concentration of CaO was achieved.
13. The crushed BC sample was submerged in CaO solution and stirred for 2 h with stirrer speed 150 rpm at room temperature.
14. 100 g of $Al_2(SO_4)_3$ was added to the solution. This ensured a concentration of 500 g/L was achieved. The solution was left to continue to stir for 4 h.
15. The activated sample was filtered using a coffee filter, and rinsed with DI water.
16. The wet CABC was packed inside the inner column cartridge.
17. The outer column cartridge was closed around the inner cartridge.
18. The inlet tube of column system was attached to the RO tap.
19. Attach outlet tube to an empty waste container.
20. The RO flow was started.
21. The inlet and outlet water was sampled using sample containers at time 0 hours and each time the waste container was filled until the fluoride concentration at the inlet was within ± 0.1 mg/L of the outlet. This was done to ensure there was no leached $PO_4$ interfering with fluoride colourimeter readings. Note: All RO flush outlet samples were filtered using the Whatman™ glass microfiber filtering method given in appendix B 4.0 before measuring using the colourimeter and FL700 probe.
22. Retained sample was dried in a toaster oven for 1.5 h at 100 °C.
23. The remaining sample was weighed and the value recorded.
24. A # 30 US standard mesh sieve was brushed with a toothbrush to ensure there were no residuals in the sieve. The sieve was kept dry.
25. A Ziploc bag containing the CABC sample was placed on a flat surface and rolled over with a piece of PVC tubing to crush the CABC.
26. The crushed CABC was placed in a # 30 US standard mesh sieve.
27. The sieve was shaken above a collection bucket until all small particles passed through the mesh.
28. Any CABC that was too big to pass through the mesh was crushed by repeating steps 25 - 27. This was repeated this until all the CABC had been crushed and sieved.
29. The CAB that passed through the mesh was weighed and the value recorded.

**B 1.4.3.4      Local Water Samples Solution:**

1. A garafón (large sealable container) was thoroughly cleaned and dried.
2. Approx. 4 L of sample water from the Ex Hacienda de Jesús well was collected in the garafón.
3. The garafón was sealed and shaken thoroughly for approx. 5 min to ensure the sample water was sufficiently mixed.
4. The water was filtered using a coffee filter to remove any suspended solids.
5. The concentration of fluoride of the sample water was measured and the value recorded. The water should had a fluoride concentration > 8.5 mg/L.
   A minimum of 6 L of sample water was accurately measured out.
6. Using ${c_1}/{c_2} = {V_2}/{V_1}$, the appropriate amount of DI water was added to ensure the sample water was at 8.5 mg/L fluoride.
7. The garafón was sealed and shaken thoroughly for approx. 5 min to ensure the sample water was sufficiently mixed.
8. The concentration of fluoride was measured and the value recorded.
9. If the fluoride concentration was > 8.5 ± 0.5 mg/L, the appropriate amount of DI water was added to decrease the concentration.
10. When the fluoride concentration was at 8.5 ± 0.5 mg/L, the arsenic concentration, pH and TDS was measured and the values recorded.

## B 1.4.4      Batch Experiment

1. Thirty-two 90 mL samples of fluoride spiked local water were measured in separate plastic tumbler containers by following the batch sample water measuring procedure detailed in appendix B 1.4.5.
2. Two samples were retained as control, and the specified doses of all other prepared media (including three doses of untreated BC) were added to other sample beakers. These were labelled blindly.
3. The beakers were placed in the tumbler and tumbled at 30 - 40 rpm for 24 hours.
4. The beakers were filtered out with a coffee filter after shaking and the filtrate was retained.
5. The filtrate was filtered again, following the Whatman™ glass microfiber filtering procedure detailed in appendix B 4.0.
6. The concentration of fluoride of all the spiked water (filtrate) samples was measured using the colourimeter and FL700 probe and their values recorded.
7. Used media was disposed of appropriately.

### *B 1.4.5      Batch Sample Water Measuring:*

1. A 100 mL volumetric flask was filled with sample water. A dropper was used to add the last few drops to ensure water was collected as accurately as possible.
2. The contents of volumetric flask was emptied into a beaker.
3. A 10 mL pipettor was used to remove 10 mL of sample water from the beaker.
4. The plastic tumbler containers were thoroughly rinsed with DI water and were completely dried.
5. The contents of the beaker was emptied into plastic tumbler container.
6. Steps 1 - 5 were repeated until the required number of tumblers had been filled with sample water.

## B 2.0 Batch Test 2

## B 2.1 Dependent Variables

1. Equilibrium fluoride concentration (i.e. concentration of fluoride in water after 24-hour batch test).
2. Production yield percentage (i.e. percentage of initial BC converted to usable adsorption media).

## B 2.2 Independent Variables

*All:*

1. Adsorption media dose: [0.05 g, 0.10 g, 0.20 g, 0.50 g, 1.00 g] i.e. [0.56 g/L, 1.11 g/L, 2.22 g/L, 5.56 g/L, 11.11 g/L]

## B 2.3 Control Variables

*All:*

1. Batch test time: 24 h
2. Batch tumbler speed: 40 rpm
3. Initial water fluoride concentration: 8 mg/L
4. Batch water sample volume: 90 mL

*RBC, BCI, BCO:*

1. Biochar barrels used in burn: 2
2. Burn temperature allowable max: 600 °C
3. Particle size: < # 30 US standard mesh (< 0.6 mm)

*SPT:*

1. Biochar barrels used in burn: 1
2. Burn temperature allowable max: 600 °C
3. Particle size: < # 30 US standard mesh (< 0.6 mm)

*BBC:*

1. Particle size: < # 30 US standard mesh (< 0.6 mm)

*H$_2$SO$_4$ BC, H$_3$PO$_4$ BC, HCl BC, KOH BC, NaOH BC:*

1. HCl activating agent concentration: 38 wt. %
2. H$_3$PO$_4$ activating agent concentration: 0.1 M
3. H$_2$SO$_4$ activating agent concentration: 0.1 M
4. NaOH activating agent concentration: 20 wt. %
5. KOH activating agent concentration: 10 wt. %
6. Activating agent soaking time: 24 h
7. Batch tumbler speed: 40 rpm
8. Activating agent solution to media ratio: 5:1 - volume:mass
9. Drying protocol: Mass taken once per hour until no change was observed
10. Activated media drying temperature: 105 °C
11. Particle size: < # 30 US standard mesh (< 0.6 mm)

## B 2.4 Procedure

### B 2.4.1 Notes

1. Batch experiments were conducted blindly and in duplicate.

### B 2.4.2 Materials

1. Representative sample RBC (minimum 1200 g)
2. Representative sample SPT (minimum 200 g)
3. BMC (minimum 200 g)
4. BOC (minimum 200 g)
5. BBC (minimum 200 g)
6. HCl (minimum 1 L)
7. 85 wt. % H$_3$PO$_4$ (minimum 1 L)
8. 98 wt. % H$_2$SO$_4$ (minimum 1 L)
9. 99 wt. % NaOH (minimum 160 g)
10. 80 wt. % KOH (minimum 60 g)
11. Sample water (minimum 9 L)
12. DI water (minimum 20 L)

Note: Amounts specified above are for a duplicate batch experiment run.

### B 2.4.3    Preparation

**B 2.4.3.1    RBC**

1. A sample (approx. 200 g) of RBC was taken, ensured to be dry and weighed. The value was recorded.
2. The sample was packed inside the inner column cartridge.
3. The outer column cartridge was closed around the inner cartridge.
4. The inlet tube of column system was attached to the RO tap.
5. The outlet tube was placed in an empty waste container.
6. The RO flow was started.
7. The inlet and outlet water was sampled using sample containers at time 0 hours and each time the waste container was filled until the fluoride concentration at the inlet was within ± 0.1 mg/L of the outlet. This was done to ensure there was no leached $PO_4$ interfering with fluoride colourimeter readings. Note: All RO flush outlet samples were filtered using the Whatman™ glass microfiber filtering method given in appendix B 4.0 before measuring using the colourimeter and FL700 probe. This was not done for the acid treated bone in the original experimental run.
8. The flushed adsorbent was removed from the column.
9. The retained sample was dried in a PID oven at 105 °C and weighed each hour until no mass change was observed.
10. The remaining sample was weighed and the value recorded.
11. Uncrushed RBC pieces were placed in a mortar and pestle and crushed.
12. A # 30 US standard mesh sieve was brushed with a toothbrush to ensure there were no residuals in the sieve. The sieve was kept dry.
13. The sieve was shaken above a collection bucket until all small particles had passed through the mesh.
14. Any BBC too big for the mesh was re-crushed by repeating steps 11 - 14. This was repeated until all BBC had been crushed and sieved.

**B 2.4.3.2    BBC**

1. A sample (approx. 200 g) of BBC was taken, ensured to be dry and weighed. The value was recorded.
2. Steps 2 - 14 of appendix B 2.4.3.1 were repeated with the BBC.

**B 2.4.3.3    BCI**

1. A representative sample (approx. 200 g) of RBC that had been subjected to a burn with two barrels of biochar was taken, ensured to be dry and the separate charred inner core separated from the outer bone. The inner char was retained and weighed. The value was recorded.
2. Steps 2 - 14 of appendix B 2.4.3.1 were repeated with the BCI.

### B 2.4.3.4    BCO

1. A representative sample (approx. 200 g) of RBC that had been subjected to a burn with two barrels of biochar was taken, ensured to be dry and the separate charred inner core separated from the outer bone. The outer char was retained and weighed. The value was recorded.
2. Steps 2 - 14 of appendix B 2.4.3.1 were repeated with the BCO.

### B 2.4.3.5    SPT

1. A representative sample (approx. 200 g) of RBC that had been subjected to a burn with one barrel of biochar was taken, ensured to be dry, and weighed. The value was recorded.
2. Steps 2 - 6 of appendix B 2.4.3.1 were repeated with the SPT.
3. The RO was left to flush the SPT until outlet water was colourless and odourless.
4. Steps 7 - 14 of appendix B 2.4.3.1 were repeated with the SPT.

### B 2.4.3.6    $H_2SO_4$ BC, $H_3PO_4$ BC, HCl BC, KOH BC, NaOH BC

1. Five initial samples of representative sample RBC (approx. 200 g each) were weighed. The values were recorded. (The crushed BC samples were kept separate throughout preparation stages to enable subsequent yield calculations for each chemical treatment method).
2. The BC was placed in a PID oven and dried at 105 °C and weighed each hour until no mass change was observed.
3. A # 30 and # 8 US standard mesh sieve were brushed with a toothbrush to ensure there were no residuals in the sieves. The sieves were kept dry.
4. The # 8 sieve was placed on top of the # 30 sieve.
5. The BC was placed in the # 8 sieve.
6. The sieves were shaken above a collection bucket until all small particles had passed through the # 8 mesh.
7. Any BC that was too big for the # 8 sieve was crushed by placing this in a Ziploc bag on a flat surface, rolling over this with a PVC tubing section and repeating steps 5 - 7.
8. The BC that passed through the # 8 sieve but was too big to pass through the # 30 sieve was weighed and the value recorded.
9. Steps 2 - 8 were repeated for the other four bags.
10. 200 mL of activating agent solutions of HCl, $H_3PO_4$, $H_2SO_4$, NaOH and KOH with concentrations as specified by the control variable list were prepared.
11. A corresponding amount of each solution for each of the BC samples was weighed in order to have a 5 : 1 ratio by weight of solution : BC.
12. The BC samples were submerged in their corresponding solutions and transferred to tumbler beakers.
13. These were tumbled at 40 rpm for 24 h at room temperature.
14. The activated samples were filtered using a coffee filter, and rinsed with DI water.

15. Steps 2 - 14 of appendix B 2.4.3.1 were repeated with the treated BC samples.

**B 2.4.3.7    Local Water Samples Solution**

1. A garafón was thoroughly cleaned and dried.
2. Approx. 10 L of sample water was collected from the CdA BC and ceramic filter production site well.
3. The garafón was sealed and shaken thoroughly for approx. 5 min to ensure the sample water was sufficiently mixed.
4. The water was filtered through a cloth column filter to remove any suspended solids.
5. The fluoride concentration of the sample water was measured and the value recorded. The water had a fluoride concentration < 8 mg/L.
6. An appropriate amount of NaF to spike water to below 8 mg/L was weighed.
7. The NaF was added to the sample water in the garafón.
8. The sample water fluoride concentration was measured and the value recorded.
9. An appropriate amount of NaF determined by the initial change in fluoride concentration of the sample water was added to get the water to 8 ± 0.5 mg/L.
10. The arsenic concentration, sample water pH and TDS were measured and their values recorded.

*B 2.4.4    Batch Experiment*

1. The 102 samples required over the duplicate batch tests were split into three lots of 34 samples. These lots were batch tested on the wheel across three 24-hour tests to ensure the wheel tumbler was not over-loaded.
2. Retaining one sample as control, specified doses of all other prepared media in one of the three lots were added to the other sample beakers. These were labelled blindly.
3. The lot of beakers were placed in the tumbler and tumbled at 40 rpm for 24 hours. Tumbler speed were reduced by adding sample beakers filled with water to increase load on this.
4. The beakers were filtered out with a coffee filter after shaking and the filtrate retained.
5. The filtrate was filtered again, following the Whatman™ glass microfiber filtering procedure detailed in appendix B 4.0.
6. The concentration of fluoride of all the filtrate samples was measured using the colourimeter and FL700 probe and their values recorded. Any comment regarding colour, odour, visual appearance (foaming, etc.) were noted.
7. The used media was disposed of appropriately.
8. Steps 2 - 7 were repeated for the other two lots, ensuring that the control sample had been included in batch tests at some point during the three lots.

### B 2.4.5    Batch Sample Water Measuring

1. Batch sample water measuring was undertaken by following the steps given in appendix B 1.4.5.

# B 3.0 RSSCT

## B 3.1 Dependent Variables

1. Sample fluoride concentration.
2. Column bed volumes passed.

## B 3.2 Independent Variables

*All:*

1. Adsorption media type: RBC, $H_3PO_4$ BC

## B 3.3 Control Variables

*All:*

1. Sample flowrate: 1.270 mL/min
2. Empty bed contact time: 152 s
3. Packed bed height: 18 cm
4. Initial water fluoride concentration: 8 mg/L
5. Sampling frequency: (15 min - 60 min)
6. BC particle size: # 100 x # 200 US standard mesh (0.108 mm < x < 1.285 mm)

## B 3.4 Procedure

### B 3.4.1    Materials

1. Representative sample RBC (minimum 50 g)
2. Representative sample $H_3PO_4$ BC (minimum 50 g)
3. Sample water (minimum 8 L)
4. DI water (minimum 4 L)

Note: Amounts specified above are for RBC and $H_3PO_4$ BC experiment runs.

### B 3.4.3　　　Preparation

1. A sample (approx. 50 g) of RBC was taken and ensured to be dry.
2. The sample was placed in a beaker and submerged in DI water.
3. The sample was stirred in the beaker at 150 rpm for 24 h to ensure the BC pores were saturated with DI water.
4. A glass wool plug was inserted at the bottom of the RSSCT column.
5. The saturated BC was sucked up from the beaker and slowly inserted into the top of the RSSCT column.
6. The side of the column was regularly tapped to ensure proper packing of the BC.
7. When the bed depth was 18 cm, the column was positioned, and connected to the chromatography water pump.
8. The pump feed was connected to a DI water source.
9. The pump was started, any trapped air was bled from the system.
10. The outlet flowrate was measured, and the pump settings adjusted until the desired flowrate was reached.

### B 3.4.3.1　　Local Water Samples Solution

1. The sample water was prepared according to the method given in appendix B 2.4.3.7.

### B 3.4.4　　　Batch Experiment

1. The DI water feed was replaced with sample water.
2. The outlet water was collected for 15 min every hour, and the outlet fluoride concentration measured.
3. When outlet water fluoride concentration was seen to increase, sampling frequency was increased to every 15 min.
4. After breakthrough, sampling frequency was again reduced back to hourly sampling until saturation.
5. Steps 1 - 10 of appendix B 3.4.3 and steps 1 - 4 of appendix B 3.4.4 were repeated with $H_3PO_4$ BC.

130

## B 4.0 Whatman™ Glass Microfiber Filtering Procedure

1. The filter base was assembled, the plastic plate was ensured to be present. This prevented the microfiber filter paper from deforming.
2. The filter paper was inserted over plastic plate with tweezers.
3. The top of the base was screwed on, securing the plastic plate to the bottom of the base.
4. The top was tightened until the lines on the side of the base matched up. If any leaks occur during the subsequent filtration, the filter base was gently tightened.
5. Approx. 5 mL of sample water was sucked up.
6. The plunger was pulled all the way up and the syringe shaken.
7. The sample water was ejected into a waste container. The syringe was rinsed at least once with new sample water between each sample taken.
8. Step 5 was repeated.
9. The sample water was ejected into a new container.
10. The container lid was closed and the container shaken.
11. The sample water was ejected into the waste container.
12. As much sample water as possible was sucked up.
13. The filter base was screwed to the syringe.
14. The sample water was ejected into the sample container through the filter.
15. The filter base was removed.
16. Steps 12-15 were repeated until no more initial sample water could be retrieved.
17. Collected sample water was retained for analysis.
18. The filter base was set aside and steps 1 - 17 were repeated using a new filter base and filter paper for the next sample.
19. Once all the filter bases had been used, these were disassembled and rinsed thoroughly in a bucket of DI water.
20. The full procedure was repeated to collect as many different samples as required.

# Appendix C: Additional Data

## C 1.0 Sample Water Chemistry

The full chemical composition of the water used in batch tests as well as RSSCT are given here. Note that ion chromatography (IC) and inductively coupled plasma mass spectrometry (ICP-MS) values reflect the results last provided by external laboratories when well samples were sent to these, and the field results were taken upon sampling in-situ (prior to this project). These values may not reflect the exact chemical composition of the samples used in these experiments.

## C 1.1 Batch Test 1

Table C 1.1.1 - Batch test 1 sample water chemical properties

| Property | CdA Lab Value | Field Testing * | IC * |
|---|---|---|---|
| Fluoride [ mg/L ] | 8.8 | 10.1 | 10.738 |
| Arsenic [ µg/L ] | 16 | 10 | - |
| TDS [ ppm ] | 286 | 345 | - |
| pH | 9.15 | 7.94 | - |
| Li [ mg/L ] | - | - | 0.279 |
| Na [ mg/L ] | - | - | - |
| $NH_4$ [ mg/L ] | - | 0.147 | < 0.01 |
| K [ mg/L ] | - | - | 2.885 |
| Mg [ mg/L ] | - | - | < 0.01 |
| Ca [ mg/L ] | - | - | 4.748 |
| Cl [ mg/L ] | - | - | 25.556 |
| $NO_2$-N [ mg/L ] | - | 0.011 | < 0.01 |
| $SO_4$ [ mg/L ] | - | 13.48 | 44.821 |
| Br [ mg/L ] | - | - | 0.164 |
| $NO_3$-N [ mg/L ] | - | 3.545 | 0.846 |
| $PO_4$ [ mg/L ] | - | - | 0.206 |
| Mn [ µg/L ] | - | 130 | - |
| Fe [ µg/L ] | - | 0 | - |
| $S_2$ [ mg/L ] | - | 0.129 | - |
| Alkalinity ($CaCO_3$ or $HCO_3$) [ mg/L ] | - | 179 | - |
| Specific Conductance [ µS/cm ] | - | 579 | - |
| Oxidation-Reduction Potential [ mV ] | - | 184.6 | - |
| Dissolved $O_2$ [ mg/L ] | - | 2.479 | - |

* Sampled 6 months prior to investigation

## C 1.2 Batch Test 2 & RSSCT

Table C 1.2.1 - Batch test 2 sample water chemical properties

| Property | CdA Lab Value | Field Testing * | IC * | ICP-MS * |
|---|---|---|---|---|
| Fluoride [ mg/L ] | 1.9 | - | 2.012 | - |
| Arsenic [ µg/L ] | 10 | - | - | 15.150 |
| TDS [ ppm ] | 199 | - | - | - |
| pH | 8.59 | 8.33 | - | - |
| Li [ mg/L ] | - | - | 0.03 | - |
| Na [ mg/L ] | - | - | 70.665 | 332.538 |
| $NH_4$ [ mg/L ] | - | - | < 0.01 | - |
| K [ mg/L ] | - | - | 0.03 | 1.370 |
| Mg [ mg/L ] | - | - | 0.03 | 0.081 |
| Ca [ mg/L ] | - | - | 8.441 | 8.505 |
| Cl [ mg/L ] | - | - | 14.911 | - |
| $NO_2$-N [ mg/L ] | - | - | 0.009 | - |
| $SO_4$ [ mg/L ] | - | - | 2.229 | - |
| Br [ mg/L ] | - | - | 0.146 | - |
| $NO_3$-N [ mg/L ] | - | - | 0.617 | - |
| $PO_4$ [ mg/L ] | - | - | 0.111 | - |
| Fe [ µg/L ] | - | - | - | 3.453 |
| $S_2$ [ mg/L ] | - | - | - | 7.839 |
| Si [ mg/L ] | - | - | - | 19.851 |
| Mo [µg/L ] | - | - | - | 3.398 |
| Cd [µg/L ] | - | - | - | 0.018 |
| Sb [µg/L ] | - | - | - | 0.045 |
| Ba [µg/L ] | - | - | - | 1.407 |
| Pb [µg/L ] | - | - | - | 0.143 |
| U [ µg/L ] | - | - | - | 2.076 |
| Al [ µg/L ] | - | - | - | 7.510 |
| P [ µg/L ] | - | - | - | 13.467 |
| Cr [ µg/L ] | - | - | - | 3.214 |
| Co [ µg/L ] | - | - | - | 0.005 |
| Ni [ µg/L ] | - | - | - | 5.074 |
| Cu [ µg/L ] | - | - | - | 1.039 |
| Zn [ µg/L ] | - | - | - | 18.082 |
| SC ** [ µS/cm ] | - | 446.1 | - | - |
| ORP *** [ mV ] | - | 8.3 | - | - |

\* Sampled 24/02/2015
\*\* Specific conductance
\*\*\* Oxidation-reduction potential

## C 2.0 RSSCT Model Parameters

Table C 2.1 gives the full list of parameters for the RSSCT model.

Table C 2.1 – PD-RSSCT model parameters

| Parameter | Large Column | Small Column |
|---|---|---|
| Flowrate ($Q$) [ mL/s ] | 0.0507 | 0.0212 |
| Mean particle size ($d_p$) [ cm ] | 0.1285 | 0.0108 |
| Bed density ($\rho_b$) [ g/cm³ ] | 0.66 | 0.66 |
| Column internal diameter ($d_i$) [ cm ] | 2.54 | 0.48 |
| Adsorbent bed depth ($L$) [ cm ] | 18 | 18 |
| Bed area ($A$) [ cm² ] | 5.07 | 0.18 |
| Bed volume ($V_{bed}$) [ cm³ ] | 91.2 | 3.2 |
| Hydraulic loading rate ($v_f$) [ cm/s ] | 0.010 | 0.119 |
| Empty bed contact time ($EBCT$) [ s ] | 1800 | 151.8 |
| Bed mass ($m$) [ g ] | 60.2 | 2.1 |
| Particle porosity ($\varepsilon_p$) | 0.46 [110] | 0.46 [110] |
| Bed porosity ($\varepsilon$) | 0.37 | 0.37 |
| Tortuosity ($\tau$) | 2.1 [110] | 2.1 [110] |
| Reynolds number ($Re$) | 0.37 | 0.37 |
| Liquid diffusivity ($\mathcal{D}_l$) [ cm²/s ] | 1.39 x 10⁻⁵ | 1.39 x 10⁻⁵ |
| Schmidt number ($Sc$) | 672 | 672 |
| Sherwood number ($Sh$) | 10.8 | 10.8 |
| Single particle Sherwood number ($Sh_p$) | 5.5 | 5.5 |
| Laminar Sherwood number ($Sh_{lam}$) | 3.5 | 3.5 |
| Turbulent Sherwood number ($Sh_{turb}$) | 0.05 | 0.05 |
| Film transfer coefficient [ cm/s ] | 1.17 x 10⁻³ | 1.39 x 10⁻² |
| Pore solute distribution parameter ($D_g$) | 0.783 | 0.783 |
| Stanton number ($St$) | 20.6 | 244.6 |
| Peclet number ($Pe$) | 93 | 1101 |
| Pore diffusion modulus ($Ed$) | 0.836 | 9.932 |
| Biot number ($Bi$) | 24.6 | 24.6 |

## C 2.0 RSSCT Model Parameters

Table C 2.1 gives the full list of parameters for the RSSCT model.

Table C 2.1 – PD-RSSCT model parameters

| Parameter | Large Column | Small Column |
|---|---|---|
| Flowrate ($Q$) [ mL/s ] | 0.0507 | 0.0212 |
| Mean particle size ($d_p$) [ cm ] | 0.1285 | 0.0108 |
| Bed density ($\rho_b$) [ g/cm$^3$ ] | 0.66 | 0.66 |
| Column internal diameter ($d_i$) [ cm ] | 2.54 | 0.48 |
| Adsorbent bed depth ($L$) [ cm ] | 18 | 18 |
| Bed area ($A$) [ cm$^2$ ] | 5.07 | 0.18 |
| Bed volume ($V_{bed}$) [ cm$^3$ ] | 91.2 | 3.2 |
| Hydraulic loading rate ($v_f$) [ cm/s ] | 0.010 | 0.119 |
| Empty bed contact time ($EBCT$) [ s ] | 1800 | 151.8 |
| Bed mass ($m$) [ g ] | 60.2 | 2.1 |
| Particle porosity ($\varepsilon_p$) | 0.46 [110] | 0.46 [110] |
| Bed porosity ($\varepsilon$) | 0.37 | 0.37 |
| Tortuosity ($\tau$) | 2.1 [110] | 2.1 [110] |
| Reynolds number ($Re$) | 0.37 | 0.37 |
| Liquid diffusivity ($\mathcal{D}_l$) [ cm$^2$/s ] | $1.39 \times 10^{-5}$ | $1.39 \times 10^{-5}$ |
| Schmidt number ($Sc$) | 672 | 672 |
| Sherwood number ($Sh$) | 10.8 | 10.8 |
| Single particle Sherwood number ($Sh_p$) | 5.5 | 5.5 |
| Laminar Sherwood number ($Sh_{lam}$) | 3.5 | 3.5 |
| Turbulent Sherwood number ($Sh_{turb}$) | 0.05 | 0.05 |
| Film transfer coefficient [ cm/s ] | $1.17 \times 10^{-3}$ | $1.39 \times 10^{-2}$ |
| Pore solute distribution parameter ($D_g$) | 0.783 | 0.783 |
| Stanton number ($St$) | 20.6 | 244.6 |
| Peclet number ($Pe$) | 93 | 1101 |
| Pore diffusion modulus ($Ed$) | 0.836 | 9.932 |
| Biot number ($Bi$) | 24.6 | 24.6 |

# C 3.0 Isotherm Model Parameters

## C 3.1 Freundlich Isotherm Parameters

Table C 3.1.1 - Freundlich isotherm model parameters

| Sample | Distribution Coefficient ($K_L$) [ $L^{1/n}/mg^{1/n-1}g$ ] | Adsorption Intensity Constant (n) |
|---|---|---|
| RBC | 2.11 | 1.74 |
| $H_3PO_4$ BC | 2.77 | 1.71 |
| $H_2SO_4$ BC | 3.26 | 1.95 |
| KOH BC | 1.40 | 1.32 |
| NaOH BC | 1.23 | 1.19 |
| SPT | 2.46 | 1.91 |
| BCI | 2.23 | 1.64 |
| BCO | 1.70 | 1.37 |
| BBC | 0.62 | 1.40 |

## C 3.2 Langmuir Isotherm Parameters

Table C 3.2.1 - Langmuir isotherm model parameters

| Sample | Maximum Adsorption Capacity ($q_{max}$) [ mg/g ] | Equilibrium Constant ($K_L$) |
|---|---|---|
| RBC | 6.69 | 0.52 |
| $H_3PO_4$ BC | 9.05 | 0.62 |
| $H_2SO_4$ BC | 6.69 | 1.32 |
| KOH BC | 8.86 | 1.32 |
| NaOH BC | 11.88 | 0.13 |
| SPT | 5.51 | 1.39 |
| BCI | 8.08 | 0.38 |
| BCO | 8.24 | 0.31 |
| BBC | 4.14 | 0.19 |

## C 3.3 Prausnitz-Radke Isotherm Parameters

Table C 3.3.1 – Prausnitz-Radke isotherm model parameters

| Sample | a [ L/g ] | b [ L/mg ] $^\beta$ | β |
|---|---|---|---|
| RBC | 2.84 | 0.26 | 1.25 |
| $H_3PO_4$ BC | 8.24 | 1.39 | 0.79 |
| $H_2SO_4$ BC | 8.81 | 1.14 | 0.94 |
| KOH BC | 2.05 | 0.36 | 0.76 |
| NaOH BC | 1.93 | 0.35 | 0.66 |
| SPT | 9.73 | 2.27 | 0.82 |
| BCI | 3.13 | 0.40 | 0.98 |
| BCO | 2.58 | 0.28 | 1.02 |
| BBC | 1.34 | 0.92 | 0.59 |